Coupled Nonlinear Aeroelasticity and Flight Dynamics for Stability Analysis of Flexible Wing Structures

Mario Natella

Technische Universiteit Delft

Delft University of Technology

Challenge the future

Coupled Nonlinear Aeroelasticity and Flight Dynamics for Stability Analysis of Flexible Wing Structures

by

Mario Natella

in partial fulfillment of the requirements for the degree of

Master of Science
in Aerospace Engineering

at the Delft University of Technology,
to be defended publicly on 11 December, 2015 at 13:00.

Thesis committee:	dr. Christos Kassapoglou,	TU Delft
	dr. ir. R. De Breuker	TU Delft
	ir. N. Werter,	TU Delft
	dr. ir. M.M. van Paassen	TU Delft

This thesis is confidential.

Declaration

I hereby certify that all material in the present MSc thesis is my own work unless otherwise referenced.

Mario Natella

Preface

I shall be telling this with a sigh
Somewhere ages and ages hence:
Two roads diverged in a wood, and I -
I took the one less traveled by,
And that has made all the difference.

- Robert Frost

Mario Natella
Delft, The Netherlands
December 2015

Alla mia famiglia. Fonte infinita di goia. [1]

[1] To my family. Inexhaustible source of joy.

Acknowledgments

What lays before your eyes is more than a mere technical report presenting my master thesis work. Behind this document there is the story of a journey, with its ups and downs, side to side with some people whose support has been vital thoughout this year.

To Roeland and Noud. Thanks for the trust placed in me from the very beginning of this journey. Thanks for bearing with me in long and interesting discussions, through the speedbumps along the way and for the invaluable support throughout.

To my family. Inexhaustible source of joy and strength despite the distance.

To Esmay. Because your love and support is invaluable to me.

Voor René. Voor de manier waarop ik ben opgenomen in de familie, waardoor ik mij altijd thuis heb gevoeld.

Voor Henriëtte en haar gezin. Ik wil jullie bedanken voor de genegenheid zoals alleen een familie kan geven.

To Mirco. Great friend from the very first day throughout the end of this journey.

To Jacqueline. For always reminding me to look sharp, despite what happens around me.

To Shahrzad. Because your legs can be giving up on you, but there's always room for one more squat.

To all my friends in Delft. For making my nights and my time off work memorable.

Por todos os meus amigos na Casa da Sua Mãe. Obrigado para fazer a minha estada no Brazil inesquecível. Será sempre um prazer ser de volta.

A Giorgio e Francesco. Perché Camigliatello non si potrá mai dimenticare.

A Gregorio, Marco, Angelo, Massimo, Fabio, Otello e tutti quelli che hanno reso i miei anni a Napoli indimenticabili tra risate, tressette e tarapia tapioco che mai potrá guastare antani, specialmente se con svergolamento a destra richiamando gli eterni fuochi fatui.

Ed per concludere in bellezza, ad Anna, Sara, Fabrizio, Alfonso, Andrea, Francesco. La vostra amicizia é stata, é, e sará inestimabile.

Abstract

State-of-the-art wing design philosophy features smart, slender and light structures. In this context, *smart* refers to proper smearing of material properties within the design by using composite materials. The enhanced flexibiliy makes aeroelasticity and flight dynamics more likely to interact at low frequencies. Effects on wing structures due to the low frequency coupling have been addressed.

The present work locates in the preliminary design evaluation phase. In this phase, medium- or low- fidelity approaches are preferred for a quick and reliable evaluation of conceptual designs, and design optimization at low computational times. The combination of vortex-lattice method (VLM) and Timoshenko beam theory (TBT) provide a low-fidelity aeroelastic framework for the evaluation of wing structures at early design stage. Fully anisotropic materials are modeled. The static aeroelastic analysis can handle large deformations and non-linearities. The dynamic aeroelaticity is linear about the nonlinear deformed configuration to facilitate stability analysis.

The aeroelastic software as such presents a solid framework to start developing more advanced analysis to be included in preliminary design assessment. The present work builds from the current aeroelastic formulation, developed by R. De Breuker et al. at the Delft University of Technology, manipulating the coupled system to model relevant phenomena associated to flexible aircraft dynamics.

The formulation has been verified against relevant test cases found in literature. The cases have shown interesting trends with regard to the flight-dynamic stability of a flexible wing structure that could be conveyed into useful guidelines in case the formulation is applied to a real-life wing design.

Mario Natella
MSc Student at Delft University of Technology

Contents

Nomenclature

Abbreviations

A/C Aircraft

AaM Department of Aeroelasticity and Morphing Wings at the TU Delft Faculty of Aerospace Engineering

AETS Aeroelastic Tailoring Software, Current Formulation

ASCM Department of Aerospace Structures and Computational Mechanics at the TU Delft Faculty of Aerospace Engineering

CFD Computational Fluid Dynamics

CFRP Carbon Fiber Reinforced Polymer

CLT Classical Lamination Theory

DLM Doublet-Lattice Method

DoF Degree of Freedom

e.a. elastic axis

EAS Equivalent Air Speed

EOM Equation of Motion

FB Flexible Body

FE Finite Element

FoR Frame of Reference

GA Genetic Algorithm

GCMMA Globally Convergent Method of Moving Asymptotes

h.t. horizontal tail

HALE High Altitude Long Endurance

LE Leading Edge

NACA National Advisory Committee for Aeronautics

NASA National Aeronautics and Space Administration

ODE	Ordinary Differential Equations
QI	Quasi Isotropic
r.b.m.	root bending moment
RB	Rigid Body
RBM	Rigid Body Motion
TAS	True Air Speed
TBE	Timoshenko Beam Element
TBT	Timoshenko Beam Theory
TE	Trailing Edge
UAV	Unmanned Air Vehicle
v.t.	vertical tail
VLM	Vortex-Lattice Method

List of symbols

Latin symbols

E Earth-fixed system

B Body-fixed system

$\mathbf{i}$ Unit vector in x direction

$\mathbf{j}$ Unit vector in y direction

$\mathbf{k}$ Unit vector in z direction

c Wing chord

$\boldsymbol{\chi}$ State vector

$\boldsymbol{\varphi}$ Perturbation vector

$\mathbf{M}$ Mass matrix

$\mathbf{K}$ Stiffness matrix

$\mathbf{R}$ Rotation matrix

$\mathbf{p}$ Position vector

$\mathbf{v}$ Velocity vector

$\mathbf{d}$ Deformation vector

T Kinetic energy

U Potential energy

δW Virtual work

$\mathbf{n}$ Normal vector

$\mathbf{t}$ Tangent vector

$\boldsymbol{\Omega}$ Spin tensor

x rigid translation in x direction

y rigid translation in y direction

z rigid translation in z direction

p Roll rate

q Pitch rate

r Yaw rate

$\mathbf{H}$ Transformation matrix

$\mathbf{T}$ Selection matrix

$\mathbf{J}$ Jacobian

Greek symbols

α Angle of attack

α_0 Angle of attack of the wing

δ Elastic deflection

λ Eigenvalue

Γ_w Doublet strength

ϕ Roll angle (first Euler angle)

θ Pitch angle (second Euler angle)

ψ Yaw angle (third Euler angle)

$\boldsymbol{\Theta}$ Combined flexible and rigid rotation vector

$\boldsymbol{\omega}$ Angular velocities

Subscripts

w Wing

a Aerodynamic

r Rigid

f Flexible

S Structural

F Flight Dynamics

lin Linear

SA Refers to a transformation from structure to aerodynamic mesh

AS Refers to a transformation from aerodynamic to structure mesh

1
Introduction

Deep-seated in the work of engineers, irregardless of the particular time in history of technology, are several aspects utterly unrelated to the physics that characterizes technological challenges. Said aspects of non-technical nature stem from society, politcs, economics and our environment. Customary in modern politics is to support world-class technology and innovation, a trend that encompasses a wide variety of scientific fields. At the same time, the fallouts of the current economic system are heavily affecting technology, including the aeronautical sector that is of particular interest in the present work. The combination of stricter environmental concerns and the need for higher revenue dictated from the private sector is determining the current, and future design challenges. Common objectives such as weight reduction, fuel consumption, increased payload, 'greener' design are constant in current aircraft design philosophy.

It is interesting to notice how externally imposed constraints have shaped the wing design concept and thus have lead to the fundamental thoughts behind the present work. The strong need for 'greener' structures implies weight reduction, a challenge that presents engineers and designers with new problems within the field of elasticity and stress analysis. Lighter structures feature high flexibility, thus making phenomena of aeroelastic nature the sizing criteria in wing design.

Since first observed in the early 1900s, aeroelastic phenomena have played a significant role in wing structural design, and have been a technological challenge for structural designers. Different ways to account for aeroelasticity in wing design have been investigated during the years, also depending upon the technological advancement at the time that particular design dates back. In fact, in the first half on the 20^{th} century, common practice advised local stiffening of wing structures to avoid aeroelastic instabilities, although the solution may have not been aligned with weight reduction policies. It was not until the late second half of the 1900s, that new engineering solutions became feasible since the understanding of the aeroelastic phenomena had grown more solid and had composite materials found their way into the aerospace industry.

Aircraft structural design philosophy changed significantly since composites have made their first appearance in aerospace industry and research. In no other circumstances, has the challenge of weight reduction seemed tangible, and most importantly within our reach. Weight reduction has made structural flexibility an important concern throughout the design process, both preliminary and detailed, with particular regard to wing structures and aeroelastic phenomena. Referring to the work of Shirk et al. (1986), the way to go is embodying "*directional stiffness into an aircraft structural design to control aeroelastic deformation [...] in such a fashion as to affect [...] structural performance [...] in a beneficial way*". These words define what we know as aeroelastic tailoring.

Aeroelastic tailoring allows for a smart use of materials, proper smearing of properties throughout the structure and utter control of the response to any perturbation. Nevertheless, modern airvehicles design have brought another challenge for structural designers. The increasing use of light and slender wings leads to structural configurations featuring low natural frequencies which can easily couple with aircraft motions, as discussed by Patil (1999), Su (2008), Cesnik et al. (2000, 2001).

Realizing the importance of aircraft motions as a consequence of the enhanced flexibility in wing structures brings a new challenge at early stages of the design process. Considerations of this kind are the ones contributing to the development of preliminary analysis tool for the design of advanced wing structures.

2
Problem Statement

Common practice in engineering design features three main phases gradually shaping the initial idea into a real-life design based on fundamental aspects dictated by both the laws of physics and designers experience. The design process features three distinct phases, namely conceptual, preliminary and detailed design. Each phase is briefly described for the sake of a clear understanding of the present work's position within the design process.

The design process begins with conceptual development. This first phase sees the rise and fall of myriads of plausible ideas that attempt to realize the design goals. Said ideas are to be quickly but effectively evaluated in terms of their feasibility and whether or not certain elemental requirements are being met. At this point, the experienced judgement of professionals comes in handy. The judgement is based on a set of rules of thumb leading to a rather accurate and thorough comprehension of crucial matters related to the idea subject to analysis. The brainstorming process selects a set of design concepts that are reckoned feasible, innovative and in agreement with the initial project requirements.

Following the conceptual phase of the design process comes the preliminary design phase. In this phase the concepts are adjusted and remodeled in a trial-and-error fashion according to several assessments, both of theoretical and experimental nature. With regard to the more theoretical part of the preliminary design evaluation, crucial within this phase is the development of low-fidelity software tools to report on fundamental aspects and features of the design. To give an example, during the development of a wing structure, one wants to ensure the design concept is free from any aeroelastic instability and if not, disregard the concept or tweak it to secure stability within the given flight envelope.

After preliminary assessment, the best set of designs enters the detailed design phase. In this phase, full-scale, expensive analysis are performed on the model for a thorough evaluation and detailed development of the design. Fabrication aspects are also addressed in this phase.

Decisive phase within the design process as a whole is the preliminary design phase. In this phase there is a strong need for quick and realiable methods for design evaluation. Moreover, several phenomena, dictated by related disciplines, are to be accounted for to enhance the quality of the design. The AETS tool, result of the hard work and dedication of R. De Breuker et al., at the ASCM/AaM department at the Delft University of Technology, serves this purpose providing a solid assessment of aeroelastic phenomena in a wing structure.

Current design tendency for civilian aircraft is oriented towards weight saving, a trend that is dictated by the pressing requirement concerning fuel reduction and the more economical side of the discussion that pushes for more payload. This inevitably faces engineers with lighter and more slender wing structures that put aeroelastic phenomena in a completely different light. Said wing structures also feature a remarkable increase in flexibility that arises more concerns with regard to stability since with the more flexibility comes large displacement and low frequency modes that can couple with aircraft rigid motions, as surrogated by the work of Patil (1999), Patil and Hodges (2005), Su (2008), Murua (2012). This line of reasoning inescapably leads to the realization that aircraft motions, or the flight dynamic stability, that displays modes at low frequency could become a point of focus at early phases of the design. Therefore stems the need to incorporate flight dynamics in low-fidelity software tools suitable for the purposes of preliminary design assessment.

With all this in mind, the present project is to be located within the preliminary design framework. The project goal can be summarized in the following statement,

with the present MSc thesis, the author aims to develop a low-fidelity flight dynamic model of an embedded flexible wing. The formulation is to be used in the development of a coupled aeroelasticity and flight dynamic model for stability assessment of composite wing structures.

3
Literature Review

Recently, within the framework of aeroelasticity and flight dynamics of wing structures, several works have significantly contributed to the body of knowledge. Detailed mathematical models have been developed to accurately describe flight dynamics of a flexible aircraft and elaborate software packages have been built to carry out static, dynamic and modal analysis on composite wing structures. Particular attention has been given to the interaction between flight dynamics and aeroelastic phenomena on particular design cases. Studies of the kind, although not discussing the effects of the coupling on the tailored composite design, have provided important observations describing crucial phenomena triggered by the interaction between flight dynamic and aeroelastic modes.

The present chapter reviews some of the relevant studies in the attempt to gather significant results and insights regarding the coupling of nonlinear aeroelasticity and flight dynamics. Each study mentioned in the sections that follow highlights different aspects of the problem, thus contributing to the process of acquiring the background knowledge needed for the present project.

3.1. Flight Dynamics

Well-established in engineering practice is the decoupling of flight dynamics and aeroelasticity. A method that is relatively effective (in terms of accuracy and simulation costs) for aircraft configurations featuring a clear separation in the frequency of aeroelastic modes and rigid modes. With the development of lighter and more slender wing structures, the choice of a decoupled system may result in a precarious assumption. Flexible flight dynamics is thus needed for a more appropriate analysis framework. Various flight dynamic formulation in literature are presented. The first concern refers to the choice of a reference frame for the EOM derivation, a choice that has been proven fundamental for the accuracy of the analytical description. Several analytical approaches that are customary within the research field are then presented.

3.1.1. Frames of Reference

A targeted choice of reference frame is fundamental for an efficient derivation of the flight dynamic equations. In this context we use *efficient* to refer to a formulation that is accurate for the purposes of the present work, while simplified in its elemental analytical terms in order to facilitate the use and solution of the system.

The first concern when selecting the frame of reference is the inertia coupling. Common practice advices the use of a Lagrangian description in body axes aligned instantaneously with the principal axes. The formulation as such leads to a diagonal inertia tensor, thus facilitating derivation and manipulation of the EOM.

It is worth mentioning that the choice of the origin has a significant impact on the flight dynamic description. A common practice in rigid aircraft dynamics is to locate the origin of the reference frame at the center of mass. With the increase in flexibility, and under severe loading conditions, the position of the center of mass varies continuously. A frame of reference that features this behaviour is referred to as *floating* reference, Shabana (1997). The complexity of a flight dynamic description in a floating reference has lead to the *mean axes* approximation, Milne (1962), Waszak and Schmidt (1990). Said approximation stems from the assumption of inertia decoupling between the structural-dynamics and rigid body equations. This leads to enforcing the linear angular momenta, due to the elastic deformation, to be zero. The interested reader can investigate the detailed mathematical formulation of the mean axes constraint, as well as its application and direct impact on the energy expressions in Meirovitch and Tuzcu (2007), Waszak and Schmidt (1990). The approach is customary in literature, although its validity is still a major point of discussions and controversies, as mentioned in Meirovitch and Tuzcu (2007).

3.1.2. Analytical Model

One of the important work on the aeroelastic properties of flexible aircraft has been presented by VanSchoor and VonFlotow (1990). The study suggests that modeling flexibility and unsteady aerodynamics is fundamental in order to properly describe aircraft dynamics. On that note, a study carried out by Waszak and Schmidt (1990) presents an analytical method in Lagrangian formulation to derive nonlinear equation of a flexible aircraft. A later study presented by Newman and Schmidt (1991) proposes a reduced order model for flight dynamics of a flexible aircraft. The method allows to get physical insights of the system itself, as well as an approximate expression of zeroes and poles for stability purposes.

The energy approach in Lagrangian formulation as proposed by Waszak and Schmidt (1990) is suitable to easily generate an accurate description of the flight dynamics of a flexible aircraft, even for unconventional configurations that feature canards or multiple tails. The system derived as such is fully coupled and nonlinear. On the other hand, although not as accurate, the reduced model is more appropriate for low-fidelity analysis in preliminary design. The underlying assumption in the reduced model presented by Newman and Schmidt (1991) is that the flight dynamics system is linearized about the deformed configuration, and therefore the perturbation is assumed relatively small compared to the wing span. The linear assumption has been widely used in literature. Relevant examples can be also found in the work of Patil (1999), Su (2008), Murua (2012).

3.2. Coupled Aeroelasticity and Flight Dynamics

Important insights about the coupling phenomena are provided in the study by Dowell et al. (2003). A wing-only type of configuration has been analysed. The configuration as such serves as a good benchmark to gather data on the coupling effect. Nevertheless, the authors note that the quality of the analysis and the predictions can be enhanced by more elaborate configurations, namely wing-horizontal tail, or wing-horizontal and vertical tail, and at last full aircraft. Important lesson from the study is that the wing-only configuration is suitable for low-fidelity predictions and preliminary design purposes. More complex configurations may be taken into account in later stages of the design phase.

The works of Nguyen et al. (2012) and Cesnik and Shearer (2005) present a finite element wing model coupled with aircraft motions about the principal axes (roll, pitch, yaw). These studies highlight the importance of flight dynamics in the aircraft modal response and flutter onset. The lighter and more slender the wing structure, the more important it is to consider aircraft motions in the wing design. This consideration becomes crucial when analysing particular aircraft configurations. On that note the work of Cesnik et al. (1996, 2000, 2001), reporting on aeroelasticity and flight dynamics of HALE aircraft (High-Altitude Long Endurance) discusses major aeroelastic effects observed in light and slender structures. Their results show that large wing deformations due to high-aspect-ratio may significantly change the aerodynamic load distribution comparing to the undeformed configuration. As a consequence, the linear approach may not be valid. The extent to which the wing structure deforms will give an indication as to what type of analysis can be performed in which particular case. The importance of low frequency coupling has been confirmed by later studies, see Livne and Weishaar (2003).

The work on HALE aircraft has been widely addressed in literature, for the effects of the flight dynamics coupling are greater in magnitude compared to conventional aircraft configurations. Important study carried out by Pendaries (1999) highlights the effect of rigid body motions on the aeroelastic characteristics. The study, again performed on HALE aircraft, uses a flexible aircraft model compared to an embedded flexible wing model on a rigid aircraft. Results show minor differences in the flutter onset in both cases. The observed discrepancies can be explained by looking at the rigid-body modes contribution to the coupling. The study also reports on the effect of the wing stiffness on aeroelastic modes, or coupled modes.

Remarkable efforts have also been done in the field of conventional aircraft. Cesnik and Su (2005a) have introduced a nonlinear aeroelastic analysis of a fully flexible aircraft, thus modeling tails and fuselage. The model allows for a thorough assessment of maneuverability, as well as aeroelastic effects on the whole aicraft. Non linear flight dynamics of flexbile aircrafts has also been presented by Chang et al. (2008). The study reports on the effect of large deformations on the aeroelastic phenomena. The strong coupling has been identified as the main cause of the high sensitivities observed in the aeroelastic analysis. In addition, the study also provides a baseline for a thorough understanding of the significance, accuracy and limitation of the results obtained at preliminary design level.

3.3. Benchmark Studies

A solid baseline is provided by the work of Drela (1999). The study presents a nonlinear aeroelastic software tool (ASWING) using a nonlinear finite element wing model coupled with a vortex wake model for steady aerodynamics. The formulation also couples flight dynamics, including full unsteady terms, and control theory, Drela (2012). The formulation has been of great influence in literature and paved the way for later studies. It is worth mentioning is the work of Palacios and Cesnik (2005) that presents an analysis software tool that can model beam theory and supports different materials formulation, as for example piezoelectric materials.

Analysis frameworks for aeroelastic tailoring have been developed more and more in the last decade. Frameworks of the kind include several disciplines, thus having to rely on several experts for the correct validation or verification of results. Important steps have been made to facilitate the analysis. The flexible wing model developed by Cesnik and Brown (2002) and Brown (2003) uses a strain-based formulation that allows for a convenient result validation using strain gauges on the real structure. Although the strain-based approach implies having to fomulate strain boundary conditions between elements, it is widely used in aeroelastic software tools.

Numerical tests on different aircraft configurations have been carried out by Patil (1999), Brown (2003) and Su (2008). The composite beam model adopted in the formulation is geometrically-exact, and coupled with 2D finite-state unsteady aerodynamics, D. A. Peters and Torrero (2006). The aircraft is modeled as fully flexible. The equation of motion is formulated from the virtual work principle, and the fully nonlinear coupled system thus derived is then linearized about the nonlinear deformed configuration.

A cantilever beam model of a wing has been used for verification purposed by Su (2008), thus showing good accordance with MSC.Patran/Nastran software package. The HALE aircraft has been used for numerical studies attempting to predict flutter onset and divergence speed including rigid body motion. Results from all three studies show good compliance with the analytical benchmark. For the HALE aircraft configuration, Patil (1999) estimates the flutter speed at 32.21 m/s, against the 32.51 m/s predicted by the analytical reference, see also Patil (1997). The difference amounts to 0.9%, thus proving the validity of both the analytical approach and the respective assumptions.

The formulation as presented in the aforementioned references encompasses a wide range of aircraft configurations. Stardard fuselage and tails configurations has been investigated, but the formulation models joined-wing aircraft, flying wings, and blended-wing bodies, Cesnik and Su (2005b, 2011, 2009).

The studies not only investigate the effect of rigid body motions on aeroelastic stability, but wing tailoring is also addressed. Ply angle in a composite wing structure has been proven to be relevant in the assessment of particular aeroelastic phenomena. In support of this statement, Patil (1999) reports on the change of divergence speed with ply angle, see Fig. (3.1). In particular, positive ply angles imply favourable bending-twisting coupling, thus increasing the divergence speed. The exact opposite holds for negative ply angles. Worth mentioning that the positive orientation is defined with respect to the wing box reference frame, as described in the aforementioned reference. Flutter is also influenced by both flight dynamics and aeroelastic tailoring, although it is more difficult to identify the direct physical quantities playing a role in the flutter onset.

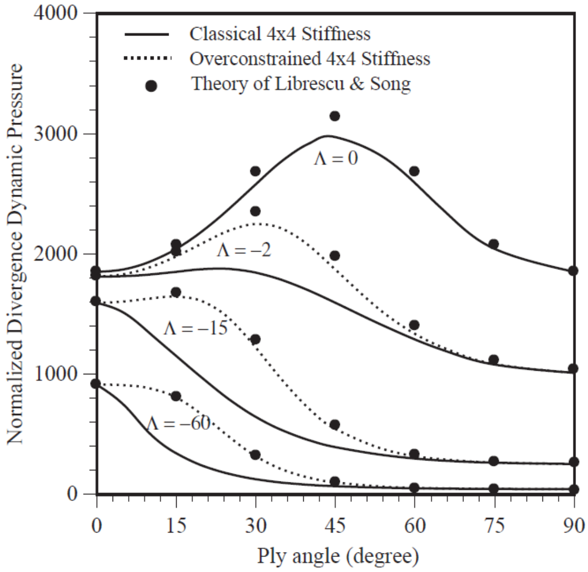

Figure 3.1: Variation of divergence dynamic pressure with ply angle, Patil (1999).

Thus proving that aeroelastic tailoring and flight dynamics indeed contribute to the development of advanced composite wing design.

3.4. Summary

To summarise, aircraft flexibility is to be taken into account in the flight dynamics model for an accurate description of the motions. Studies present a difference in the fully flexible system and the embedded flexible wing formulation. The former can be more accurate, the latter more suitable for preliminary design analysis. Main effects of the coupling between aeroelasticity and flight dynamics result in change of aerodynamic loads, flutter onset and low frequency modes coupling. On the other hand, the effect on the wing tailored design is not yet clear, and central point of discussion of the present study.

4

Thesis Plan

4.1. Methodology

The main hypothesis behind the present research lies in acknowledging that despite the advancement of state-of-the-art aeroelastic software tools, the extent to which wing structural design is affected by the coupling between aeroelasticity and flight dynamics is not clearly understood. The discussion is ongoing, and surrogated by relevant works in different institutions, research groups all over the world, see Nguyen et al. (2012), Nguyen and Tuzcu (2012), Cesnik and Shearer (2005).

The first step is to identify the proper flight dynamic model for an accurate description of aircraft motions. Main works to surrogates the model are presented by Waszak and Schmidt (1990), VanSchoor and VonFlotow (1990) and Newman and Schmidt (1991), that set the basis for flight dynamics of a flexible aircraft model. Then it is important to fully understand the coupling mechanics and implement it. Studies investigating the coupling have been carries out by Pendaries (1999) and Cesnik and Su (2005a). Finally, once the model is set and verified, we can start convey the observed trend and results into useful guidelines.

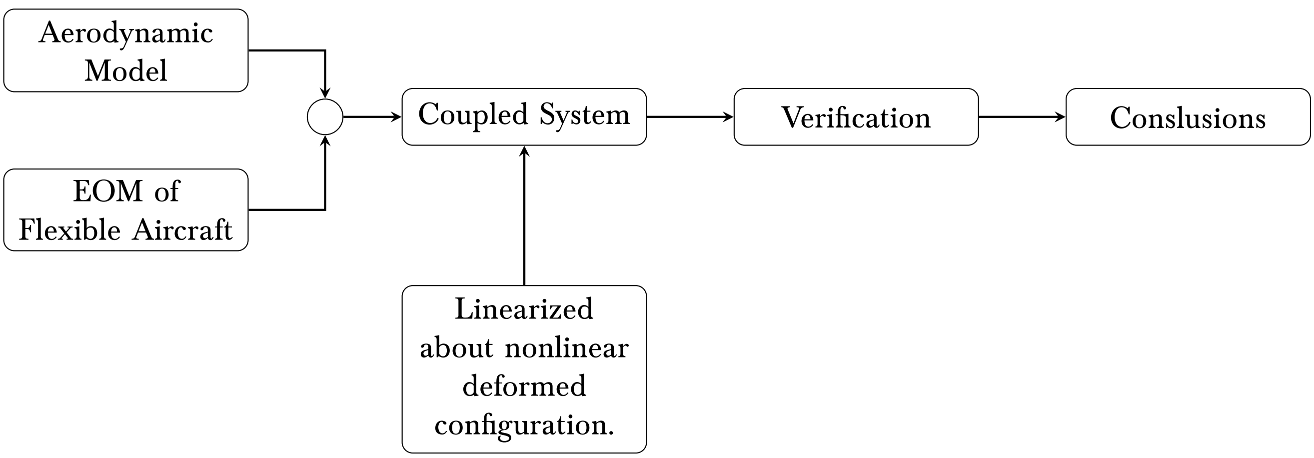

A crucial step within the framework of this research is to convey the results of the analysis into useful recommendations to be utilized during the preliminary design phase. It is worth mentioning that preliminary design is the starting point from which stems the optimized design. On that note, the quality of the optimized design depends upon the quality of the starting point. Thus, enhancing the quality of preliminary design is expected to increase the quality of the optimized design as well as improve the computational time needed for the search.

4.2. Verification Cases

The main intention at this point of the project is to test the flight dynamics code, the aeroelastic software tool and the coupled system when run on real-life wing design. Particular attention is to be given to the benchmark case selected. Among the myriad of studies that can be found in literature, the ones with similar assumptions and similar models (main focus is to be given to the assumptions behind the flight dynamics model and the aerodynamic model) will be used for verification and validation purposes. Compliance to said cases will therefore provide a solid assessment of plausibility and veracity of the results.

Together with benchmark studies provided in the literature, compliance to conventional software packages is also a valid way of testing. As far as the present study is concerned, Abaqus is the software package of choice. The reasoning for that lies in the fact that multiple type of analysis can be easily dealt with simultaneously by defining the different sets of loads and boundary conditions to describe a particular analysis. Another choice could be MSC.Patran/Nastran, that although easier to link to other computational software (e.g. Matlab), requires more elaborate settings to conduct different type of analysis on the same model.

Standard practice suggests the use of simple structural models, so that the chances of errors in the input formulation are kept to the lowest. Another aspects that contribute to lowering modeling errors is the amount of information that can be collected about the test case, and the assumptions behind the analysis found in literature. In either case, by lowering chances of modeling errors, the focus can be put on to checking the mathematical formulation.

Having said that, a good test model for the purposes of the present study is a cantilever beam subject to aeroelastic loads, see the work of Su (2008) for extensive details, and the 3D cantilever bend, with reference to the work of Crisfield and Jelenic (1999). This setting gives the chance to test the static and dynamic response, as well as the structural part of the coupled system that includes flight dynamics. Flying-wing configurations are appropriate models for aeroelastic phenomena of interest as flutter onset, divergence and stability, and modes of the fully coupled system (namely structure, aerodynamics and flight dynamics). Depending on which analysis is taken into consideration, it is important to identify the key physical quantities to monitor and verify. As far as the present project is concerned, lift distribution, incidence and trim history, bending deflection, twist rotation, flutter speed and modes are among the quantities of interest since they characterize the wing design and its performance.

5

Aeroelastic Framework

This chapter introduces the aeroelastic framework developed by De Breuker et al. (2015), used as a basis for the development of the current formulation for coupled flight dynamics and aeroelasticity.

The aeroelastic framework comprises of two models. The structural model is discussed in Sec. 5.1, whereas Sec. 5.2 covers the aerodynamic model. The aim of this chapter is to present information about the aeroelastic software that are relevant both for a thorough understanding and to the development of the current formulation. The interested reader can find further details in the referenced literature.

5.1. Structural Model

The wing structure is modeled with Timoshenko beam elements described in a corotational frame of reference (FoR), De Breuker et al. (2015). The corotational frame is rigidly connected to the element and moves with the deformation of the beam at the particular point . A detailed mathematical derivation of the structural system in a corotational framework is presented in the the work of Battini and Pacoste (2002). The main advantage presented by the corotational approach is that the rigid connection renders the direction of the aerodynamic element constant irregardless of the local deformation.

A logical chart of the structural analysis is shown in Fig. 5.1. The analysis commences with the modeling of the structural properties, described in terms of lamination parameters. Said parameters are then translated in cross-sectional properties assigned to a particular node locations. The formulation as such is suitable for both analysis and optimization of composite wing structures. Customary in optimization of composite structure is to opt for a discrete formulation of the problem, given the discrete nature of the thickness of a composite laminate. However, the introduction of lamination parameter allows for a continuous formulation of the optimization problem yielding to a convex design space wherein lies the optimum.

From classical lamination theory (CLT), any given laminate is defined by 15 lamination parameters and the material invariants, Gurdal et al. (1999). The aeroelastic framework

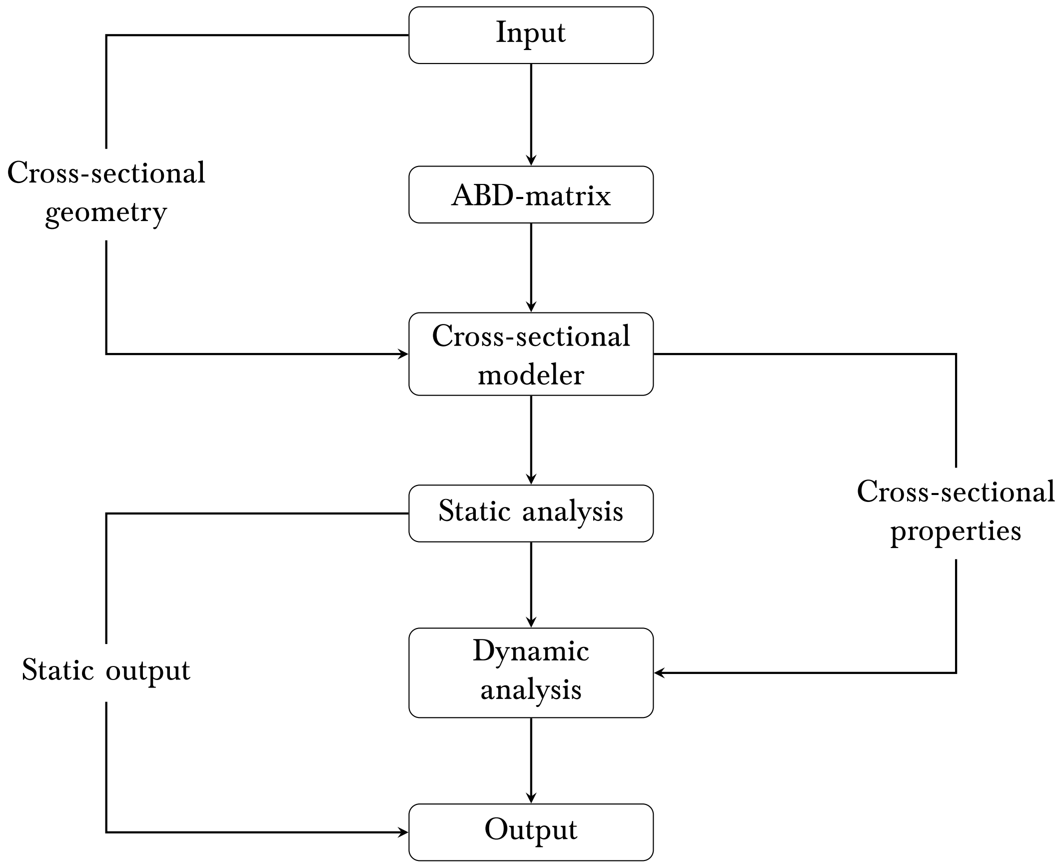

Figure 5.1: Structural analysis flow chart, De Breuker et al. (2015).

assumes symmetric laminate, thus reducing the lamination parameters to 10 for a thorough description of the laminate. From this assumption also follows the de-coupling between in-plane and out-of-plane deformations, and prevention of out-of-plane warping. Unbalanced laminate are allowed, thus accounting for the bending-torsion coupling in composite laminates, a key-stone in aeroelastic tailoring optimization.

Once the laminate has been properly described, the cross-sectional properties are to be translated in equivalent properties to lump in a specific node of the wing FE model. The computation of the equivalent properties is performed by means of the cross-sectional modeler, see Fig. 5.1, developed by Willaert et al. (2010). The formulation as such evaluates the Timoshenko stiffness matrix of a thin-walled cross-section, discretized in N elements. Material properties and thickness are assumed constant within an element, although changes between elements are allowed. From the Timoshenko stiffness matrix, the static response of the wing is thus determined.

The dynamic analysis, linear about the nonlinear static equilibrium point, is then performed. The cross-sectional modeler feeds the mass matrix evaluated from the area and inertia properties of the cross-section. Area and inertia are computed under the assumption of constant density across the section. For analytical details refer to De Breuker et al. (2015).

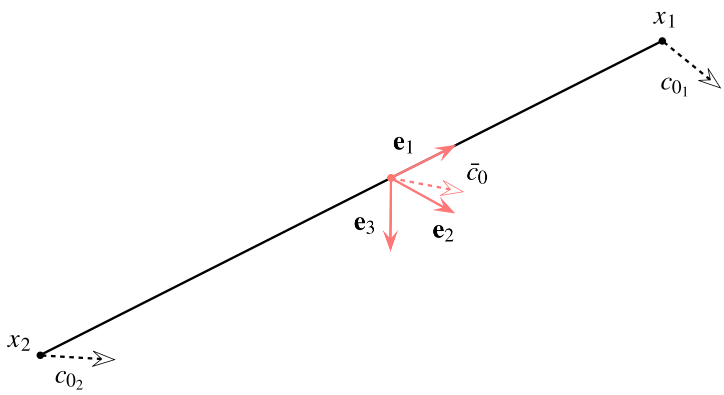

Figure 5.2: Linear cross-sectional element of the wing FE model.

Relevant for the purposes of the present work is the stiffness matrix derivation, the reason for this will become clear in Chap. 6, where the flight dynamic formulation is presented. Below, mesh generation and the FE model are discussed.

Brief Overview of the FE Model

The beam is modeled with N nodes, and $N-1$ elements, depending on the input specified in the input file. The length of the element is then evaluated. The number of mesh points of each section is determined by rounding up the length of the element divided by the average element length. The beam orientation is determined by the unit vectors $\mathbf{e}_1$, $\mathbf{e}_2$ and $\mathbf{e}_3$. The unit vector $\mathbf{e}_1$ is defined along the beam as shown in Fig. 5.2,

$$\mathbf{e}_1 = \frac{\mathbf{x}_2 - \mathbf{x}_1}{|\mathbf{x}_2 - \mathbf{x}_1|} \tag{5.1}$$

with 1 and 2 being the two end nodes of the beam element. The unit vector $\mathbf{e}_3$ is defined using $\mathbf{e}_1$ and the average chord direction $\mathbf{c}_{\text{avg}}$. Note that the average chord direction is the average of the chord directions at the end nodes. Having said that, unit vector $\mathbf{e}_3$ is given by,

$$\mathbf{e}_3 = \frac{\mathbf{e}_1 \times \mathbf{c}_{\text{avg}}}{|\mathbf{e}_1 \times \mathbf{c}_{\text{avg}}|} \tag{5.2}$$

The unit vector $\mathbf{e}_2$ is derived from $\mathbf{e}_1$ and $\mathbf{e}_3$ as follows,

$$\mathbf{e}_2 = \frac{\mathbf{e}_3 \times \mathbf{e}_1}{|\mathbf{e}_3 \times \mathbf{e}_1|} \tag{5.3}$$

For each structural elements thus generated, the local stiffness matrix is determined. The global matrix is then assembled using the co-rotational framework as developed and discussed in the work of Battini and Pacoste (2002).

5.2. Aerodynamic Model

The aerodynamic module employed in this work is based on the unsteady vortex-lattice method. The model is based on the unsteady potential flow theory under the assumption of incompressible, inviscid and irrotational flow, Werter et al. (2015). The governing equations can thus be written as,

$$\nabla^2 \Phi = 0 \tag{5.4}$$

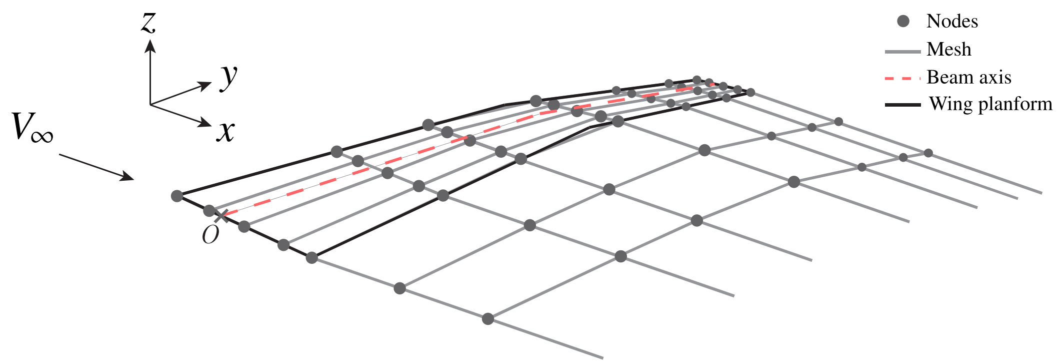

Figure 5.3: Aerodynamic mesh in the aeroelastic framework developed by De Breuker et al. (2015).

subject to flow tangency (Eq. 5.5) and far-field boundary conditions (Eq. 5.6),

$$(\nabla\Phi + \mathbf{v}_\infty) \cdot \mathbf{n} = 0 \tag{5.5}$$

$$\lim_{d\to\infty} \nabla\Phi = 0 \tag{5.6}$$

For a unique solution of the aerodynamic problem, the wake has to be taken into account making sure that the Kutta condition is satisfied at the trailing edge, see Fig. 5.3 for a visual representation of the wake in the current aeroelastic framework. This means that the vortex strength has to be zero at the trailing edge. For the sake of completion, the shed vorticity can also be calculated remembering that the circulation $\mathbf{\Gamma}$ is zero around a curve enclosing the wing as proven by the Kelvin's theorem.

Omitting the extensive analytical derivation, that can be found in the work of De Breuker et al. (2015), from the unsteady flow theory the following set of equations in state space formulation is obtained as follows,

$$\begin{bmatrix} \dot{\mathbf{\Gamma}}_w \\ \dot{\boldsymbol{\alpha}} \end{bmatrix} = \begin{bmatrix} \mathbf{K}_8 & \mathbf{K}_9 \\ \mathbf{0} & \mathbf{0} \end{bmatrix} \begin{bmatrix} \mathbf{\Gamma}_w \\ \boldsymbol{\alpha} \end{bmatrix} + \begin{bmatrix} \mathbf{0} \\ \mathbf{I} \end{bmatrix} \dot{\boldsymbol{\alpha}} \tag{5.7}$$

Important for the aeroelastic coupling is the aerodynamic output in terms of forces and moments acting on the wing. The outputs are then to be lumped to the beam location at the particular section. Without going into details of the analytical formulation, extensively illustrated in the work of Werter et al. (2015) and Mohammadi-Amin et al. (2012) [1], the output equation can be written as follows,

$$\begin{bmatrix} \mathbf{F} \\ \mathbf{M} \end{bmatrix} = \begin{bmatrix} \mathbf{L}_8 & \mathbf{L}_9 \end{bmatrix} \begin{bmatrix} \mathbf{\Gamma}_w \\ \boldsymbol{\alpha} \end{bmatrix} + \mathbf{L}_7\dot{\boldsymbol{\alpha}} \tag{5.8}$$

The aerodynamic model thus formulated is to be coupled with the structural and flight dynamic module. The latter is illustrated in the following chapter.

[1] N.P.M. Werter, R. De Breuker, M.M. Abdalla, *Continuous-time state-space unsteady aerodynamic modelling for efficient aeroelastic load analysis.* International Forum on Aeroelasticity and Structural Dynamics, June 2015, Saint Petersburg, Russia.

6
Flight Dynamics

This section presents the mathematical formulation that describes the coupled aeroelasticity and flight dynamics system developed for the purposes of the present project. The flight dynamic model builds upon the aeroelastic framework, develped by De Breuker et al. (2015). An embedded flexible wing formulation has been adopted. The aircraft is thus modeled using rigid fuselage, rigid horizontal and vertical tails, and flexible composite wings.

6.1. Frames of Reference

Let $\hat{\mathbf{i}}_E$, $\hat{\mathbf{j}}_E$, $\hat{\mathbf{k}}_E$ be the unit vectors of an *Earth-fixed* intertial frame (E-frame), and $\hat{\mathbf{i}}_B$, $\hat{\mathbf{j}}_B$, $\hat{\mathbf{k}}_B$, the unit vectors of a *body-fixed* frame attached to the aircraft (B-frame). With the purpose of simplifying the analytical description, let us define a third frame of reference that shall be referred to as *body-oriented*, identified by the unit vectors $\hat{\mathbf{i}}_O$, $\hat{\mathbf{j}}_O$, $\hat{\mathbf{k}}_O$. Said frame of reference originates in the E-frame, but its unit vector are parallel to the B-frame. The advantages of deriving the equations of motion in a frame thus built will become clear later in this chapter.
The vector $\mathbf{C} - \mathbf{O}$ describes the position of the aircraft as a function of time. The orientation of the B-frame is defined and discussed in Sec. (6.2).

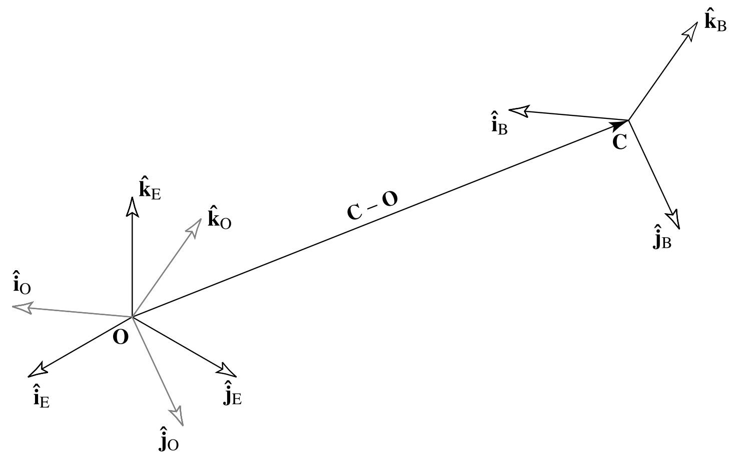

Figure 6.1: Frames of reference.

The transformation matrix from the inertial frame E to the B-frame ($\mathbf{R}_{\text{EtoB}}$) can be written as a combination of the Euler fundamental rotations ϕ, θ, ψ, thus,

$$\mathbf{R}_{\text{EtoB}} = \mathbf{R}_{\psi}\mathbf{R}_{\theta}\mathbf{R}_{\phi} \tag{6.1}$$

where $\mathbf{R}_{\phi}, \mathbf{R}_{\theta}$ and $\mathbf{R}_{\psi}$ are given by,

$$\mathbf{R}_{\phi} = \begin{bmatrix} 1 & 0 & 0 \\ 0 & \cos\phi & -\sin\phi \\ 0 & \sin\phi & \cos\phi \end{bmatrix} \tag{6.2}$$

$$\mathbf{R}_{\theta} = \begin{bmatrix} \cos\theta & 0 & \sin\theta \\ 0 & 1 & 0 \\ -\sin\theta & 0 & \cos\theta \end{bmatrix} \tag{6.3}$$

$$\mathbf{R}_{\psi} = \begin{bmatrix} \cos\psi & -\sin\psi & 0 \\ \sin\psi & \cos\psi & 0 \\ 0 & 0 & 1 \end{bmatrix} \tag{6.4}$$

Therefore, with $\mathbf{p}_{\text{E}}$ and $\mathbf{p}_{\text{B}}$ being the position of a generic point $\mathbf{P}$ on the aircraft in the E- and B-frame respectively, it follows,

$$\mathbf{p}_{\text{B}} = \mathbf{R}_{\text{EtoB}}\mathbf{p}_{\text{E}} \tag{6.5}$$

Same logic applies to other quantities, if needed to be transformed in a particular frame.

6.2. Aircraft Orientation

The aircraft orientation is described with elemental rotations ϕ, θ and ψ about the principal axes. The formulation is a variant of the Euler formulation that uses 3 different axes to define the elemental rotations.

Let x, y, z be the body reference frame in its initial undeformed position. The first rotation ϕ is defined about the x axis, and defines the intermediate reference frame x, y', z'. The second rotation θ is then defined about the y' axis, thus defining the new intermediate frame x', y', z''. Third and last rotation ψ is defined about the z'' axis, and the reference frame rotates into its final position x'', y'', z''.

Having in mind the orientation definition, the elemental rotations can be related to angular velocity $\boldsymbol{\omega}_0^T = [p \;\; q \;\; r]$ as follows,

$$\boldsymbol{\omega}_0 = \mathbf{R}_{\phi}\begin{bmatrix} \dot{\phi} \\ 0 \\ 0 \end{bmatrix} + \mathbf{R}_{\theta}\mathbf{R}_{\phi}\begin{bmatrix} 0 \\ \dot{\theta} \\ 0 \end{bmatrix} + \mathbf{R}_{\psi}\mathbf{R}_{\theta}\mathbf{R}_{\phi}\begin{bmatrix} 0 \\ 0 \\ \dot{\psi} \end{bmatrix} \tag{6.6}$$

that yields to the nonlinear set of equations,

$$\begin{cases} p = \dot{\phi} - \dot{\psi}\sin\theta \\ q = \dot{\psi}\cos\theta\sin\phi + \dot{\theta}\cos\phi \\ r = \dot{\psi}\cos\theta\cos\phi - \dot{\theta}\sin\phi \end{cases} \tag{6.7}$$

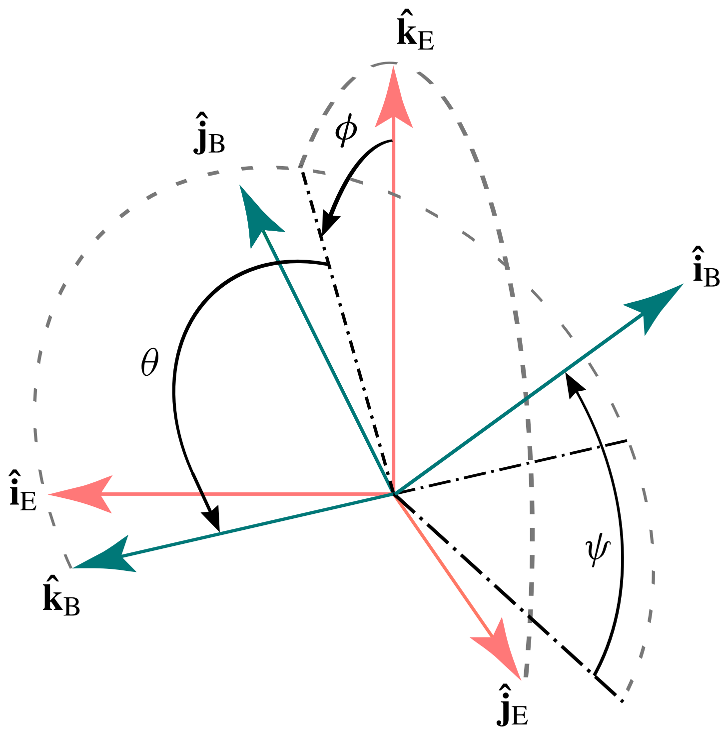

Figure 6.2: Euler angles in Tait-Bryant fomulation (pitch ϕ, roll θ, yaw ψ).

6.3. Lagrangian Formulation

Energy method in its Lagrangian formulation has been used to generate the equation of motion (EOM) of a flexible aircraft model. In its abstract form, once the energy has been properly formulated, the equation of motion can be written as,

$$\frac{d}{dt}\frac{\partial T}{\partial \dot{\chi}_i} - \frac{\partial T}{\partial \chi_i} + \frac{\partial U}{\partial \chi_i} = \frac{\partial(\delta W)}{\partial \chi_i} \tag{6.8}$$

where T refers to the total kinetic energy of the system, U the strain and potential energy and δW the virtual work along the degrees of freedom q_i. The degrees of freedom account for both the structural degrees of freedom and the flight dynamics state. The state vector $\boldsymbol{\chi}$ is thus,

$$\boldsymbol{\chi}^T = [\delta_x^1,\ \delta_y^1,\ \delta_z^1,\ \theta_x^1,\ \theta_y^1,\ \theta_z^1,\ \cdots,\ \delta_x^N,\ \delta_y^N,\ \delta_z^N,\ \theta_x^N,\ \theta_y^N,\ \theta_z^N,\ x,\ y,\ z,\ \phi,\ \theta,\ \psi] \tag{6.9}$$

where $\delta_x^i, \delta_y^i, \delta_z^i, \theta_x^i, \theta_y^i, \theta_z^i$ are the structural degrees of freedom of the i^{th} node, and $x, y, z, \phi, \theta, \psi$ are the flight dynamics degrees of freedom. The number of equations needed is therefore $6(N+1)$, with N being the number of structural nodes.

It is important to remember that the Lagrangian formulation automatically satisfies the force equilibrium, which for a Newtonian approach one would have to derive separately. The virtual work δW is given by,

$$\delta W = \mathbf{F}\delta\mathbf{r} \tag{6.10}$$

with $\mathbf{F}$ including both forces and moments.

The equation can be further extended as follows,

$$\delta W = \mathbf{F}\frac{\partial r_i}{\partial q_j}\delta q_j \tag{6.11}$$

where q refers to the state variables. The term $\partial r_i/\partial q_j$ refers to the Jacobian of the applied forces, and translates the force distribution in generalized forces acting along both the structural and flight dynamic DoFs. The use of this particular Jacobian will become clear when we go into more details on the coupling between the aerodynamic and the structural model.

6.4. Fundamental Description

Let $\mathbf{P}$ be a generic point belonging to the aircraft. Its position in the B-frame is described by the vector $\mathbf{r}_P^B$ defined as,

$$\mathbf{r}_P^B = \mathbf{r}_0 + \mathbf{d} \tag{6.12}$$

where $\mathbf{r}_0$ is the position of point P in the undeformed configuration, whereas $\mathbf{d}$ the deformation vector also defined in the B-frame,

$$\mathbf{d}^T = [\delta_x \;\; \delta_y \;\; \delta_z] \tag{6.13}$$

Note that the deformation vector is zero for the rigid components (fuselage and tails). Remembering that the position of the aircraft is given by $d^E_{\mathbf{C}-\mathbf{O}}$, with,

$$d^E_{\mathbf{C}-\mathbf{O}} = \mathbf{C} - \mathbf{O} \tag{6.14}$$

the position of point $\mathbf{P}$ in the BO-frame is,

$$\mathbf{r}_P^{BO} = d^{BO}_{\mathbf{C}-\mathbf{O}} + \mathbf{r}_0 + \mathbf{d} \tag{6.15}$$

where,

$$d^{BO}_{\mathbf{C}-\mathbf{O}} = \mathbf{R}_{EtoB}(\mathbf{C} - \mathbf{O}) \tag{6.16}$$

Its velocity is obtained by the time derivative of $\mathbf{r}_P^{BO}$, thus,

$$\mathbf{v}_P^{BO} = \frac{d}{dt}\left(\mathbf{R}_{EtoB}\mathbf{C}\right) - \frac{d}{dt}\left(\mathbf{R}_{EtoB}\mathbf{O}\right) + \dot{\mathbf{r}_0} + \dot{\mathbf{d}} + \tilde{\boldsymbol{\omega}}_0(\mathbf{r}_0 + \mathbf{d}) \tag{6.17}$$

where $\tilde{\boldsymbol{\omega}}_0$ is the second order tensor obtained from the angular velocitiy vector $\boldsymbol{\omega}_0^T = [p \;\; q \;\; r]$,

$$\tilde{\boldsymbol{\omega}}_0 = \begin{bmatrix} 0 & -r & q \\ r & 0 & -p \\ -q & p & 0 \end{bmatrix} \tag{6.18}$$

The velocity can be further manipulated into,

$$\mathbf{v}_P^{BO} = \dot{\mathbf{R}}_{EtoB}\mathbf{C} + \mathbf{R}_{EtoB}\dot{\mathbf{C}} - \dot{\mathbf{R}}_{EtoB}\mathbf{O} - \mathbf{R}_{EtoB}\dot{\mathbf{O}} + \dot{\mathbf{r}_0} + \dot{\mathbf{d}} + \tilde{\boldsymbol{\omega}}_0(\mathbf{r}_0 + \mathbf{d}) \tag{6.19}$$

Observing that $\dot{\mathbf{O}}$ and $\dot{\mathbf{r}_0}$ are both zero, the velocity of point $\mathbf{P}$ can be rewritten as,

$$\mathbf{v}_P^{BO} = \dot{\mathbf{R}}_{EtoB}\mathbf{C} + \mathbf{R}_{EtoB}\dot{\mathbf{C}} - \dot{\mathbf{R}}_{EtoB}\mathbf{O} + \dot{\mathbf{d}} + \tilde{\boldsymbol{\omega}}_0(\mathbf{r}_0 + \mathbf{d}) \tag{6.20}$$

With $\boldsymbol{\Theta}$ being the aeroelastic angular deformation vector defined about the B-frame axes,

$$\boldsymbol{\Theta}^T = [\theta_x \;\; \theta_y \;\; \theta_z] \tag{6.21}$$

the total angular velocity can be thus described by the vector,

$$\boldsymbol{\omega}_P = \boldsymbol{\omega}_0 + \dot{\boldsymbol{\Theta}} \tag{6.22}$$

The equation only holds for small perturbations about the deformed configuration. A more elaborate relationship between $\boldsymbol{\omega}$ and $\dot{\boldsymbol{\Theta}}$ is developed in Battini and Pacoste (2002).

6.4.1. Kinetic Energy

Kinetic energy in its fundamental components is,

$$T = T_{\mathrm{w}} + T_{\mathrm{r}} \tag{6.23}$$

where T_{w} describes the contribution to the kinetic energy due to the elastic wing, and T_{r} the one due to the rigid parts, namely fuselage and tails. The latter can be further decomposed into,

$$T_{\mathrm{r}} = T_{\mathrm{r}}^{\mathrm{v}} + T_{\mathrm{r}}^{\omega} \tag{6.24}$$

with $T_{\mathrm{r}}^{\mathrm{v}}$ accounting for rigid translation, and T_{r}^{ω} for rigid rotation. The total kinetic energy can be thus written as,

$$T = T_{\mathrm{w}} + T_{\mathrm{r}}^{\mathrm{v}} + T_{\mathrm{r}}^{\omega} \tag{6.25}$$

All components are discussed and elaborated in details.

6.4.2. Elastic Wing

The wing has been modeled with Timoshenko beam elements, and therefore the kinetic energy of a generic element can be written as,

$$T_{\mathrm{el}} = \frac{1}{2}\int_V \rho \mathbf{v}^T \mathbf{v} dV \tag{6.26}$$

as supported by the work of Chen and Chern (1993), Sabuncu and Evran (2006).
Let $\boldsymbol{\chi}_s$ be the state vector of the structural system, defined as,

$$\boldsymbol{\chi}_s^T = [\delta_x^1,\;\; \delta_y^1,\;\; \delta_z^1,\;\; \theta_x^1,\;\; \theta_y^1,\;\; \theta_z^1,\;\; \cdots,\;\; \delta_x^N,\;\; \delta_y^N,\;\; \delta_z^N,\;\; \theta_x^N,\;\; \theta_y^N,\;\; \theta_z^N] \tag{6.27}$$

the structural mass matrix is thus given by the Hessian of the kinetic energy in eq. (6.26) with respect to $\boldsymbol{\chi}_s$,

$$M_{\mathrm{ij}} = \frac{\partial^2 T_{\mathrm{el}}}{\partial \dot{\chi_s}^i \partial \dot{\chi_s}^j} \tag{6.28}$$

In Sec. (6.4), the velocity and angular velocity of a generic point $\mathbf{P}$ belonging to the aircraft has been discussed. In case of the an elastic wing model the deformation vectors $\mathbf{d}$, $\boldsymbol{\Theta}$ are $\neq 0$, and more importantly both $\mathbf{v}$ and $\boldsymbol{\omega}$ are a function of both the structural DoFs ($\boldsymbol{\chi}_s$) and the flight dynamic states (that will be referred to as $\boldsymbol{\chi}_f$). The latter is defined as,

$$\boldsymbol{\chi}_f^T = [x,\;\; y,\;\; z,\;\; \phi,\;\; \theta,\;\; \psi] \tag{6.29}$$

The element kinetic energy can be thus formulated as,

$$T_{\mathrm{w}} = \frac{1}{2}\int_V \rho \mathbf{v}^T(\boldsymbol{\chi}_s, \boldsymbol{\chi}_f)\mathbf{v}(\boldsymbol{\chi}_s, \boldsymbol{\chi}_f)dV \tag{6.30}$$

Recalling the general format of the Lagrangian equation of motion, shown in eq. (6.8), it follows,

$$\frac{d}{dt}\frac{\partial T_{\mathrm{w}}}{\partial \dot{\chi}_i} - \frac{\partial T_{\mathrm{w}}}{\partial \chi_i} = \begin{bmatrix} \mathbf{M}_{SS} & \mathbf{M}_{SF} \\ \mathbf{M}_{SF}^T & \mathbf{M}_{FF} \end{bmatrix} \ddot{\boldsymbol{\chi}} \tag{6.31}$$

where $\mathbf{M}_{SS}$ is the element mass matrix, $\mathbf{M}_{FF}$ is the mass matrix related to the flight dynamics degrees of freedom and $\mathbf{M}_{SF}$ couples the flight dynamics degrees of freedom to the structural ones. Mathematically speaking, the mass matrices can be built by evaluating the following Hessians of the kinetic energy,

$$(M_{SS})_{\mathrm{ij}} = \frac{\partial^2 T_{\mathrm{w}}}{\partial \dot{\chi_s}^i \partial \dot{\chi_s}^j} \qquad (M_{FF})_{\mathrm{ij}} = \frac{\partial^2 T_{\mathrm{w}}}{\partial \dot{\chi_f}^i \partial \dot{\chi_f}^j} \tag{6.32}$$

$$(M_{SF})_{\mathrm{ij}} = \frac{\partial^2 T_{\mathrm{w}}}{\partial \dot{\chi_s}^i \partial \dot{\chi_f}^j} \tag{6.33}$$

6.4.3. Rigid Fuselage and Tails

Fuselage, horizontal and vertical tails are assumed to be rigid as far as this study is concerned. As discussed in Sec. (6.4.1), the kinetic contribution given by the rigid components can be split in two parts, namely $T_{\mathrm{r}}^{\mathrm{v}}$ accounting for the rigid translation and T_{r}^{ω} for the rigid rotation. In more details,

$$T_{\mathrm{r}}^{\mathrm{v}} = \frac{1}{2}m_{\mathrm{R}}\mathbf{v}^T\mathbf{v} \qquad T_{\mathrm{r}}^{\omega} = \frac{1}{2}\boldsymbol{\omega}^T\mathbf{I}\boldsymbol{\omega} \tag{6.34}$$

The relationships hold for constant mass density, and are evaluated about the element center of gravity thus canceling out inertia coupling terms.

In a similar fashion as in previous section, from the Lagrangian equation of motion we have,

$$\frac{d}{dt}\frac{\partial T_{\mathrm{r}}^{\mathrm{v}}}{\partial \dot{\chi}_i} - \frac{\partial T_{\mathrm{r}}^{\mathrm{v}}}{\partial \chi_i} = \begin{bmatrix} 0 & 0 \\ 0 & \mathbf{M}_{\mathrm{R}}^{\mathrm{v}} \end{bmatrix} \ddot{\boldsymbol{\chi}} \tag{6.35}$$

$$\frac{d}{dt}\frac{\partial T_{\mathrm{r}}^{\omega}}{\partial \dot{\chi}_i} - \frac{\partial T_{\mathrm{r}}^{\omega}}{\partial \chi_i} = \begin{bmatrix} 0 & 0 \\ 0 & \mathbf{M}_{\mathrm{R}}^{\omega} \end{bmatrix} \ddot{\boldsymbol{\chi}} \tag{6.36}$$

The assumption of rigid bodies implies that the kinetic energy is not dependent on the structural degrees of freedom. It therefore follows that the only non-zero Hessians are,

$$(M_{\mathrm{r}}^{\mathrm{v}})_{\mathrm{ij}} = \frac{\partial^2 T_{\mathrm{r}}^{\mathrm{v}}}{\partial \dot{\chi_f}^i \partial \dot{\chi_f}^j} \tag{6.37}$$

$$(M_{\mathrm{r}}^{\omega})_{\mathrm{ij}} = \frac{\partial^2 T_{\mathrm{r}}^{\omega}}{\partial \dot{\chi_f}^i \partial \dot{\chi_f}^j} \tag{6.38}$$

6.4.4. Strain Energy

Strain energy is defined as,

$$U_{\mathrm{e}} = \frac{1}{2}\boldsymbol{\chi}_s^T \mathbf{K} \boldsymbol{\chi}_s \tag{6.39}$$

where $\boldsymbol{\chi}_s$ is the structural state vector, and $\mathbf{K}$ the stiffness matrix of the finite element wing model. The relevant details regarding the derivation of the stiffness matrix are given in the work of De Breuker et al. (2015). Since the strain energy is only dependent on the structural degrees of freedom, any derivative with respect to the flight dynamics degrees of freedom is zero. Thus, from the Lagrangian equation of motion,

$$\frac{\partial U_{\mathrm{e}}}{\partial \chi_i} = \begin{bmatrix} \mathbf{K} & 0 \\ 0 & 0 \end{bmatrix} \boldsymbol{\chi} \tag{6.40}$$

6.4.5. Potential Energy

Gravitational energy in its integral form is given by Waszak and Schmidt (1990),

$$U_{\mathrm{g}} = -\int_V \mathbf{g}^T \mathbf{r} \rho dV \tag{6.41}$$

where $\mathbf{g}$ is the gravitational acceleration vector, and $\mathbf{r}$ the position vector. The total gravitational energy can be split in two terms, one for the elastic wing, one for the rigid parts of the aircraft,

$$U_{\mathrm{g}} = (U_{\mathrm{g}})_{\mathrm{w}} + (U_{\mathrm{g}})_{\mathrm{R}} \tag{6.42}$$

Assuming constant mass density, we have,

$$(U_{\mathrm{g}})_{\mathrm{w}} = \sum_i m_i \mathbf{g}^T \mathbf{r}_i \tag{6.43}$$

$$(U_{\mathrm{g}})_{\mathrm{R}} = m_{\mathrm{R}} \mathbf{g}^T \mathbf{r} \tag{6.44}$$

with $\mathbf{r}$ evaluated with respect to the element center of gravity. Thus, from the Lagrangian equation of motion follows,

$$\frac{\partial U_{\mathrm{g}}}{\partial \chi_i} = \begin{bmatrix} \mathbf{K}^{\mathrm{g}}_{SS} & \mathbf{K}^{\mathrm{g}}_{SF} \\ (\mathbf{K}^{\mathrm{g}}_{SF})^T & \mathbf{K}^{\mathrm{g}}_{FF} \end{bmatrix} \boldsymbol{\chi} \tag{6.45}$$

The stiffness matrices can be derived from the Hessians of the potential energy as follows,

$$(K^{\mathrm{g}}_{SS})_{\mathrm{ij}} = \frac{\partial^2 U_{\mathrm{g}}}{\partial \chi_s^i \partial \chi_s^j} \qquad (K^{\mathrm{g}}_{FF})_{\mathrm{ij}} = \frac{\partial^2 U_{\mathrm{g}}}{\partial \chi_f^i \partial \chi_f^j} \tag{6.46}$$

$$(K^{\mathrm{g}}_{SF})_{\mathrm{ij}} = \frac{\partial^2 U_{\mathrm{g}}}{\partial \chi_s^i \partial \chi_f^j} \tag{6.47}$$

6.5. Nonlinear System

The fully nonlinear system obtain with the Lagrangian formulation is shown,

$$\left\{ \begin{bmatrix} \mathbf{M}_{SS} & \mathbf{M}_{SF} \\ \mathbf{M}_{SF}^T & \mathbf{M}_{FF} \end{bmatrix} + \begin{bmatrix} 0 & 0 \\ 0 & \mathbf{M}_{\mathrm{R}}^{\mathrm{v}} \end{bmatrix} + \begin{bmatrix} 0 & 0 \\ 0 & \mathbf{M}_{\mathrm{R}}^{\omega} \end{bmatrix} \right\} \ddot{\boldsymbol{\chi}} + \left\{ \begin{bmatrix} \mathbf{K} & 0 \\ 0 & 0 \end{bmatrix} + \begin{bmatrix} \mathbf{K}^{\mathrm{g}}_{SS} & \mathbf{K}^{\mathrm{g}}_{SF} \\ (\mathbf{K}^{\mathrm{g}}_{SF})^T & \mathbf{K}^{\mathrm{g}}_{FF} \end{bmatrix} \right\} \boldsymbol{\chi} = \mathbf{R} \tag{6.48}$$

The vector of generalized forces is unknown, and it is to be determined by coupling the system to the aerodynamic model. The details are shown in Sec. (6.9).

6.6. Linearized System

The fully nonlinear system has been linearized about the nonlinear deformed configuration (denoted by δ) to facilitate the stability analysis. The underlying assumption is that the state vector can be written as,

$$\chi = \chi_\delta + \varphi \tag{6.49}$$

where χ_δ refers to the state vector in the nonlinear deformed configuration, while φ to the perturbation. The perturbation is assumed to be reasonably small compared to the nonlinear deformation. The linearization process is hereby discussed, further details of the derivation can be found in Appendix A.

Analytical overview

Let us write the nonlinear system in its compact form as,

$$\mathbf{M}\ddot{\chi} + \mathbf{K}\chi = \mathbf{R}(\chi) \tag{6.50}$$

To simplify the mathematical formulation of the variational equations needed to linearize the system, the following auxiliary functions are hereby defined,

$$\boldsymbol{f}_1 = \mathbf{M}\ddot{\chi} \tag{6.51}$$

$$\boldsymbol{f}_2 = \mathbf{K}\chi \tag{6.52}$$

The Taylor expansion of the nonlinear functions $\boldsymbol{f}_1$ and $\boldsymbol{f}_2$ is,

$$\boldsymbol{f}_1 = \boldsymbol{f}_1(\delta) + \left(\frac{\partial \boldsymbol{f}_1^i}{\partial \ddot{\boldsymbol{\chi}}_j}\right)_\delta \ddot{\varphi} + \left(\frac{\partial \boldsymbol{f}_1^i}{\partial \dot{\boldsymbol{\chi}}_j}\right)_\delta \dot{\varphi} + \left(\frac{\partial \boldsymbol{f}_1^i}{\partial \boldsymbol{\chi}_j}\right)_\delta \varphi + o(2) \tag{6.53}$$

$$\boldsymbol{f}_2 = \boldsymbol{\xi}_2(\delta) + \left(\frac{\partial \boldsymbol{f}_2^i}{\partial \ddot{\boldsymbol{\chi}}_j}\right)_\delta \ddot{\varphi} + \left(\frac{\partial \boldsymbol{f}_2^i}{\partial \dot{\boldsymbol{\chi}}_j}\right)_\delta \dot{\varphi} + \left(\frac{\partial \boldsymbol{f}_2^i}{\partial \boldsymbol{\chi}_j}\right)_\delta \varphi + o(2) \tag{6.54}$$

recalling the assumption in eq. (6.49) the higher order terms can be neglected thus having,

$$\boldsymbol{f}_1 \approx \boldsymbol{f}_1(\delta) + \left(\frac{\partial \boldsymbol{f}_1^i}{\partial \ddot{\boldsymbol{\chi}}_j}\right)_\delta \ddot{\varphi} + \left(\frac{\partial \boldsymbol{f}_1^i}{\partial \dot{\boldsymbol{\chi}}_j}\right)_\delta \dot{\varphi} + \left(\frac{\partial \boldsymbol{f}_1^i}{\partial \boldsymbol{\chi}_j}\right)_\delta \varphi \tag{6.55}$$

$$\boldsymbol{f}_2 \approx \boldsymbol{f}_2(\delta) + \left(\frac{\partial \boldsymbol{f}_2^i}{\partial \ddot{\boldsymbol{\chi}}_j}\right)_\delta \ddot{\varphi} + \left(\frac{\partial \boldsymbol{f}_2^i}{\partial \dot{\boldsymbol{\chi}}_j}\right)_\delta \dot{\varphi} + \left(\frac{\partial \boldsymbol{f}_2^i}{\partial \boldsymbol{\chi}_j}\right)_\delta \varphi \tag{6.56}$$

Since $\boldsymbol{f}_1$ is only a function of $\ddot{\chi}$, and $\boldsymbol{f}_2$ only dependent on χ, the linear approximations become,

$$\boldsymbol{f}_1 \approx \boldsymbol{f}_1(\delta) + \left(\frac{\partial \boldsymbol{f}_1^i}{\partial \ddot{\boldsymbol{\chi}}_j}\right)_\delta \ddot{\varphi} \tag{6.57}$$

$$\boldsymbol{f}_2 \approx \boldsymbol{f}_2(\delta) + \left(\frac{\partial \boldsymbol{f}_2^i}{\partial \boldsymbol{\chi}_j}\right)_\delta \varphi \tag{6.58}$$

Substituting the linearized function in the initial equation of motion in eq.(6.50),

$$\boldsymbol{f}_1(\delta) + \left(\frac{\partial \boldsymbol{f}_1^i}{\partial \ddot{\boldsymbol{\chi}}_j}\right)_\delta \ddot{\varphi} + \boldsymbol{f}_2(\delta) + \left(\frac{\partial \boldsymbol{f}_2^i}{\partial \boldsymbol{\chi}_j}\right)_\delta \varphi = \mathbf{R}(\delta) + \mathbf{R}(\varphi) \tag{6.59}$$

where the generalized forces $\mathbf{R}$ have been decomposed into the two contributions $\mathbf{R}(\delta)$ in the nonlinear deformed configuration and $\mathbf{R}(\varphi)$ in the perturbed state. Worth to mention that the break down of the generalized forces only holds under the small perturbation assumption.

We now note that the following part of the linear equation of motion in eq. (6.5),

$$\boldsymbol{f}_1(\delta) + \boldsymbol{f}_2(\delta) = \mathbf{R}(\delta) \tag{6.60}$$

is nothing other than the solution of the nonlinear deformed configuration. Thus eq.(6.59) can be reduced to,

$$\left(\frac{\partial \boldsymbol{f}_1^i}{\partial \ddot{\chi}_j}\right)_\delta \ddot{\varphi} + \left(\frac{\partial \boldsymbol{f}_2^i}{\partial \chi_j}\right)_\delta \varphi = \mathbf{R}(\varphi) \tag{6.61}$$

Where the Jacobians of $\boldsymbol{f}_1$ and $\boldsymbol{f}_2$ represent the linear mass matrix and the linear stiffness matrix respectively.

$$\mathbf{M}_{\text{lin}}\ddot{\varphi} + \mathbf{K}_{\text{lin}}\varphi = \mathbf{R}(\varphi) \tag{6.62}$$

The linear system is now to be coupled to the aerodynamic model in order to determine the unknown forces on the perturbed state and assess stability about the nonlinear deformed configuration.

6.7. The Structural State Space

Let us write the coupled structural system as,

$$\mathbf{M}\ddot{\chi} + \mathbf{K}\chi = \mathbf{F} \tag{6.63}$$

For reasons that will become clear when we will discuss the coupling to the aerodynamic system of equation, it is convenient to rewrite the structural equation is state space format. It thus follows,

$$\begin{bmatrix} \ddot{\chi} \\ \dot{\chi} \end{bmatrix} = \begin{bmatrix} \mathbf{0} & -\mathbf{M}^{-1}\mathbf{K} \\ \mathbf{I} & \mathbf{0} \end{bmatrix} \begin{bmatrix} \dot{\chi} \\ \chi \end{bmatrix} + \begin{bmatrix} \mathbf{M}^{-1} \\ \mathbf{0} \end{bmatrix} \mathbf{F} \tag{6.64}$$

and in a more compact version,

$$\dot{\mathbf{X}}_s = \mathbf{A}_s\mathbf{X}_s + \mathbf{B}_s\mathbf{F}_s \tag{6.65}$$

6.8. The Angle of Attack

Fundamental in the formulation of the coupled system is to define the correct angle of attack that also includes flight dynamics variables. With reference to the work of Waszak and Schmidt (1990) and De Breuker et al. (2012), the angle of attack can be formulated as,

$$\boldsymbol{\alpha} = \boldsymbol{\alpha}_{\text{air}} + \boldsymbol{\Theta} + \frac{\dot{\boldsymbol{\Theta}}_s}{V_\infty}(\boldsymbol{x}_{\text{p}} - x_{\text{ref}}) + \frac{q}{V_\infty}(\boldsymbol{x}_{\text{p}} - x_{\text{ref}}) - \frac{\dot{\boldsymbol{h}}_s}{V_\infty} - \frac{\dot{\boldsymbol{h}}_r}{V_\infty} \tag{6.66}$$

where $\boldsymbol{\alpha}_{\text{air}}$ is the incidence angle, $\boldsymbol{\Theta}$ is the combined rotation (that includes both the rigid rotation and the elastic deformation $\boldsymbol{\Theta}_s$), the term q refers to the pitch rate while $\dot{\boldsymbol{h}}_s$ and $\dot{\boldsymbol{h}}_r$ are respectively the structural and rigid plunge rates.

6.8.1. Contribution of the combined flexible and rigid rotation

The most delicate term in the equation is the combined rotation angle $\boldsymbol{\Theta}$, which is a function of both χ_s (the structural DoFs) and χ_f (the flight dynamic states). In more details, the problem is that we have to combine the twist rotations θ_x, θ_y, θ_z with the consecutive rotation angles (Euler angles) ϕ, θ, ψ. This particular problem does not exist for angular velocities, which are always additive. We will now explain how to derive the combined rotation in details.

Let us begin with the rigid component, given in Euler angles. The three consecutive rotation define the following rotation matrix,

$$\mathbf{R}^{\text{r}} = \mathbf{R}_\psi \mathbf{R}_\theta \mathbf{R}_\phi \tag{6.67}$$

with the elemental rotation matrices in ϕ, θ, ψ are defined in Sec. 6.1.

The amount of rotation that results from the structural deformation is described by three non-consecutive rotations. This makes the derivation of the rotation matrix less straight forward compared to the rigid case. Therefore, let us now consider the three rotations in question, θ_x, θ_y, θ_z, that define the vector $\boldsymbol{\theta}_s$. To this vector we can associate a 3-by-3 skew-symmetric matrix, $\boldsymbol{\Omega}$, usually called the *spin tensor*,

$$\boldsymbol{\Omega} = \mathbf{spin}(\boldsymbol{\theta}_s) = \begin{bmatrix} 0 & -\theta_z & \theta_y \\ \theta_z & 0 & -\theta_x \\ -\theta_y & \theta_z & 0 \end{bmatrix} \equiv -\boldsymbol{\Omega}^T \tag{6.68}$$

The problem we have now is the construction of a rotation matrix $\mathbf{R}^{\text{f}}$ (where f stands for flexible) from the rotation angles $\boldsymbol{\theta}_s$. Considering that $\mathbf{R}^{\text{f}}$ is analytical in $\boldsymbol{\Omega}$, that tells us that the Taylor expansion exists and thus the rotation matrix can be written as,

$$\mathbf{R}^{\text{f}} = \mathbf{I} + \sum_i c_i \boldsymbol{\Omega}^i \tag{6.69}$$

At this point, one can refer to the Cayley-Hamilton theorem, Birkoff and MacLane (1996), that proves the following property of the spin matrix,

$$\boldsymbol{\Omega}^n = -||\boldsymbol{\theta}_s||\boldsymbol{\Omega}^{n-2} \tag{6.70}$$

for $n \geq 3$, which allows us to write c_1 and c_2 as,

$$c_1 = \sum_{n=0}^{+\infty} (-1)^n \frac{||\boldsymbol{\theta}_s||^{2n+1}}{(2n+1)!} \tag{6.71}$$

$$c_2 = 1 - \sum_{n=0}^{+\infty} (-1)^n \frac{||\boldsymbol{\theta}_s||^{2n}}{2n!} \tag{6.72}$$

that are the generic expressions for the Taylor expansion of the following trigonometric functions,

$$c_1 = \sin ||\boldsymbol{\theta}_s|| \tag{6.73}$$

$$c_2 = 1 - \cos ||\boldsymbol{\theta}_s|| \equiv \frac{\sin 0.5||\boldsymbol{\theta}_s||}{||\boldsymbol{\theta}_s||} \tag{6.74}$$

thus the flexible rotation matrix becomes,

$$\mathbf{R}^{\mathrm{f}} = \mathbf{I} + \sin ||\boldsymbol{\theta}_s||\boldsymbol{\Omega} + \frac{\sin 0.5||\boldsymbol{\theta}_s||}{||\boldsymbol{\theta}_s||} \boldsymbol{\Omega}^2 \tag{6.75}$$

and finally we can write the combined rotation matrix as,

$$\mathbf{R} = \mathbf{R}^{\mathrm{f}}\mathbf{R}^{\mathrm{r}} \tag{6.76}$$

From combined rotation matrix to the amount of rotation

The problem we are now facing is the calculation of the amount of rotation that is dictated by the rotation matrix. A simple way is advised in the standard theory of finite rotations, where given a rotation matrix **R**, the spin tensor associated with the rotation vector is nothing other than,

$$\boldsymbol{\Omega} = \log \mathbf{R} \tag{6.77}$$

Let us now introduce the *axial* operator, such that given a matrix **A**,

$$\mathbf{axial}(A) = \begin{bmatrix} A_{32} - A_{23} \\ A_{13} - A_{31} \\ A_{21} - A_{12} \end{bmatrix} \tag{6.78}$$

This allows to define the normalized axis of rotation **n** as,

$$\mathbf{n} = \mathbf{axial}(\mathbf{R} - \mathbf{R}^T) \tag{6.79}$$

and,

$$\tau = \frac{1}{2}||\mathbf{axial}(\mathbf{R} - \mathbf{R}^T)|| \tag{6.80}$$

so that the spin tensor can be expressed in its closed form as,

$$\boldsymbol{\Omega} = \frac{\sin^{-1} \tau}{2\tau}\mathbf{n} \tag{6.81}$$

from the spin tensor the rotation vector is obtained by simply reversing the spin operator,

$$\boldsymbol{\theta} = \mathbf{spin}^{-1}(\boldsymbol{\Omega}) \tag{6.82}$$

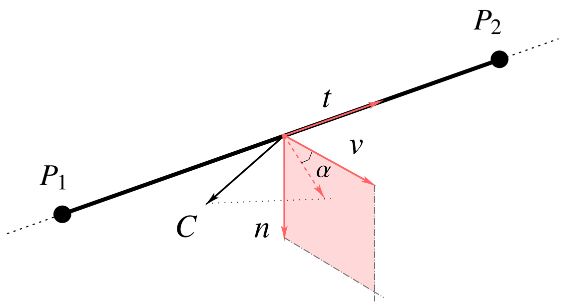

Figure 6.3: Vectorial derivation of the angle of attack.

From local rotation to angle of attack

Let us consider an element of the aerodynamic mesh, delimited by the points P_1, P_2. This element is subject to a rotation, appropriately translated from the structural mesh, that will influence on the local angle of attack. We will hereby go into the details of how to transform the rotations into an angle of attack, see Fig. 6.3.

Let $\mathbf{t}$ be the tangent vector to the element, positive from P_1 towards P_2. Assuming that,

$$P_1 = [x_1 \;\; y_1 \;\; z_1] \tag{6.83}$$

$$P_2 = [x_2 \;\; y_2 \;\; z_2] \tag{6.84}$$

the tangent vector is defined as,

$$\mathbf{t} = \begin{bmatrix} 0 \\ \dfrac{y_2 - y_1}{\sqrt{(y_2-y_1)^2 + (z_2-z_1)^2}} \\ \dfrac{z_2 - z_1}{\sqrt{(y_2-y_1)^2 + (z_2-z_1)^2}} \end{bmatrix} = \begin{bmatrix} 0 \\ t_2 \\ t_3 \end{bmatrix} \tag{6.85}$$

It is important to mention that the aerodynamic element between P_1 and P_2 is not curved. The tangent vector is important because it is the axis of rotation of the element.

Now, let $\mathbf{v}$ be the velocity vector, with coordinates,

$$\mathbf{v}^T = [1 \;\; 0 \;\; 0] \tag{6.86}$$

that is perpendicular to the tangent vector $\mathbf{t}$. Finally, their cross-product,

$$\mathbf{n} = \mathbf{t} \times \mathbf{v} \tag{6.87}$$

is nothing other than the normal to the element with respect to the plane ($\mathbf{t}$,$\mathbf{v}$). The three vectors form a right-handed base system that will allow to define a robust formulation for the angle of attack. The base rotation matrix $\mathbf{R}_\mathrm{B}$ is,

$$\mathbf{R}_\mathrm{B} = \begin{bmatrix} \mathbf{v} & \mathbf{t} \times \mathbf{v} & \mathbf{t} \end{bmatrix} \tag{6.88}$$

and it is defined in such a way that the following two conditions are true,

$$\mathbf{v} = \mathbf{R}_{\mathrm{B}}^{\mathrm{T}} \begin{bmatrix} 1 \\ 0 \\ 0 \end{bmatrix} \tag{6.89}$$

$$\mathbf{t} = \mathbf{R}_{\mathrm{B}}^{\mathrm{T}} \begin{bmatrix} 0 \\ 0 \\ 1 \end{bmatrix} \tag{6.90}$$

From the coordinates of **v** and **t**, we have,

$$\mathbf{n} = \mathbf{t} \times \mathbf{v} \tag{6.91}$$

using the spin operator on **t**, we have,

$$\mathbf{n} = \begin{bmatrix} 0 & -t_3 & t_2 \\ t_3 & 0 & 0 \\ -t_2 & 0 & 0 \end{bmatrix} \begin{bmatrix} 1 \\ 0 \\ 0 \end{bmatrix} = \begin{bmatrix} 0 \\ t_3 \\ -t_2 \end{bmatrix} \tag{6.92}$$

thus the base matrix becomes,

$$\mathbf{R}_{\mathrm{B}} = \begin{bmatrix} 1 & 0 & 0 \\ 0 & t_3 & -t_2 \\ 0 & t_2 & t_3 \end{bmatrix} \tag{6.93}$$

We now have all the ingredients to finalize the derivation of the angle of attack.

Consider a vector $\mathbf{C}_0$ initially equal to,

$$\mathbf{C}_0 = \mathbf{v} = \begin{bmatrix} 1 \\ 0 \\ 0 \end{bmatrix} \tag{6.94}$$

that it is then rotated by pre-multiplying by the combined rotation matrix **R**,

$$\mathbf{C}' = \mathbf{R}\mathbf{C}_0 \tag{6.95}$$

and brought into the base system previously defined,

$$\mathbf{C} = \mathbf{R}_{\mathrm{B}}\mathbf{R}\mathbf{C}_0 \tag{6.96}$$

The angle of attack is the angle between **C** and $\mathbf{C}_0$ in the plane (**v**,**n**). Since all the vectors are defined in the same local frame of reference, the angle of attack is given by,

$$\alpha = \tan^{-1}\left(\frac{C_y}{C_x}\right) \tag{6.97}$$

The equation is non-linear in the state variables (in this case only the structural rotations, and the Euler angles). The angle of attack can be thus approximated as,

$$\alpha = \alpha_0 + \frac{\partial \alpha}{\partial \chi}\delta\chi + o(2) \tag{6.98}$$

From eq. 6.97, the variation of α with respect to one of the state variables is given by,

$$d\alpha \approx \frac{1}{1+\left(\frac{C_y}{C_x}\right)^2} \; \frac{dC_y C_x - C_y dC_x}{C_x^2} \tag{6.99}$$

where the variation of $\mathbf{C}$ is obtained with the chain rule on eq. 6.96,

$$d\mathbf{C} = \mathbf{R}_{\mathrm{B}} d\mathbf{R} \mathbf{C}_0 \tag{6.100}$$

The formulation has three advantages,

- the sign of alpha is directly obtained by the ration C_y/C_x,
- the derivative is defined for any real number, thus showing no singularities,
- the derivative exists if $\mathbf{C}$ and $\mathbf{C}_0$ are aligned.

The third point is crucial when weighing the different mathematical options to define the angle of attack. To give an example, another equivalent way to define α is the following,

$$\alpha = \cos^{-1}\left(\mathbf{C} \cdot \mathbf{C}_0\right) \tag{6.101}$$

assuming both vectors are normalized. Its variation is thus,

$$d\alpha = \frac{1}{\sqrt{1-\left(\mathbf{C} \cdot \mathbf{C}_0\right)^2}} \; d\mathbf{C} \cdot \mathbf{C}_0 \tag{6.102}$$

a function that is singular when,

$$\mathbf{C} \cdot \mathbf{C}_0 = 1 \tag{6.103}$$

that means the two vectors are aligned. In case the angle of attack had been formulated using the arcsin,

$$\alpha = \sin^{-1}\left(||\mathbf{C} \times \mathbf{C}_0||\right) \tag{6.104}$$

with both vector normalized, the variation is again singular if $\mathbf{C}$ and $\mathbf{C}_0$ are aligned.

6.8.2. Contribution of the plunge rates

As we have seen from eq. 6.66, there is two contributions to the angle of attack due to the plunge rate. The structural plunge is the local motion of the element described by the following equation,

$$\dot{h}_s = \mathbf{n} \cdot \dot{\boldsymbol{\delta}}_s \tag{6.105}$$

with $\mathbf{n}$ being the element normal. Atop of it, we have the rigid plunge that instead is a function of rigid translations hereby referred to as $\mathbf{X}$,

$$\dot{h}_r = \mathbf{n} \cdot \dot{\mathbf{X}} \tag{6.106}$$

that applies uniformly to all the elements in the structure.

6.9. Coupled System

Let us recall the expression of the angle of attack as presented in eq. 6.66,

$$\boldsymbol{\alpha} = \boldsymbol{\alpha}_{\text{air}} + \boldsymbol{\Theta} + \frac{\dot{\boldsymbol{\Theta}}_s}{V_\infty}(\boldsymbol{x}_{\text{p}} - x_{\text{ref}}) + \frac{q}{V_\infty}(\boldsymbol{x}_{\text{p}} - x_{\text{ref}}) - \frac{\dot{\boldsymbol{h}}_s}{V_\infty} - \frac{\dot{\boldsymbol{h}}_r}{V_\infty} \tag{6.107}$$

which is an essential term to couple the structural state space (that includes the flight dynamic degrees of freedom) to the aerodynamic system of equations. The angle of attack determines the force distribution on the structure that is the mathematical link between the two systems, given a proper translation of the forces between the aerodynamic and the structural mesh. In the current formulation, the transformation is performed using the *nearest neighbor* interpolation, refer to De Breuker et al. (2015). The author's work builds from the existing aeroelastic coupled system from De Breuker et al. (2015) in the attempt to extend the system to include the flight dynamic state variables.

In more generic terms, the angle of attack is a function of the following quantities,

- θ_x, θ_y, θ_z
- $\dot{\theta}_x^s$, $\dot{\theta}_y^s$, $\dot{\theta}_z^s$
- q
- $\dot{\delta}_x$, $\dot{\delta}_y$, $\dot{\delta}_z$
- $\dot{x}$, $\dot{y}$, $\dot{z}$

It is important to remember that when we refer to the element rotation, it is always intended a combined flexible and rigid rotation. The angular velocity, on the other hand, are additive and we can thus treat the two components (structural and rigid) as separate.

Three important remarks will now follow before moving into the details of the coupling equations.

Remark no. 1
The pitch rate q is defined around the y-axis, in the body frame of reference. When calculating its contribution to the local angle of attack, one should only consider the rotation in the direction of the element tangent vector (also local axis of rotation). The same holds for the structural rotation derivatives. Let then $\mathbf{t}$ be the tangent vector with coordinates,

$$\mathbf{t}^T = \begin{bmatrix} t_1 & t_2 & t_3 \end{bmatrix} \tag{6.108}$$

from which we can define the following auxiliary matrices,

$$\mathbf{T}_1 = \begin{bmatrix} (t_1)_1 & 0 & 0 & \dots & 0 \\ 0 & (t_1)_2 & 0 & \dots & 0 \\ \dots & & & & \\ 0 & 0 & 0 & \dots & (t_1)_{N_{el}} \end{bmatrix}_{(N_{el}\times N_{el})} \tag{6.109}$$

$$\mathbf{T}_2 = \begin{bmatrix} (t_2)_1 & 0 & 0 & \dots & 0 \\ 0 & (t_2)_2 & 0 & \dots & 0 \\ \dots & & & & \\ 0 & 0 & 0 & \dots & (t_2)_{N_{el}} \end{bmatrix}_{(N_{el}\times N_{el})} \tag{6.110}$$

$$\mathbf{T}_3 = \begin{bmatrix} (t_3)_1 & 0 & 0 & \dots & 0 \\ 0 & (t_3)_2 & 0 & \dots & 0 \\ \dots & & & & \\ 0 & 0 & 0 & \dots & (t_3)_{N_{el}} \end{bmatrix}_{(N_{el} \times N_{el})} \tag{6.111}$$

If $\boldsymbol{\theta}_x$, $\boldsymbol{\theta}_y$, $\boldsymbol{\theta}_z$ are the x, y and z sturctural rotation on the elements, the components aligned with the rotation axis are,

$$(\boldsymbol{\theta}_x)_t = \mathbf{T}_1 \boldsymbol{\theta}_x \tag{6.112}$$

$$(\boldsymbol{\theta}_y)_t = \mathbf{T}_2 \boldsymbol{\theta}_y \tag{6.113}$$

$$(\boldsymbol{\theta}_z)_t = \mathbf{T}_3 \boldsymbol{\theta}_z \tag{6.114}$$

Analogously, for the pitch rate (which refers to a rotation about the y-axis in the body frame of reference), we define the vector,

$$\mathbf{t}_2 = \begin{bmatrix} (t_2)_1 \\ (t_2)_2 \\ \dots \\ (t_2)_{N_{el}} \end{bmatrix} \tag{6.115}$$

that allows us to write q in the direction of the rotation axis as,

$$\mathbf{q}_t = \mathbf{t}_2 q \tag{6.116}$$

Remark no. 2

The translation rates, in the three axial directions, are essential for the correct determination of the effect of a non-zero plunge rate onto the angle of attack. In this case, the significant contribution is the one in the direction of the element normal vector. In a similar fashion as in the previous case, we define $\mathbf{n}$ as the element normal vector with coordinates,

$$\mathbf{n}^T = [\, n_1 \;\; n_2 \;\; n_3 \,] \tag{6.117}$$

from which we can define the following auxiliary matrices,

$$\mathbf{N}_1 = \begin{bmatrix} (n_1)_1 & 0 & 0 & \dots & 0 \\ 0 & (n_1)_2 & 0 & \dots & 0 \\ \dots & & & & \\ 0 & 0 & 0 & \dots & (n_1)_{N_{el}} \end{bmatrix}_{(N_{el} \times N_{el})} \tag{6.118}$$

$$\mathbf{N}_2 = \begin{bmatrix} (n_2)_1 & 0 & 0 & \dots & 0 \\ 0 & (n_2)_2 & 0 & \dots & 0 \\ \dots & & & & \\ 0 & 0 & 0 & \dots & (n_2)_{N_{el}} \end{bmatrix}_{(N_{el} \times N_{el})} \tag{6.119}$$

$$\mathbf{N}_3 = \begin{bmatrix} (n_3)_1 & 0 & 0 & \dots & 0 \\ 0 & (n_3)_2 & 0 & \dots & 0 \\ \dots & & & & \\ 0 & 0 & 0 & \dots & (n_3)_{N_{el}} \end{bmatrix}_{(N_{el} \times N_{el})} \tag{6.120}$$

If $\boldsymbol{\delta}_x$, $\boldsymbol{\delta}_y$, $\boldsymbol{\delta}_z$ are the x, y and z sturctural deformation of the elements, the components aligned with the normal axis are,

$$(\boldsymbol{\delta}_x)_n = \mathbf{N}_1\boldsymbol{\delta}_x \tag{6.121}$$

$$(\boldsymbol{\delta}_y)_n = \mathbf{N}_2\boldsymbol{\delta}_y \tag{6.122}$$

$$(\boldsymbol{\delta}_z)_n = \mathbf{N}_3\boldsymbol{\delta}_z \tag{6.123}$$

For the rigid translation rates $\dot{x}$, $\dot{y}$, $\dot{z}$, we define the vectors,

$$\mathbf{n}_1 = \begin{bmatrix} (n_1)_1 \\ (n_1)_2 \\ \dots \\ (n_1)_{N_{el}} \end{bmatrix} \tag{6.124}$$

$$\mathbf{n}_2 = \begin{bmatrix} (n_2)_1 \\ (n_2)_2 \\ \dots \\ (n_2)_{N_{el}} \end{bmatrix} \tag{6.125}$$

$$\mathbf{n}_3 = \begin{bmatrix} (n_3)_1 \\ (n_3)_2 \\ \dots \\ (n_3)_{N_{el}} \end{bmatrix} \tag{6.126}$$

that allows us to write the rates in the direction of the rotation axis as,

$$\dot{\boldsymbol{x}}_n = \mathbf{n}_1\dot{x} \tag{6.127}$$

$$\dot{\boldsymbol{y}}_n = \mathbf{n}_2\dot{y} \tag{6.128}$$

$$\dot{\boldsymbol{z}}_n = \mathbf{n}_3\dot{z} \tag{6.129}$$

Remark no. 3
It is always crucial to remember that anglular contributions are not additive. Nevertheless, when dealing with variation of angular contribution with respect to state variables, the partial derivatives can be treated as separate terms. This observation will be useful when writing the angle of attack as a function of the states, with particular regard to the influence of structural deformations and Euler angles.

Remembering that $\boldsymbol{\Theta}$ is a function of,

$$\boldsymbol{\Theta} = f(\theta_x^s, \theta_y^s, \theta_z^s, \phi, \theta, \psi) \tag{6.130}$$

we can linearize its i^{th} term as,

$$\Theta_i \approx \Theta_0 + \frac{\partial\Theta_i}{\partial(\theta_x^s)_i}\delta(\theta_x)_i + \frac{\partial\Theta_i}{\partial(\theta_y^s)_i}\delta(\theta_y)_i + \frac{\partial\Theta_i}{\partial(\theta_z^s)_i}\delta(\theta_z)_i + \frac{\partial\Theta_i}{\partial\phi}\delta\phi + \frac{\partial\Theta_i}{\partial\theta}\delta\theta + \frac{\partial\Theta_i}{\partial\psi}\delta\psi \tag{6.131}$$

By the same logic, we can calculate the variation for each and every element, thus defining the following matrices,

$$(\mathbf{T}_\alpha)_1 = \frac{\partial\Theta_i}{\partial(\theta_x)_j} \tag{6.132}$$

$$(\mathbf{T}_\alpha)_2 = \frac{\partial \Theta_i}{\partial (\theta_y)_j} \tag{6.133}$$

$$(\mathbf{T}_\alpha)_3 = \frac{\partial \Theta_i}{\partial (\theta_z)_j} \tag{6.134}$$

$$(\mathbf{T}_\alpha)_4 = \begin{bmatrix} \frac{\partial \Theta_i}{\partial \phi} & \frac{\partial \Theta_i}{\partial \theta} & \frac{\partial \Theta_i}{\partial \psi} \end{bmatrix} \tag{6.135}$$

The angle of attack as a function of the states

The equation for the angle of attack is to be related to the state vector of the coupled system. By means of transformation matrices between the structural and the aerodynamic mesh, and appropriate boolean matrices [1], the relevant quantities in eq.(6.66) can be written as,

$$\boldsymbol{\Theta}_x = \mathbf{T}_\alpha^1 \mathbf{H}_{\text{SA}} \mathbf{T}_\Theta \boldsymbol{\chi} \tag{6.136}$$

$$\boldsymbol{\Theta}_y = \mathbf{T}_\alpha^2 \mathbf{H}_{\text{SA}} \mathbf{T}_\Theta \boldsymbol{\chi} \tag{6.137}$$

$$\boldsymbol{\Theta}_z = \mathbf{T}_\alpha^3 \mathbf{H}_{\text{SA}} \mathbf{T}_\Theta \boldsymbol{\chi} \tag{6.138}$$

$$\boldsymbol{\Theta} = \mathbf{T}_\alpha^4 \begin{bmatrix} \mathbf{T}_\phi \\ \mathbf{T}_\theta \\ \mathbf{T}_\psi \end{bmatrix} \boldsymbol{\chi} \tag{6.139}$$

$$\dot{\boldsymbol{\Theta}}_x^s = \mathbf{T}_1 \mathbf{H}_{\text{SA}} \mathbf{T}_{\dot{\Theta}_s} \boldsymbol{\chi} \tag{6.140}$$

$$\dot{\boldsymbol{\Theta}}_y^s = \mathbf{T}_2 \mathbf{H}_{\text{SA}} \mathbf{T}_{\dot{\Theta}_s} \boldsymbol{\chi} \tag{6.141}$$

$$\dot{\boldsymbol{\Theta}}_z^s = \mathbf{T}_3 \mathbf{H}_{\text{SA}} \mathbf{T}_{\dot{\Theta}_s} \boldsymbol{\chi} \tag{6.142}$$

$$q = \mathbf{t}_2 \mathbf{T}_q \boldsymbol{\chi} \tag{6.143}$$

$$\dot{\boldsymbol{\delta}}_s = \mathbf{N}_1 \mathbf{H}_{\text{SA}} \mathbf{T}_{\dot{\delta}_s} \boldsymbol{\chi} \tag{6.144}$$

$$\dot{\boldsymbol{\delta}}_s = \mathbf{N}_2 \mathbf{H}_{\text{SA}} \mathbf{T}_{\dot{\delta}_s} \boldsymbol{\chi} \tag{6.145}$$

$$\dot{\boldsymbol{\delta}}_s = \mathbf{N}_3 \mathbf{H}_{\text{SA}} \mathbf{T}_{\dot{\delta}_s} \boldsymbol{\chi} \tag{6.146}$$

$$\dot{x} = \mathbf{n}_1 \mathbf{T}_{\dot{x}} \boldsymbol{\chi} \tag{6.147}$$

$$\dot{y} = \mathbf{n}_2 \mathbf{T}_{\dot{y}} \boldsymbol{\chi} \tag{6.148}$$

$$\dot{z} = \mathbf{n}_3 \mathbf{T}_{\dot{z}} \boldsymbol{\chi} \tag{6.149}$$

[1]The mathematical details of the boolean matrices can be found in Appendix B

The coupling equations

Let us begin recalling the aerodynamic system of equations as illustrated in eq. 5.7,

$$\begin{bmatrix} \dot{\mathbf{\Gamma}}_w \\ \dot{\boldsymbol{\alpha}} \end{bmatrix} = \begin{bmatrix} \mathbf{K}_8 & \mathbf{K}_9 \\ \mathbf{0} & \mathbf{0} \end{bmatrix} \begin{bmatrix} \mathbf{\Gamma}_w \\ \boldsymbol{\alpha} \end{bmatrix} + \begin{bmatrix} \mathbf{0} \\ \mathbf{I} \end{bmatrix} \dot{\boldsymbol{\alpha}}_{\text{air}} \tag{6.150}$$

including all the contributions to the angle of attack, the system becomes,

$$\begin{bmatrix} \dot{\mathbf{\Gamma}}_w \\ \dot{\boldsymbol{\alpha}} \end{bmatrix} = \begin{bmatrix} \mathbf{K}_8 & \mathbf{K}_9 & \mathbf{K}_9\Xi_1 \\ \mathbf{0} & \mathbf{0} & \mathbf{0} \end{bmatrix} \begin{bmatrix} \mathbf{\Gamma}_w \\ \boldsymbol{\alpha} \\ \mathbf{\Theta} \\ \dot{\mathbf{\Theta}}_s \\ q \\ \dot{\boldsymbol{\delta}}_s \\ \dot{x} \\ \dot{y} \\ \dot{z} \end{bmatrix} + \begin{bmatrix} \mathbf{0} \\ \mathbf{I} \end{bmatrix} \dot{\boldsymbol{\alpha}}_{\text{air}} \tag{6.151}$$

where Ξ_1 is a matrix that acts on the contributions to the angle of attack, and it is build based on the three remarks presented before. Details on this matrix can be found in Appendix C. In a more compact notation, the system can be written as,

$$\begin{bmatrix} \dot{\mathbf{\Gamma}}_w \\ \dot{\boldsymbol{\alpha}} \end{bmatrix} = \mathbf{H}_1 \begin{bmatrix} \mathbf{\Gamma}_w \\ \boldsymbol{\alpha} \\ \mathbf{\Theta} \\ \dot{\mathbf{\Theta}}_s \\ q \\ \dot{\boldsymbol{\delta}}_s \\ \dot{x} \\ \dot{y} \\ \dot{z} \end{bmatrix} + \mathbf{H}_7 \dot{\boldsymbol{\alpha}}_{\text{air}} \tag{6.152}$$

The second equation needed at this point is the force equation, again from the aerodynamic model, presented already in eq. 5.8,

$$\mathbf{F}_a = \begin{bmatrix} \mathbf{L}_8 & \mathbf{L}_9 \end{bmatrix} \begin{bmatrix} \mathbf{\Gamma}_w \\ \boldsymbol{\alpha} \end{bmatrix} + \mathbf{L}_7 \dot{\boldsymbol{\alpha}}_{\text{air}} \tag{6.153}$$

that when all contributions to alpha are included becomes,

$$\mathbf{F}_a = \begin{bmatrix} \mathbf{L}_8 & \mathbf{L}_9 & \mathbf{L}_9\Xi_2 \end{bmatrix} \begin{bmatrix} \mathbf{\Gamma}_w \\ \boldsymbol{\alpha} \\ \mathbf{\Theta} \\ \dot{\mathbf{\Theta}}_s \\ q \\ \dot{\boldsymbol{\delta}}_s \\ \dot{x} \\ \dot{y} \\ \dot{z} \end{bmatrix} + \mathbf{H}_3 \begin{bmatrix} \ddot{\boldsymbol{\theta}}_s \\ \dot{q} \\ \ddot{\boldsymbol{\delta}}_s \\ \ddot{x} \\ \ddot{y} \\ \ddot{z} \end{bmatrix} + \mathbf{L}_7 \dot{\boldsymbol{\alpha}}_{\text{air}} \tag{6.154}$$

Extensive details on the matrices Ξ_2 and $\mathbf{H}_3$ are presented in Appendix D. In a similar fashion as in the previous case,

$$\mathbf{F}_a = \mathbf{H}_2 \begin{bmatrix} \mathbf{\Gamma}_w \\ \boldsymbol{\alpha} \\ \mathbf{\Theta} \\ \dot{\mathbf{\Theta}}_s \\ q \\ \dot{\boldsymbol{\delta}}_s \\ \dot{x} \\ \dot{y} \\ \dot{z} \end{bmatrix} + \mathbf{H}_3 \begin{bmatrix} \ddot{\boldsymbol{\theta}}_s \\ \dot{q} \\ \ddot{\boldsymbol{\delta}}_s \\ \ddot{x} \\ \ddot{y} \\ \ddot{z} \end{bmatrix} + \mathbf{L}_7 \dot{\boldsymbol{\alpha}}_{\text{air}} \tag{6.155}$$

Note that the equations are still not an explicit function of the structural and flight dynamic states. Remembering the logic behind the boolean selection matrices, the aerodynamic model can be written as,

$$\begin{bmatrix} \dot{\mathbf{\Gamma}}_w \\ \dot{\boldsymbol{\alpha}} \end{bmatrix} = \mathbf{H}_1 \mathbf{T}_1 \begin{bmatrix} \mathbf{\Gamma}_w \\ \boldsymbol{\alpha} \\ \chi \end{bmatrix} + \mathbf{H}_7 \dot{\boldsymbol{\alpha}}_{\text{air}} \tag{6.156}$$

$$\mathbf{F}_a = \mathbf{H}_2 \mathbf{T}_1 \begin{bmatrix} \mathbf{\Gamma}_w \\ \boldsymbol{\alpha} \\ \chi \end{bmatrix} + \mathbf{H}_3 \mathbf{T}_2 \dot{\chi} + \mathbf{L}_7 \dot{\boldsymbol{\alpha}}_{\text{air}} \tag{6.157}$$

We also observe that the vector,

$$\begin{bmatrix} \mathbf{\Gamma}_w \\ \boldsymbol{\alpha} \\ \chi \end{bmatrix} \tag{6.158}$$

is nothing other than the states of the fully coupled system (that includes aerodynamics, structure and flight dynamics). We will refer to this vector as $\mathbf{X}$.

$$\mathbf{X} = \begin{bmatrix} \mathbf{\Gamma}_w \\ \boldsymbol{\alpha} \\ \chi \end{bmatrix} \tag{6.159}$$

The equations are thus,

$$\begin{bmatrix} \dot{\mathbf{\Gamma}}_w \\ \dot{\boldsymbol{\alpha}} \end{bmatrix} = \mathbf{H}_1 \mathbf{T}_1 \mathbf{X} + \mathbf{H}_7 \dot{\boldsymbol{\alpha}}_{\text{air}} \tag{6.160}$$

$$\mathbf{F}_a = \mathbf{H}_2 \mathbf{T}_1 \mathbf{X} + \mathbf{H}_3 \mathbf{T}_2 \dot{\chi} + \mathbf{L}_7 \dot{\boldsymbol{\alpha}}_{\text{air}} \tag{6.161}$$

The aerodynamic equations are now in the right format to be coupled to the structural system of equations.

From the structural state space in eq. 6.65, we have,

$$\dot{\chi} = \mathbf{A}_s \chi + \mathbf{B}_s \mathbf{F}_s \tag{6.162}$$

Therefore, in order to finalize the coupling, the aerodynamic forces $\mathbf{F}_a$ are to be translated on generalized forces that act along both the structural and flight dynamic degrees of freedom. At this point, we need to refer to the Jacobian matrix of the force vector, mentioned in Sec. 6.3. The nearest neighbor interpolation gives us a tranformation matrix from aerodynamic to structure that allows us to calculate the forces along the structural degrees o freedom as,

$$\mathbf{F}'_s = \mathbf{H}_{\mathrm{AS}}\mathbf{F}_a \tag{6.163}$$

Recalling that the Jacobian of the force vector is given by,

$$(J_f)_{i,j} = \frac{\partial r_i}{\partial \chi_j} \tag{6.164}$$

the force vector becomes,

$$\mathbf{F}_s = \mathbf{J}_f\mathbf{H}_{\mathrm{AS}}\mathbf{F}_a = \mathbf{H}^*_{\mathrm{AS}}\mathbf{F}_a \tag{6.165}$$

It is important to remember that the transformation matrix $\mathbf{H}_{\mathrm{AS}}$ should include the root note (usually clamped) to translate the reaction forces properly along the new state vector.

With the forces properly transformed, the structural state space becomes,

$$\dot{\chi}_s = \mathbf{A}_s\chi + \mathbf{B}_s\,\mathbf{H}^*_{\mathrm{AS}}\,\mathbf{F}_a \tag{6.166}$$

from the force expression in eq. 6.161,

$$\dot{\chi}_s = \mathbf{A}_s\chi + \mathbf{B}_s\,\mathbf{H}^*_{\mathrm{AS}}\left(\mathbf{H}_2\mathbf{T}_1\mathbf{X} + \mathbf{H}_3\mathbf{T}_2\dot{\chi} + \mathbf{L}_7\dot{\boldsymbol{\alpha}}_{\mathrm{air}}\right) \tag{6.167}$$

that can be rearranged as,

$$\left(\mathbf{I} - \mathbf{B}_s\,\mathbf{H}^*_{\mathrm{AS}}\mathbf{H}_3\mathbf{T}_2\right)\dot{\chi} = \left(\mathbf{A}_s\mathbf{T}_3 + \mathbf{B}_s\,\mathbf{H}^*_{\mathrm{AS}}\,\mathbf{H}_2\mathbf{T}_1\right)\mathbf{X} + \mathbf{B}_s\mathbf{H}^*_{\mathrm{AS}}\mathbf{L}_7\dot{\boldsymbol{\alpha}}_{\mathrm{air}} \tag{6.168}$$

that in a more compact format becomes,

$$\mathbf{H}_4\dot{\chi} = \mathbf{H}_5\mathbf{X} + \mathbf{H}_6\dot{\boldsymbol{\alpha}}_{\mathrm{air}} \tag{6.169}$$

with,

$$\mathbf{H}_4 = \mathbf{I} - \mathbf{B}_s\,\mathbf{H}^*_{\mathrm{AS}}\mathbf{H}_3\mathbf{T}_2 \tag{6.170}$$

$$\mathbf{H}_5 = \mathbf{A}_s\mathbf{T}_3 + \mathbf{B}_s\,\mathbf{H}^*_{\mathrm{AS}}\,\mathbf{H}_2\mathbf{T}_1 \tag{6.171}$$

$$\mathbf{H}_6 = \mathbf{B}_s\mathbf{H}^*_{\mathrm{AS}}\mathbf{L}_7 \tag{6.172}$$

note that the extra matrix $\mathbf{T}_3$ is an auxiliary matrix defined such that,

$$\chi = \mathbf{T}_3\mathbf{X} \equiv \begin{bmatrix} \mathbf{0} \\ \mathbf{I} \end{bmatrix}\mathbf{X} \tag{6.173}$$

Picking up from eq. 6.174, and solving for $\dot{\chi}$,

$$\dot{\chi} = \mathbf{H}_4^{-1}\mathbf{H}_5\mathbf{X} + \mathbf{H}_4^{-1}\mathbf{H}_6\dot{\boldsymbol{\alpha}}_{\mathrm{air}} \tag{6.174}$$

and thus,

$$\dot{\mathbf{X}} = \begin{bmatrix} \mathbf{H}_1\mathbf{T}_1 \\ \mathbf{H}_4^{-1}\mathbf{H}_5 \end{bmatrix}\mathbf{X} + \begin{bmatrix} \mathbf{H}_7 \\ \mathbf{H}_4^{-1}\mathbf{H}_6 \end{bmatrix}\dot{\boldsymbol{\alpha}}_{\mathrm{air}} \tag{6.175}$$

which is the state space formulation of the fully coupled system.

7

Numerical Verification

This chapter presents the numerical verification of the mathematical formulation developed for the purposes of the current work.

Two different approaches have been used in selecting benchmark cases. First, similar studies within relevant literature have been replicated to assess the accuracy of the present formulation. Second, test cases have been run on standard software packages that provide a solid reference for verification purposes. ABAQUS FEA® is software package of choice as far as this study is concerned.

The numerical verification encompasses the formulation in all its submodules, namely structural, aerodynamic and flight dynamic module. Five different test cases have been selected. A classic cantilever beam, discussed in Sec. 7.1, and a more complex 3D beam model, known as the *3D cantilever bend* described in Sec. 7.2, see. Crisfield and Jelenic (1999). These first two models already allow a thorough verification of the formulation in all its modules. For the sake of completeness, three more test cases are also used. The HALE aircraft model, Sec. 7.3, used for aeroelastic analyses. In addition to that, a flying-wing and a blended-wing-body configuration have been chosen for further test cases on the flight dynamic module.

7.1. Cantilever Beam Configuration

A cantilever beam model of a wing is used for static and dynamic tests of the formulation. The static test is performed under constant tipload. The dynamic tests are used to verify the linearized dynamic formulation. An equivalent cantilever beam model has been created in ABAQUS FEA® , and the same analyses have been run to generate benchmark results.

The set up as such has been widely used for verification purposes in literature, see Goland (1945), Patil (1999), Su (2008). In the present work, the beam has been discretized with 8 structural elements, thus ensuring fully converged results. Material and geometric properties of the cantilever beam model can be found in Table 7.1.

Table 7.1: Material properties of test beam, Su (2008).

Property	Value	SI Unit
Length	1.00	m
Extensional stiffness	1.00E6	Pa·m^2
Torsional stiffness	8.00E1	N·m^2
Flatwise bending stiffness	5.00E1	N·m^2
Chordwise bending stiffness	1.25E3	N·m^2
Mass density	0.10	kg/m
Rotational inertia (x-axis)	1.30E-4	kg·m
Flatwise bending inertia (y-axis)	5.00E-6	kg·m
Chordwise bending inertia (z-axis)	1.25E-4	kg·m

Figure 7.1: Cantilever beam under constant tipload.

7.1.1. Static Test

The cantilever beam is subject to a constant tip load of 150 N, see Fig. 7.1. A quasi-isotropic composite layup has been adopted. Vertical displacement is shown against the benchmark given in ABAQUS FEA® in Fig. 7.2. Results are in perfect agreement.

7.1.2. Dynamic Response About Undeformed Configuration

The beam model is now subject to a sinusoidal tip load of $30\sin(20t)$ N applied to the undeformed configuration. The dynamic system is solved with adaptive time step in the current formulation. Different time steps have been used in ABAQUS to assess convergence. Results shown in Fig. 7.3.

7.1.3. Dynamic Response About Nonlinear Deformed Configuration

The purpose of this test is to verify the dynamic formulation when linearized about a non linear equilibrium point. Therefore, the cantilever beam is first brought to a non linear range of deformation by applying a static load of 1000 N. Subsequent to that, the non linear equilibrium position is perturbed by applying a sinusoidal tip load of $100\sin(20t)$ N. Results are shown in Fig. 7.4.

As one can observe, the non linear response generated by ABAQUS FEA® shows the presence of damping, that is absent in the prediction by the current formulation. As previously stated, the dynamic system is linear about the non linear deformed configuration. For the linearization process, the present work uses the linear mass matrix of the non linear deformed structure. Therefore, the additional damping and stiffness generated by the non linear mass matrix is not accounted for, thus explaining the absence of damping in the system.

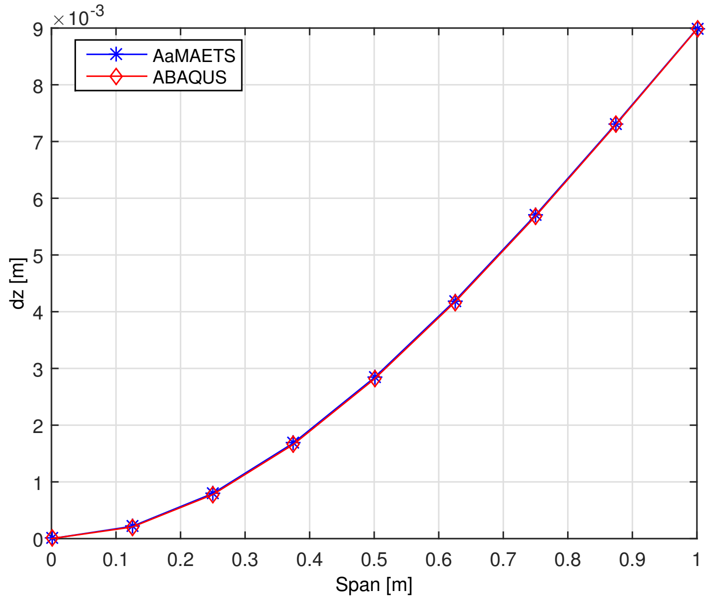

Figure 7.2: Deflection under constant tipload of 150 N.

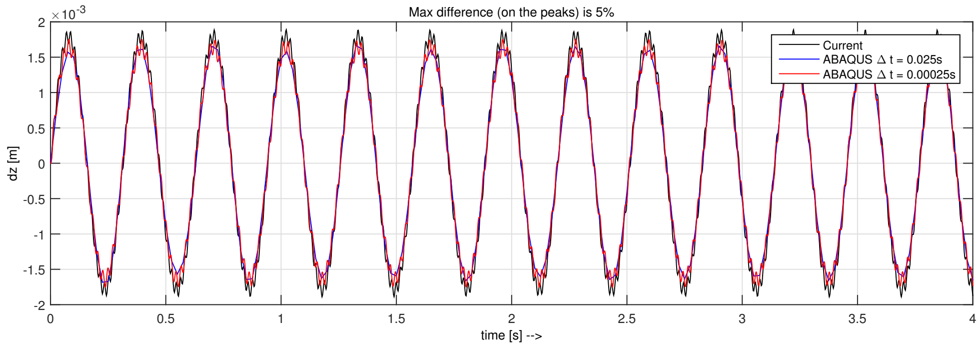

Figure 7.3: Deflection under sinusoidal tipload of $30 \sin 20t$ N.

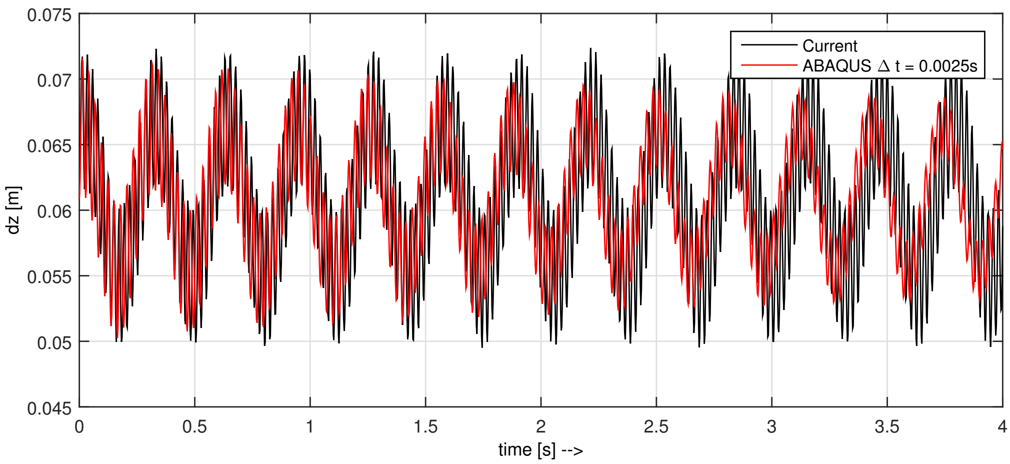

Figure 7.4: Deflection under sinusoidal tipload of $100 \sin 20t$ N applied on a nonlinearly deformed configuration.

Table 7.2: Material properties of the 3D cantilever bend, Crisfield and Jelenic (1999).

Property	Value	SI Unit
EA	1E7	Pa·m^2
GA_2 = GA_3	5E6	Pa·m^2
EI_2 = EI_3	8.33E5	N·m^2

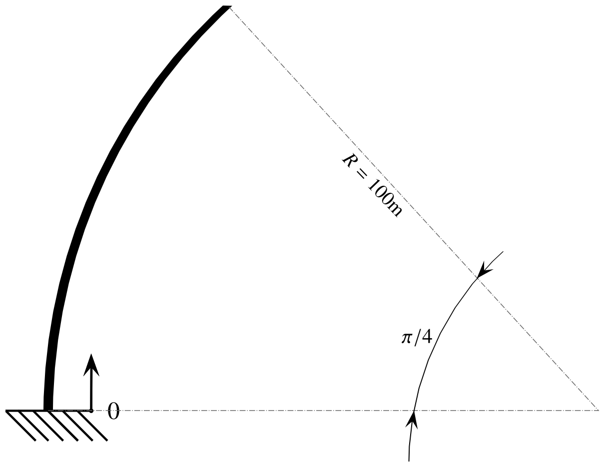

Figure 7.5: Geometrical details of Crisfield beam model.

7.2. 3D Cantilever Bend

The *3D cantilever bend*, as described in Crisfield and Jelenic (1999), is a three-dimensional curved cantilever beam of 100m radius. The details of the geometry and material properties are given in Fig. 7.5 and Tab 7.2 respectively.

In the first test, a sinusoidal tip load has been applied to the structure to study its dynamic response. The purpose of this test is to assess the accuracy of the model and rule out any possible input error to have a reliable verification of the flight dynamic module. An equivalent model is build in ABAQUS FEA® to verify the current formulation against. The dynamic response obtained is illustrated in Fig. 7.6 compared to the benchmark response.

After having verified the input model, the flight dynamic formulation has been tested. In the second test case, a 6 DOF input motion has been prescribed to the root node to test the structural response. The input motion is a periodic function in its most general format,

$$f(t) = A\sin(\omega t + \phi) \tag{7.1}$$

From a mathematical point of view, there is two ways to prescribe the input motion. The first method uses the purely structural system of equations, and it is the solution method adopted in ABAQUS FEA® . The second, instead, uses the fully coupled system including the rigid DOFs, and it is adopted in the current formulation. Both approaches are hereby discussed in details.

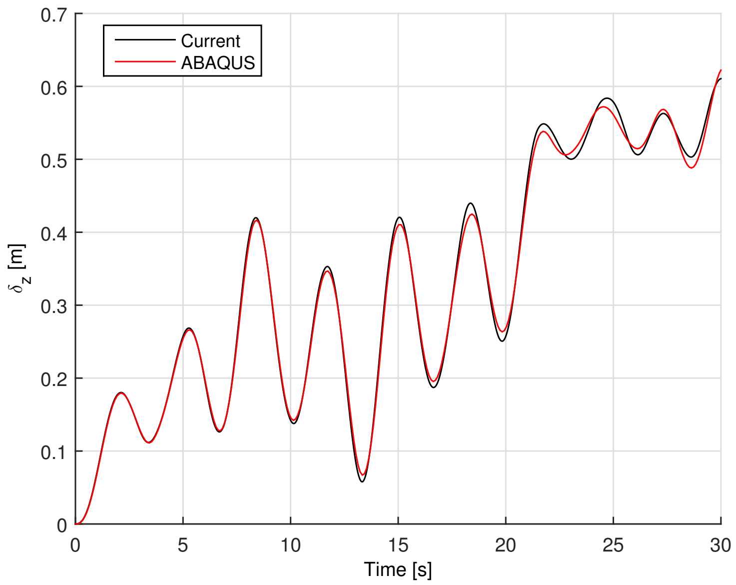

Figure 7.6: Deflection under sinusoidal tipload of $100 \sin 2t$ N.

First solution method

In the first solution method, the input motion prescribes a time-dependent boundary condition of the DOFs of the root node, that are referred to as χ_{11}. From the structural system of equations,

$$\mathbf{M}\ddot{\chi}_S + \mathbf{K}\chi_S = \mathbf{R} \tag{7.2}$$

assuming that the state vector can be split as follows,

$$\chi_S^T = [\chi_{11}, \ \chi'_S] \tag{7.3}$$

with χ'_S being the independent DOFs (not prescribed by the input motion), the full system can be rearranged as,

$$\begin{bmatrix} \mathbf{M}_{11} & \mathbf{M}_{1S} \\ \mathbf{M}_{1S}^T & \mathbf{M}_{SS} \end{bmatrix} \begin{bmatrix} \ddot{\chi}_1 \\ \ddot{\chi}'_S \end{bmatrix} + \begin{bmatrix} \mathbf{K}_{11} & \mathbf{K}_{1S} \\ \mathbf{K}_{1S}^T & \mathbf{K}_{SS} \end{bmatrix} \begin{bmatrix} \chi_1 \\ \chi'_S \end{bmatrix} = \begin{bmatrix} \mathbf{R}_1 \\ \mathbf{R}'_S \end{bmatrix} \tag{7.4}$$

that leads to,

$$\mathbf{M}_{1S}^T\ddot{\chi}_1 + \mathbf{M}_{SS}\ddot{\chi}'_S + \mathbf{K}_{1S}^T\chi_1 + \mathbf{K}_{SS}\chi'_S = \mathbf{R}_S \tag{7.5}$$

Assuming that no external force is acting on the structure, the independent DOFs are solution of the following system of equations,

$$\mathbf{M}_{SS}\ddot{\chi}'_S + \mathbf{K}_{SS}\chi'_S = -\mathbf{M}_{1S}^T\ddot{\chi}_1 - \mathbf{K}_{1S}^T\chi_1 \tag{7.6}$$

It is important to observe that both the input motion and its second derivative contribute to the input function. In presence of damping, there would be a contribution of the first derivative of the input motion.

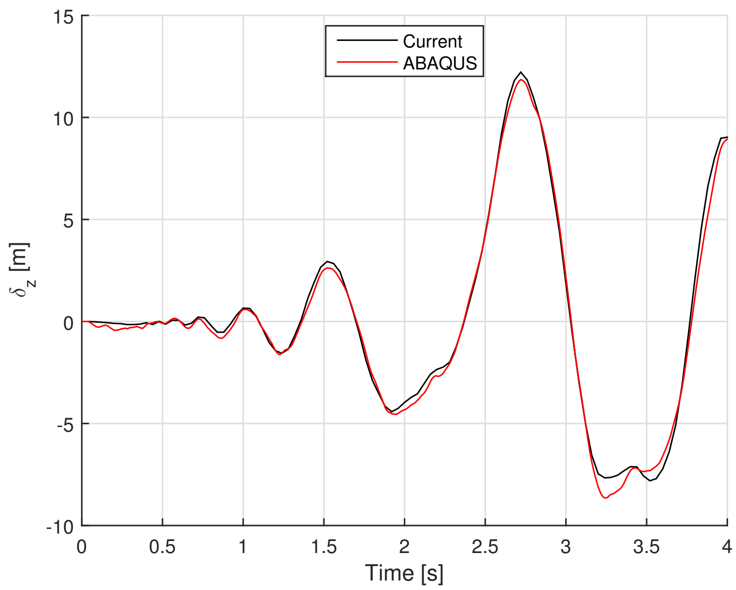

Figure 7.7: Deflection under a 6 DOF input motion applied at the root node.

Second solution method

In the second solution method, the deformation at every node is described by a flexible and rigid DOF. The input motion in this method prescribes the rigid DOFs of the stucture, while the flexible DOFs are the only unknown of the system. From the fully coupled system, that includes the rigid-body degrees of freedom, we have,

$$\mathbf{M}\ddot{\chi} + \mathbf{K}\chi = \mathbf{R} \tag{7.7}$$

can also be used to study the wing response to a flight dynamics input (e.g. sinusoidal pitch motion applied at the root). From eq. 7.7, remembering that the state vector can be decomposed in the structural and flight dynamic degrees of freedom, we have,

$$\begin{bmatrix} \mathbf{M}_{SS} & \mathbf{M}_{SF} \\ \mathbf{M}_{SF}^T & \mathbf{M}_{FF} \end{bmatrix} \begin{bmatrix} \ddot{\chi}_{\text{S}} \\ \ddot{\chi}_{\text{F}} \end{bmatrix} + \begin{bmatrix} \mathbf{K}_{SS} & \mathbf{K}_{SF} \\ \mathbf{K}_{SF}^T & \mathbf{K}_{FF} \end{bmatrix} \begin{bmatrix} \chi_{\text{S}} \\ \chi_{\text{F}} \end{bmatrix} = \begin{bmatrix} \mathbf{R}' \\ \mathbf{R}'' \end{bmatrix} \tag{7.8}$$

where χ_{S} refers to the structural DoFs, defined as,

$$\chi_{\mathbf{S}}^T = \left[\delta_x^1, \ \ \delta_y^1, \ \ \delta_z^1, \theta_x^1, \ \ \theta_y^1, \ \ \theta_z^1, \ \ \ldots \ \ , \ \ \delta_x^N, \ \ \delta_y^N, \ \ \delta_z^N, \theta_x^N, \ \ \theta_y^N, \ \ \theta_z^N \right] \tag{7.9}$$

while $\chi_{\mathbf{F}}$ is,

$$\chi_{\mathbf{F}}^T = [x, \ \ y, \ \ z, \ \ \phi, \ \ \theta, \ \ \psi] \tag{7.10}$$

Considering the first equation of the system in eq. 7.8,

$$\mathbf{M}_{SS}\ddot{\chi}_{\text{S}} + \mathbf{M}_{SF}\ddot{\chi}_{\text{F}} + \mathbf{K}_{SS}\chi_{\text{S}} + \mathbf{K}_{SF}\chi_{\text{F}} = \mathbf{R}' \tag{7.11}$$

that is rearranged as follows,

$$\mathbf{M}_{SS}\ddot{\chi}_{\text{S}} + \mathbf{K}_{SS}\chi_{\text{S}} = \mathbf{R}' - \mathbf{M}_{SF}\ddot{\chi}_{\text{F}} - \mathbf{K}_{SF}\chi_{\text{F}} \tag{7.12}$$

since the terms $\mathbf{M}_{SF}\ddot{\chi}_{\mathrm{F}}$ and $\mathbf{K}_{SF}\chi_{\mathrm{F}}$ are input to the system. If $\mathbf{R} = 0$, that refer to a purely structural analysis, eq. 7.14 describes the wing behaviour under the applied rigid motion. For aeroelastic analysis with prescribed pitching motion, eq. 7.14 is to be coupled with the aerodynamic model to be solved. In case of a pure input motion applied to the structure, with no relative motion with respect to the flow, eq. 7.14 alone suffices to obtain a dynamic analysis of the structure (since $\mathbf{R}' = 0$).

The two approaches are equivalent. We can quickly prove the statement by a simple thought experiment. If we imagine an infinitely stiff structure (perfectly rigid), with the first method the motion applied to the root point would transfer unchanged to all points in the strucure. With the second method, the flexible DOFs would be zero, and the position and orientation of the structure is only dictated by the prescribed input motion.

The structural response due to a 6 DOF input motion is shown in Fig. 7.7. The input motion adopted for this example is the following,

- $x(t) = \sin(30t + 10),\ y(t) = \sin(20t),\ z(t) = \sin(10t)$
- $\phi(t) = \sin(5t),\ \theta(t) = \sin(10t),\ \psi(t) = \sin(5t + 10)$

The results are in good agreement, further validating the statement about the equivalence of the two approaches to the problem.

One final comment before moving to the second phase of the verification. The two mathematical approaches to applying an input motion present only one fine difference. In the first approach, where the input is prescribed as a time-dependent boundary condition on the root node, the system,

$$\mathbf{M}_{SS}\ddot{\chi}'_{\mathrm{S}} + \mathbf{K}_{SS}\chi'_{\mathrm{S}} = -\mathbf{M}_{1S}^{T}\ddot{\chi}_{1} - \mathbf{K}_{1S}^{T}\chi_{1} \tag{7.13}$$

results in a vector χ'_{S} which is a measure for both the structural deformation and the rigid applied motion. On the other hand, in the second approach, the system,

$$\mathbf{M}_{SS}\ddot{\chi}_{\mathrm{S}} + \mathbf{K}_{SS}\chi_{\mathrm{S}} = -\mathbf{M}_{SF}\ddot{\chi}_{\mathrm{F}} - \mathbf{K}_{SF}\chi_{\mathrm{F}} \tag{7.14}$$

separates the two terms, thus it follows,

$$\chi'_{\mathrm{S}} = \chi_{\mathrm{S}} + \chi_{\mathrm{F}} \tag{7.15}$$

Figure 7.8: Example of HALE concept for air recoinnassance, 2005, NOAA and NASA Collaboration.

7.3. Highly Flexible Wing Configuration

The **H**igh-**A**ltitude **L**ong-**E**ndurance vehicles are aircraft concepts developed for a wide range of applications, from environmental sensing to telecommunication, and even air reconnaissance. They feature very slender wings at high aspect ratio, and the main purpose behind the choise is the optimization of the lift/drag ratio. On the other hand, these wings undergo large deformations due to their high level of flexibility, and aeroelastic phenomena become a relevant problem even under conditions that for most aircraft are not reckoned as extreme.

An example of HALE unmanned airvehicle is illustrated in Fig. 7.8. The aircraft was a 2005 NOAA and NASA cooperation called *Altair*. Altair is able to reach altitudes of up to 15 kilometers and stay aloft for more than 20 hours.

In this chapter, aeroelastic analyses are performed on high-aspect-ratio wing, in the HALE aircraft configuration as presented in Patil (1999). In addition to that, the work of Goland (1945) and Su (2008) are used as benchmark for the purposes of this section. The analysis covers natural modes, flutter and divergence prediction.

7.3.1. Wing Geometry

The wing model of choice for the aeroelastic analysis features 32m span, with 1m chord. Sweep and dihedral angle are zero. Further details on the geometry can be found in Fig. 7.9. Additional properties as provided in the work by Patil (1999) are shown in Table 7.4. The wingbox geometry refers to the Goland wing, as presented in the work by Goland (1945). The structural model signifies the standard composite wing model, widely used in literature for benchmark and feasibility studies. Material properties of the Goland wing are presented in Table 7.3.

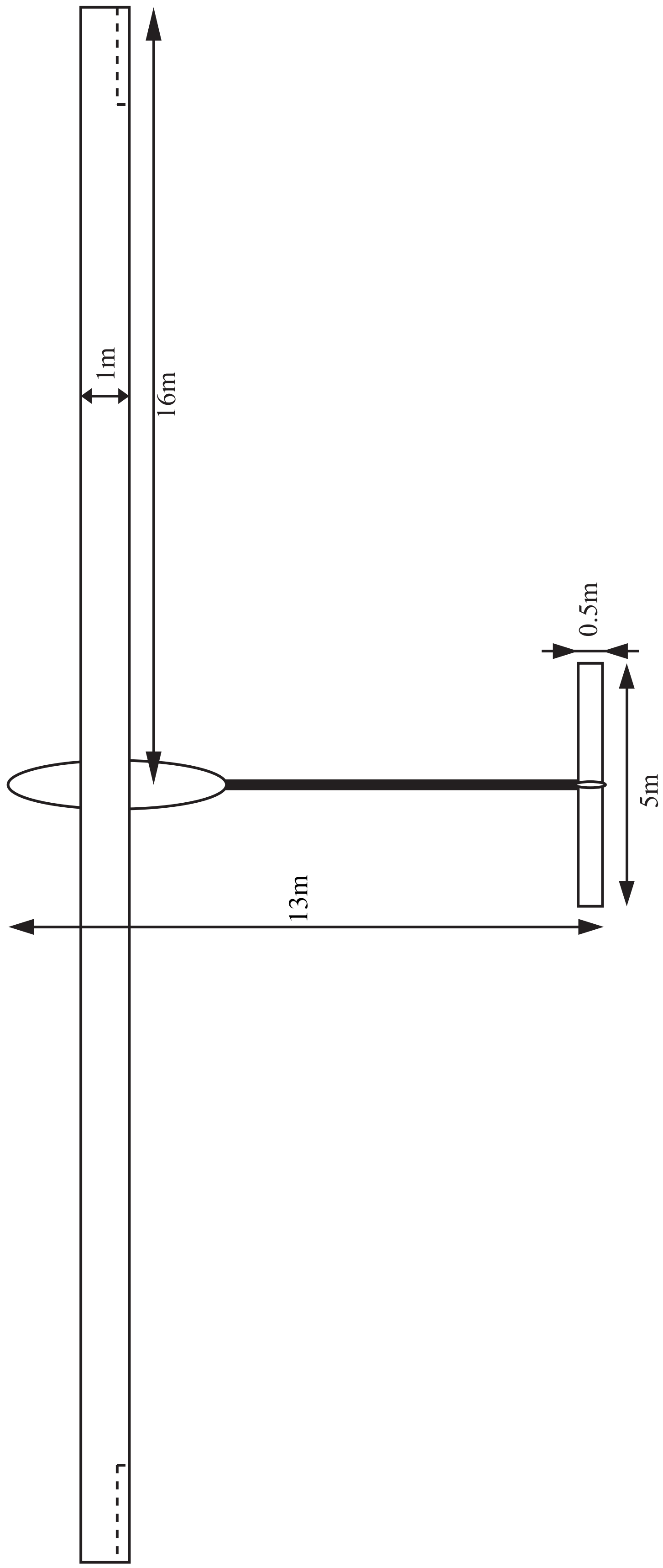

Figure 7.9: Geometrical detail of the HALE aircraft.

Table 7.3: Material properties of the Goland wing, Goland (1945).

Property	Value	SI Unit
E_1	20.6E11	Pa
$E_2 = E_3$	5.17E9	Pa
G_{12}	3.10E9	Pa
$G_{13} = G_{23}$	2.55E9	Pa
$\nu_{12} = \nu_{13} = \nu_{23}$	0.25	-

Table 7.4: Material properties of test HALE configuration, Patil (1999).

Property	Value	SI Unit
Half span	16	m
Chord	1.00	m
Mass per unit length	0.75	kg/m
Moment of inertia (50% chord)	0.1	kg·m
Spanwise elastic axis	0.5	-
Center of gravity	0.5	-
Torsional rigidity	1E4	N·m^2
Flatwise bending rigidity	2E4	N·m^2
Chordwise bending rigidity	4E6	N·m^2

Table 7.5: Natural modes of current formulation compared to reference data.

Mode	Current [rad/s]	Analytical Ref. [rad/s]	Patil (1999) [rad/s]	Su (2008) [rad/s]
1	2.270	2.245	2.247	2.247
2	14.22	14.03	14.60	14.30
3	31.94	31.05	31.15	31.08
4	31.29	31.75	31.74	31.77
5	39.81	39.36	44.01	41.06

Table 7.6: Flutter and divergence predictions compared to reference data.

	Current [m/s]	Brown (2003) [m/s]	Rel. Diff. [%]
Flutter Speed	30.5	32.2	-5.2
Divergence Speed	37.0	37.3	-0.8

7.3.2. Aeroelastic Analysis

The natural modes of the undeformed configuration are shown in Table 7.5, compared to the analytical reference in Brown (2003), and numerical studies carried by Su (2008) and Patil (1999). The analysis has been performed to rule out possible errors coming from input data or the structural module.

Flutter and divergence prediction has been carried at zero angle of attack, at the altitude of 20000m, typical of HALE aircraft. Air density at the given altitude amounts to 0.0899 kg/m^3. Tesults are summarized in Table 7.6. The divergence speed is in excellent agreement, while the flutter speed has been registered with approximately -5% difference.

Despite flutter is predicted at a lower speed, making the current formulation conservative compared to the reference, the frequency shows excellent agreement when the aeroelasticity is evaluated at the reference speed of 32.51 m/s. Frequency predicted by the current formulation is 22.9 rad/s, compared to the 22.37 rad/s in Brown (2003), resulting in only +2.4% relative difference.

Figure 7.10: Example of blended-wing-body aircraft for military purposes, Northrop YB-49.

7.4. Blended-Wing-Body Aircraft

The blended-wing-body is a aircraft concept that features a fixed-wing that gradually blends into a body-structure. The aircraft is designed in such a way that there will be no clear distinction between the wings and fuselage. Others among the classical components of a aircarft are usually not adopted, making the blended-wing-body a challengind design in terms of lateral-directional stability. Historical example of a blended-wing-body aircraft prototype is the Northrop YB-49, designed and manufactured post World War II, see Fig. 7.10.

One of the main advantages of adopting a blended-wing-body concept is the remarkable lift-drag ratio that such a configuration allows. The main reason is that atop of the lift generated by the wings, the contribution of the body (which is airfoil-shaped) is rather significant. And a high lift-drag ratio is directly linked to a lower fuel consumption. The combination of the two advantages has made this aircraft configuration extremely interesting for designers.

Regarding the purposes of this verification study, the blended-wing-body aircraft makes an appropriate test case to verify the mathematical model that couples aeroelasticity and flight-dynamics. The reason for said choice is that the current aeroelastic code runs for a wing-only type of configuration. Fuselage, horizontal and vertical tails, although present as rigid parts in the flight dynamic formulation, are not accounted for in the aeroelastic module. The approach to modeling the blended-wing-body is thus the following. Ideally, the aircraft can be thought of as a wing-only symmetric structure. By applying symmetric boundary conditions at the middle plane, the problem is reduced to a single flying-wing. The wing structure is divided in two main property sections (using a Nastran-like terminology), (*i*) the inboard property (assigned to the body), (*ii*) the outboard properties (assigned to the rest of the wing). Control surfaces are not considered in this study.

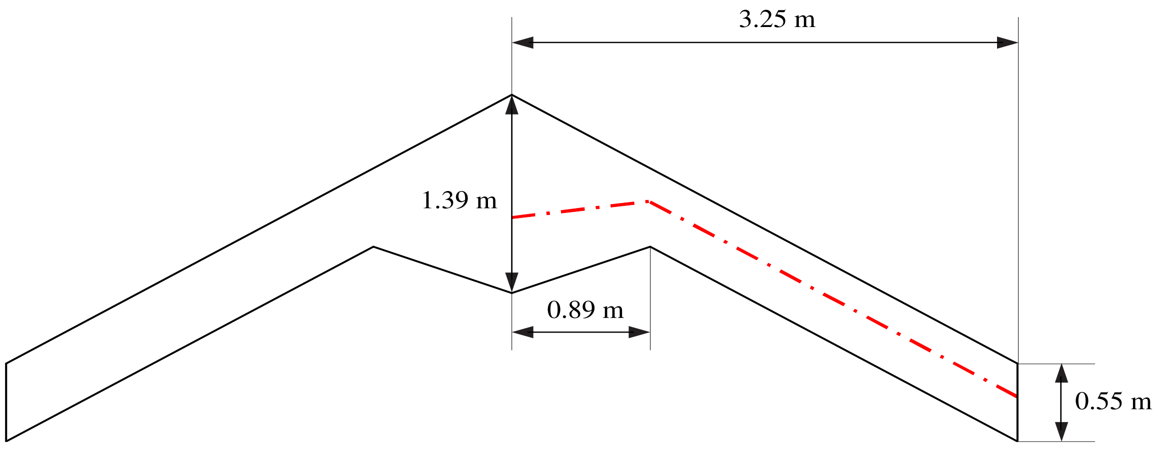

Figure 7.11: Blended-wing-body aircraft. The red dash-dotted line indicates the beam reference axis.

Table 7.7: Body properties of the blended-wing-body aircraft, Cesnik and Su (2010)

Property	Value	SI Unit
Elastic (reference) axis	0.6438/0.4650	-
Center of gravity	0.6438/0.4650	-
Torsional rigidity	2.25E6	N·m^2
Flatwise bending rigidity	7.50E5	N·m^2
Chordwise bending rigidity	3.50E7	N·m^2
Mass per unit length	50.00	kg/m
Rotational inertia (x-axis)	4.50	kg·m
Flat bending inertia (y-axis)	0.70	kg·m
In-plane bending inertia (z-axis)	22.0	kg·m

Table 7.8: Wing properties of the blended-wing-body aircraft, Cesnik and Su (2010)

Property	Value	SI Unit
Elastic (reference) axis	0.4650/0.4650	-
Center of gravity	0.4650/0.4650	-
Torsional rigidity	1.10E4	N·m^2
Flatwise bending rigidity	1.17E4	N·m^2
Chordwise bending rigidity	1.30E5	N·m^2
Mass per unit length	6.20	kg/m
Rotational inertia (x-axis)	5.08E-3	kg·m
Flat bending inertia (y-axis)	5.00E-4	kg·m
In-plane bending inertia (z-axis)	4.63E-3	kg·m

Table 7.9: Flight conditions.

ID	EAS [m/s]	H [m]	Mach [-]	n_z [-]
1	68.0	0	0.20	1.0
2	238	0	0.70	1.0
3	23.5	15000	0.20	1.0
4	82.1	15000	0.70	1.0

7.4.1. Analysis Settings

The aircraft, in both its body and wing, is modeled as a beam, as shown in Fig. 7.11. As discussed in the introduction, the model features two sets of material properties. The properties assigned to the body are in Tab. 7.7, while Tab. 7.8 refers to the wing properties. A concentrated mass of 80 kg is positioned in the middle plane, 0.89m in front of the reference axis. Nine non-structural masses (20 kg each for a total of 180 kg) are then distributed uniformly in spanwise direction. The analysis settings are with reference to the study from Cesnik and Su (2010).

In this study we will focus on flight dynamic stability of the blended-wing-body aircraft. In particular, we will assess stability under two different Mach numbers ($M = 0.2$, $M = 0.7$), and at two different altitude levels ($H = 0\,\mathrm{m}$, $H = 15000\,\mathrm{m}$). The analysis in performed in equivalent airspeed (EAS), thus the air density stays constant at 1.225 kg/m^3. For the sake of completeness, from altitude (H) and Mach number (M), the EAS is given by,

$$EAS = a_0 M \sqrt{\frac{p(H)}{p_0}} \tag{7.16}$$

with $a_0 \approx 340\,\mathrm{m/s}$ being the speed of sound at sea level, $p(H)$ the static pressure at altitude H, and $p_0 = 101325\,\mathrm{Pa}$ the static pressure at sea level. The flight conditions used in this study are summarized in Tab. 7.9.

7.4.2. Flight Dynamic Stability

The current flight dynamic formulation, coupled with the aeroelastic codes De Breuker et al. (2012), allows for the assessment of symmetric modes of a flexible wing structure, namely the short-period and the phugoid. We will now go into some details of both modes.

Short-Period Mode

Short-period modes refer to symmetric modes of motion at a constant speed. The angle of attack and pitch vary periodically during the motion, as well as the velocity vector in its direction only (its magnitude is constant per definition). The mode features oscillation at relatively high frequency and damping. The high damping makes the mode barely noticeable in flight, since it is usually damped in a matter of seconds. This also means that even if a pilot may notice it, it is still diffult of correct the motion due to the short span of time in which it occurs.

Table 7.10: Eigenvalues obtained with current formulation compared to Cesnik and Su (2010).

			M = 0.2		M = 0.7	
	H [m]		Real	Imag	Real	Imag
Phugoid	0	Ref.	-0.00800	0.0330	-0.000100	0.01350
	0	Current	-0.00828	0.0367	-0.000167	0.01354
	15000	Ref.	-0.0331	0.0360	-0.000780	0.01280
	15000	Current	-0.0336	0.0379	-0.000840	0.0131
Short-Period	0	Ref.	-4.39	1.88	-21.00	7.51
	0	Current	-4.43	1.92	-21.34	7.55
	15000	Ref.	-1.47	1.09	-7.08	4.26
	15000	Current	-1.52	1.11	-7.18	4.32

Phugoid Mode
Phugoid mode refers to a symmetric mode of motion at a constant angle of attack, characterized by low frequency and damping. The motion occurs in a longer span of time (if compared to the phugoid), and displays as a periodic plunge and pitch. The low frequency at which the motion occurs can trigger the coupling between aeroelastic modes resulting into instability. It is precisely for this reason that the phugoid is of high interest in stability assessment and aeroelastic phenomena.

The results of the analysis, compared to the reference found in the relevant literature, are summarized in Tab. 7.10. The results are in good agreement, with a better match for the frequencies. Details regarding the mode shapes can be found in Appendix E.

Analysis of Results
Consider the case where the altitude is constant and we vary the Mach number only. With reference to eq. 7.16, a change in Mach number at constant altitude varies the equivalent airspeed. Let us now look at the phugoid mode at sea level altitude,

- at $M = 0.2$, the eigenvalue of the phugoid mode is -0.008828 + 0.03670i, while
- at $M = 0.7$, the eigenvalue of the phugoid mode is -0.000167 + 0.01354i.

This shows that as we increase the Mach number (at constant H), the phugoid shifts towards areas in the real-imaginary plane at lower damping and lower frequencies.

For the short-period mode, the following eigenvalues have been obtained (at sea level),

- at $M = 0.2$, the eigenvalue is -4.43+1.92i, while
- at $M = 0.7$, the eigenvalue is -21.34+7.55i.

The results for the short period suggest the exact opposite trend observed for the phugoid. The mode features higher damping and higher frequency as the Mach increases (at constant H). The same holds if we look at the eigenvalues at $H = 15000\,\text{m}$.

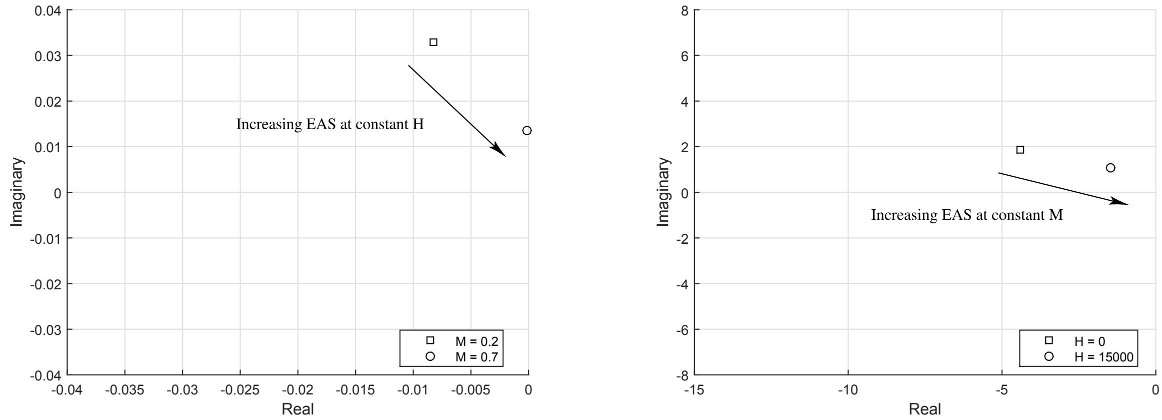

(a) Shift of the phugoid mode.

(b) Shift of the short-period mode.

Figure 7.12: Summary of how the flight dynamic modes change with an increase in EAS.
NOTE: te phugoid shifts due to a change in EAS at constant H, the short-period due to a change in EAS at constant M.

Let us now perform the opposite analysis. We will keep the Mach number constant, and vary the altitude.

If $M = 0.2$, the following is observed for the phugoid mode,

- at $H = 0$, the eigenvalue is -0.00828+0.0367i, while
- at $H = 15000$, the eigenvalue is -0.0336+0.0379i.

The frequency shows little variation resulting from a change in altitude. The damping increases, thus making the mode less dangerous as far as stability is concerned.

For the short-period at $M = 0.2$, results show that,

- at $H = 0$, the eigenvalue is -4.43+1.92i, while
- at $H = 15000$, the eigenvalue is -1.52+1.11i.

We observe that as altitude increases (at constant Mach), the short period lowers both its frequency and damping.

Note that if a mode shifts towards areas at lower damping and lower frequencies, not only is the mode more likely to activate a low-frequency coupling with aeroelastic modes, but it is also moving towards the unstable area. An example is shown in Fig. 7.12. This trend is really important because it allows us to understand which of the mode becomes critical for the low-frequency coupling of a flexible wing in flight. With that in mind, we conclude that,

- a change in equivalent airspeed at constant H, makes the phugoid mode more critical for low-frequency coupling,
- a change in equivalent airspeed at constant M, makes the short-period more likely to trigger the coupling.

Table 7.11: Material properties of test flying-wing configuration, Patil and Hodges (2005).

Property	Value	SI Unit
Elastic (reference) axis	0.25	-
Torsional rigidity	1.65E5	N·m^2
Flatwise bending rigidity	1.03E6	N·m^2
Chordwise bending rigidity	1.24E7	N·m^2
Mass per unit length	8.93	kg/m
Rotational inertia (x-axis)	4.15	kg·m
Flat bending inertia (y-axis)	0.69	kg·m
In-plane bending inertia (z-axis)	3.46	kg·m

Table 7.12: Details of the different settings of the flying-wing configuration, Patil and Hodges (2005).

	Empty	*Heavy*	SI Unit
Pod mass	27.30	22.70	kg
Payload	27.2	254	kg
Thrust	37.11	37.02	N

7.5. Flying-Wing Configuration

In light of what has been shown in the previous study on flight dynamic stability, the flying-wing configuration has been analysed. In particular this test case sheds light on the effect of payload (hence flexibility) on the flight dynamic stability. The connection is rather straight forward. An increase in payload causes an increase in deformation, thus calls for an increase in structural flexibility.

This section discusses some of the relevant properties of the configuration. The phugoid mode is evaluated and compared to benchmark found in related literature. More results on the flying-wing configuration can be investigated in Appendix F.

7.5.1. Properties

The beam equivalent of the flying-wing configuration attempts to reproduce the *Helios* concept developed by NASA in 1999. The wing features a span of about 72.8 m, with a fixed breadth of 2.44 m. The details of the wing configuration are shown in Fig. 7.13. Additional properties are provided in Patil and Hodges (2005) and shown in Table 7.11.

7.5.2. Analysis Settings

Half of the flying-wing configuration is modeled for symmetry reasons. The model thus reduced features two pods. The central pod has a mass of 27.30 kg, while the lateral pod (positioned at 2/3 span) 22.70 kg. The payload can vary from 27.2 kg, referred to as *empty* configuration and 254 kg, as *heavy* configuration. There is a total of 5 propulsive units along the wing span. The thrust per unit is 37.11 N for the *empty* configuration, while 37.02 N for the *heavy*. All details are givens in Table 7.12.

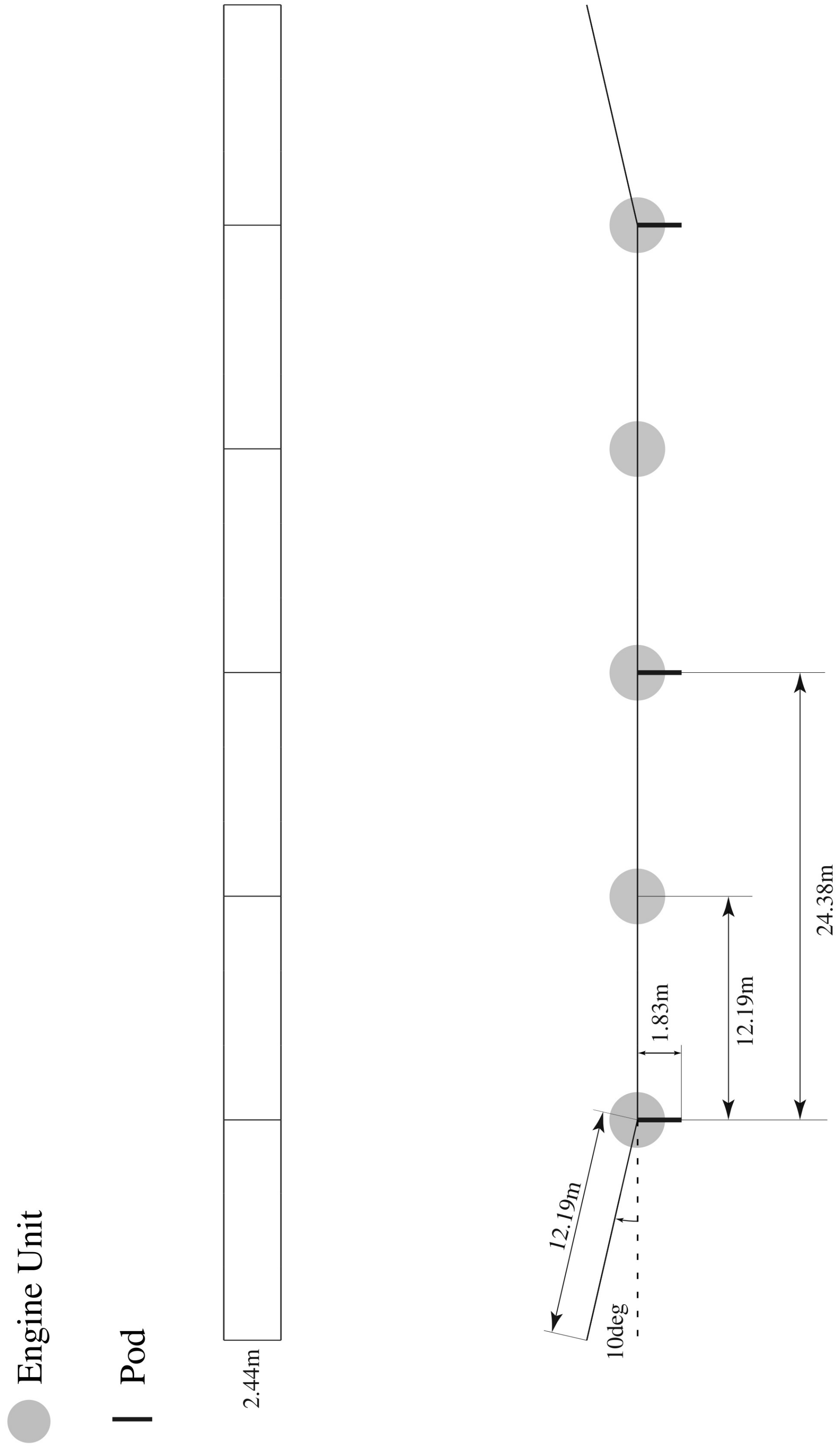

Figure 7.13: Initial undeformed configuration.

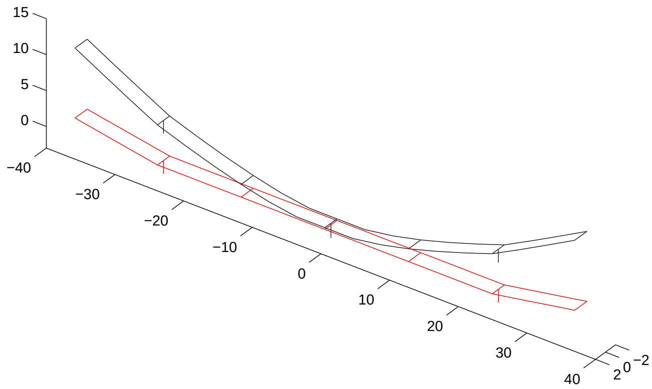

(a) 3D view.

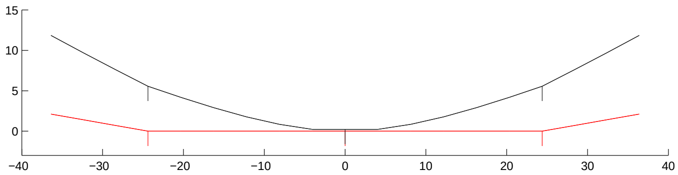

(b) Front view.

Figure 7.14: Elastic deformation of the flying-wing configuration at trim. In red the underformed configuration.

Before assessing flight dynamic stability, the flying-wing is trimmed at the speed of 12.2 m/s in both its empty and heavy configuration. Results of the trim analysis are shown in Fig. 7.14. As one can observe, the empty configuration remains in the linear range of deformation, while the heavy configuration reaches a tip displacement of approx. 30% of the span thus entering the non linear range. In both cases, the flight dynamic stability is assessed linearly about the deformed configuration.

7.5.3. The Phugoid Mode

The eigenvalues of the phugoid mode are shown in Tab. 7.13 for different payload configurations compared to Patil and Hodges (2005). The results show good agreement with the reference study. An interesting phenomenon is observed in this case, a phenomenon that proves the severity of the mode in terms of stability as the payload, thus flexibility, is increased. At maximum payload, the phugoid crosses the imaginary axis into the instable domain. Both modes are illustrated in Fig. 7.15.

Table 7.13: Phugoid mode of flying-wing configuration.

Payload	Current	Patil and Hodges (2005)	Su (2008)
Full	0.1453 + 0.5309i	0.1470 + 0.586i	0.1070 + 0.498i
Empty	-0.1048 + 0.1160i	-0.1.08 + 0.142i	-0.0077 + 0.086i

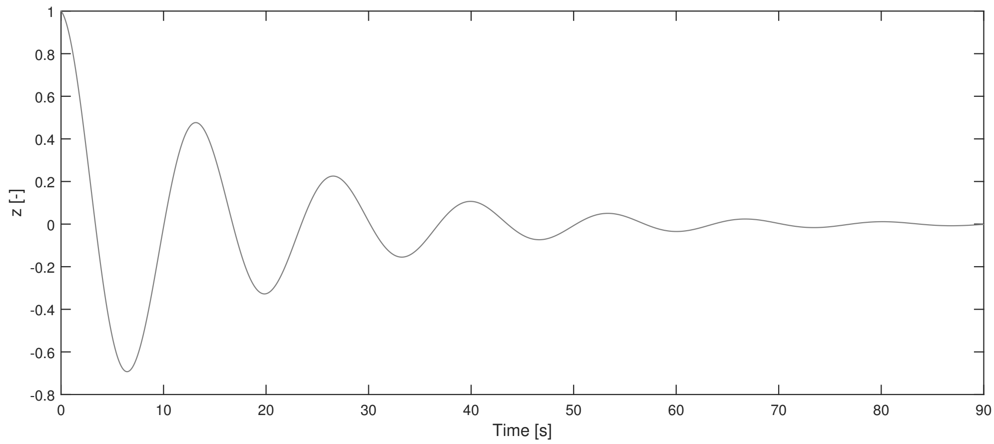

(a) Empty payload.

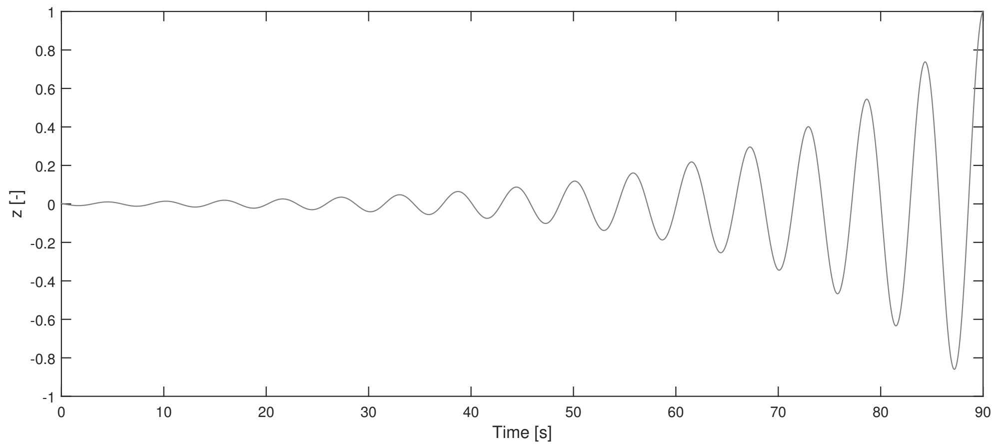

(b) Full payload.

Figure 7.15: Phugoid modes.

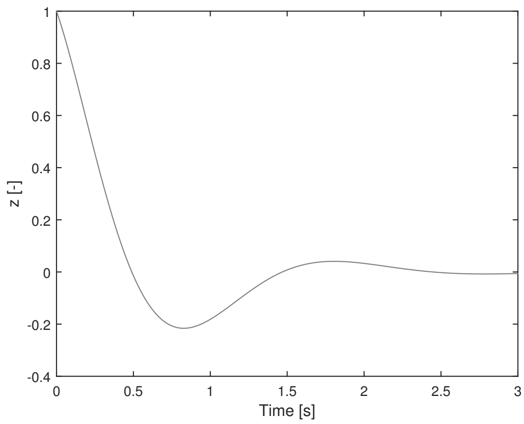

Figure 7.16

Table 7.14: Short-period mode of flying-wing configuration.

Payload	Current	Patil and Hodges (2005)	Su (2008)
Empty	-2.73 + 1.68i	-2.74 + 1.76i	-

7.5.4. The Short-Period Mode

The short period mode has only been found for the configuration at empty payload, as also reported in Patil and Hodges (2005). The eigenvalues corresponding to the mode are shown in Tab. 7.14. It is important to notice that the model at full payload is mainly driven by the unstable phugoid mode. In addition to that, we remember that the wing at full payload reached a significant amount of deformation in trimmed flight. The deformed U-shape of the wing leads to an order of magnitude increase in the pitch moment of inertia (due to non-linear effects), and thus follows a corresponding increase in frequency. As a result of that, the highly flexible wing does not show a classical short period mode in its deformed state, provided it is sufficiently loaded.

8
Conclusions and Future Work

The present work locates within the framework of preliminary design optimization of composite wing structures. The enhanced flexibility of modern structures as a result of the pressing requirements in terms of weight saving, fuel efficiency and increasing payload has made stability, in its broader sense, a crucial concern in structural design and optimization.

A flight dynamic description of an embedded flexible wing has been derived and coupled to the aeroelastic framework developed at the Delft University of Technology by De Breuker et al. (2015).

The flight dynamic module has been verified on the 3D cantilever bend, the blended-wing-body and the flying-wing configuration. In either cases, the current formulation predicts results in the same range of frequencies and damping shown in literature despite the differences in the analysis softwares adopted, lack of data regarding the model, assumptions and analysis settings. Generating an extensive set of benchmark cases would benefit future developments within the present research field.

Two main trends have been observed in flight dynamic stability when studying how the stability evolves with increasing equivalent speed. The phugoid mode shows decreasing damping and frequency with an increase in equivalent speed at constant altitude. A decrease in damping pushes the design dangerously towards the instable zone at positive damping. Moreover, the lower the frequency, the higher the chance of low-frequency coupling with aeroelastic modes, the more recurrent the instabilities. On the other hand, short-period mode shows a similar trend as a result of an increase in equivalent speed at constant Mach number.

Interesting results have been obtained when varying the flexibility of the structure, as in the flying-wing example. The phugoid mode becomes unstable as a result of increasing the flexibility of the structure. The reason for that it to be found in the large displacement the structure undergoes in trimmed conditions at full payload. Under the same conditions, the short period mode has not been found. The relatively high amount of deformation increases the pitch moment of inertia thus suppressing the mode.

As it is the case in research, there is always room for improvement and the present work is not spared. Hereby are some points of improvement in future work,

1. The aeroelastic framework used in current formulation works with a wing-only type of configuration. The next step would be to include the horizontal and vertical tail. The fuselage can still be excluded from the aerodynamics because of its negligible contribution to aerodynamic loads.

2. Aerodynamic control surfaces are to be modeled and included in the aeroelastic framework. With this addition, lateral-directional flight and stability analysis become possible and would significantly extend the potentiality of the framework.

3. With the inclusion of tails and fuselage in the aerodynamic and structural module, the flight dynamic formulation can be extended to fully flexible aircraft. This would have a significant potential in terms of generation of benchmark cases and analysis.

4. The coupled aeroelasticity and flight dynamic system is to be included in the global gradient-based optimization to extend the use of the current formulation to a real-life wing design study. As mentioned at the beginning of this work, including these concerns at preliminary design level is believed to improve the quality of the design, thus ensuring a better initial point in an optimization.

Appendices

A

Details on the Linear EOM

In Sec. 6.4, it has been shown that the velocity ($\mathbf{v}$) and the angular velocity ($\boldsymbol{\omega}$) are a function of both the structural degrees of freedom, indicated by $\boldsymbol{\chi}_s$, and the flight dynamic states, indicated by $\boldsymbol{\chi}_f$. The state vector that includes all DOFS, both structural and rigid will be referred to as $\boldsymbol{\chi}$.

$$\mathbf{v} = f(\boldsymbol{\chi}_s, \boldsymbol{\chi}_f) \tag{A.1}$$

$$\boldsymbol{\omega} = f(\boldsymbol{\chi}_s, \boldsymbol{\chi}_f) \tag{A.2}$$

Let $\mathbf{M}$ be the structural mass matrix, for every point of the wing structure, an auxiliary vector can be defined,

$$\boldsymbol{\xi}^T = [\mathbf{v}(\boldsymbol{\chi}_s, \boldsymbol{\chi}_f), \boldsymbol{\omega}(\boldsymbol{\chi}_s, \boldsymbol{\chi}_f)] \tag{A.3}$$

that allows us to write the kinetic energy as,

$$T = \frac{1}{2}\boldsymbol{\xi}^T \mathbf{M} \boldsymbol{\xi} \tag{A.4}$$

The term (i, j) of the mass matrix is nothing other than the Hessian of the kinetic energy with respect to the first derivative of the state vector, thus,

$$M_{i,j} = \frac{\partial^2 T}{\partial \dot{\chi}_i \partial \dot{\chi}_j} \tag{A.5}$$

From eq. A.4, we have,

$$M_{i,j} = \frac{1}{2} \frac{\partial^2}{\partial \dot{\chi}_i \partial \dot{\chi}_j} \left(\boldsymbol{\xi}^T \mathbf{M} \boldsymbol{\xi}\right) \tag{A.6}$$

that leads to,

$$M_{i,j} = \frac{1}{2} \frac{\partial}{\partial \dot{\chi}_j} \left(\frac{\partial \boldsymbol{\xi}^T}{\partial \dot{\chi}_i} \mathbf{M} \boldsymbol{\xi} + \boldsymbol{\xi}^T \mathbf{M} \frac{\partial \boldsymbol{\xi}}{\partial \dot{\chi}_i}\right) \tag{A.7}$$

and thus,

$$M_{i,j} = \frac{1}{2} \left(\frac{\partial^2 \boldsymbol{\xi}^T}{\partial \dot{\chi}_i \partial \dot{\chi}_j} \mathbf{M} \boldsymbol{\xi} + \frac{\partial \boldsymbol{\xi}^T}{\partial \dot{\chi}_i} \mathbf{M} \frac{\boldsymbol{\xi}}{\partial \dot{\chi}_j} + \frac{\partial \boldsymbol{\xi}^T}{\partial \dot{\chi}_j} \mathbf{M} \frac{\boldsymbol{\xi}}{\partial \dot{\chi}_i} + \boldsymbol{\xi}^T \mathbf{M} \frac{\partial^2 \boldsymbol{\xi}}{\partial \dot{\chi}_i \partial \dot{\chi}_j}\right) \tag{A.8}$$

From the linearized EOM in eq. 6.61, we know that,

$$\left(\frac{\partial \boldsymbol{f}_1^i}{\partial \ddot{\boldsymbol{\chi}}_j}\right)_\delta \ddot{\boldsymbol{\varphi}} + \left(\frac{\partial \boldsymbol{f}_2^i}{\partial \boldsymbol{\chi}_j}\right)_\delta \boldsymbol{\varphi} = \mathbf{R}(\boldsymbol{\varphi}) \tag{A.9}$$

where $\boldsymbol{f}_1$ and $\boldsymbol{f}_2$ are defined as,

$$\boldsymbol{f}_1 = \mathbf{M}\ddot{\boldsymbol{\chi}} \tag{A.10}$$

$$\boldsymbol{f}_2 = \mathbf{K}\boldsymbol{\chi} \tag{A.11}$$

In particular, the jacobian,

$$\left(\frac{\partial \boldsymbol{f}_1^i}{\partial \ddot{\boldsymbol{\chi}}_j}\right)_\delta \tag{A.12}$$

is nothing other than the mass matrix linearized about the deformed configuration δ. From eq. A.8, the generic term of the jacobian can be written as,

$$2M_{i,j}^{\text{lin}} = \frac{\partial}{\partial \ddot{\chi}_k}\left[\left(\frac{\partial^2 \boldsymbol{\xi}^T}{\partial \dot{\chi}_i \partial \dot{\chi}_j}\mathbf{M}\boldsymbol{\xi} + \frac{\partial \boldsymbol{\xi}^T}{\partial \dot{\chi}_i}\mathbf{M}\frac{\boldsymbol{\xi}}{\partial \dot{\chi}_j} + \frac{\partial \boldsymbol{\xi}^T}{\partial \dot{\chi}_j}\mathbf{M}\frac{\boldsymbol{\xi}}{\partial \dot{\chi}_i} + \boldsymbol{\xi}^T\mathbf{M}\frac{\partial^2 \boldsymbol{\xi}}{\partial \dot{\chi}_i \partial \dot{\chi}_j}\right)\ddot{\chi}_k\right] \tag{A.13}$$

if we note that,

$$\frac{\partial^2 \boldsymbol{\xi}^T}{\partial \dot{\chi}_i \partial \dot{\chi}_j}\mathbf{M}\boldsymbol{\xi} = \boldsymbol{\xi}^T\mathbf{M}\frac{\partial^2 \boldsymbol{\xi}}{\partial \dot{\chi}_i \partial \dot{\chi}_j} = 0 \tag{A.14}$$

and,

$$\frac{\partial \boldsymbol{\xi}^T}{\partial \ddot{q}_k} = 0 \tag{A.15}$$

the only non-zero terms of the jacobian are,

$$2M_{i,j}^{\text{lin}} = \frac{\partial \boldsymbol{\xi}^T}{\partial \dot{\chi}_i}\mathbf{M}\frac{\boldsymbol{\xi}}{\partial \dot{\chi}_j}\frac{\partial \ddot{q}_k}{\partial \ddot{q}_k} + \frac{\partial \boldsymbol{\xi}^T}{\partial \dot{\chi}_j}\mathbf{M}\frac{\boldsymbol{\xi}}{\partial \dot{\chi}_i}\frac{\partial \ddot{q}_k}{\partial \ddot{q}_k} \tag{A.16}$$

The last term of the derivative is the Kroenecker operator, that in this particular case is equal to 1, thus,

$$2M_{i,j}^{\text{lin}} = \frac{\partial \boldsymbol{\xi}^T}{\partial \dot{\chi}_i}\mathbf{M}\frac{\boldsymbol{\xi}}{\partial \dot{\chi}_j} + \frac{\partial \boldsymbol{\xi}^T}{\partial \dot{\chi}_j}\mathbf{M}\frac{\boldsymbol{\xi}}{\partial \dot{\chi}_i} \tag{A.17}$$

B

Selection Matrices

In this chapter we will discuss the derivation of the selection matrices $\mathbf{T}_{\boldsymbol{\Theta}}$ and $\mathbf{T}_q$. The reason is that the two matrices are the only that operate on a quantity ($\boldsymbol{\Theta}$ and q) that are functions of the states. The rest of the selection matrices are purely boolean matrices since they operate directly on the state variables.

Selection of the combined rotation $\mathbf{T}_{\boldsymbol{\Theta}}$

In Sec.6.8. we discussed how to derive the angle of attack that results from a combined flexible and rigid rotation $\boldsymbol{\Theta}$. We also remember, as presented in eq. 6.97, that the angle of attack can be calculated as,

$$\alpha = \tan^{-1}\left(\frac{C_y}{C_x}\right) \tag{B.1}$$

The objective is now to write α, that is non-linear in the state variables, in the following format,

$$\alpha = \mathbf{T}_{\boldsymbol{\Theta}}\boldsymbol{\chi} \tag{B.2}$$

with $\boldsymbol{\chi}$ signifying the state vector. By taking the Taylor expansion of the non-linear equation, we have,

$$\alpha = \alpha_0 + \frac{\partial \alpha_i}{\partial \chi_j}\delta\chi_j + o(2) \tag{B.3}$$

recalling that $\alpha_0 = 0$,

$$\alpha = \frac{\partial \alpha_i}{\partial \chi_j}\delta\chi_j \tag{B.4}$$

The Jacobian,

$$J_{i,j} = \frac{\partial \alpha_i}{\partial \chi_j} \equiv (\mathbf{T}_{\boldsymbol{\Theta}})_{i,j} \tag{B.5}$$

is precisely the selection matrix that we were looking for, a matrix that relates the angle of attack to the state vector.

Let us now go into more details of the selection matrix $\mathbf{T}_{\boldsymbol{\Theta}}$.

The variation of α with respect to any of the state variables is given by,

$$d\alpha \approx \frac{1}{1+\left(\frac{C_y}{C_x}\right)^2} \; \frac{dC_yC_x - C_ydC_x}{C_x^2} \tag{B.6}$$

Recalling that $\mathbf{C}$ is nothing other than,

$$\mathbf{C} = \mathbf{R}_B\mathbf{R}^{\mathrm{f}}\mathbf{R}^{\mathrm{r}}\mathbf{C}_0 \tag{B.7}$$

we have,

$$d\mathbf{C} = \mathbf{R}_B d\mathbf{R}^{\mathrm{f}}\mathbf{R}^{\mathrm{r}}\mathbf{C}_0 + \mathbf{R}_B\mathbf{R}^{\mathrm{f}}d\mathbf{R}^{\mathrm{r}}\mathbf{C}_0 \tag{B.8}$$

For the i^{th} element in the structure, the matrix entries are hereby given.

$$\frac{\partial \alpha_i}{\partial \delta_x} = 0 \tag{B.9}$$

$$\frac{\partial \alpha_i}{\partial \delta_y} = 0 \tag{B.10}$$

$$\frac{\partial \alpha_i}{\partial \delta_z} = 0 \tag{B.11}$$

$$\frac{\partial \alpha_i}{\partial \theta_x} = \frac{1}{1+\left(\frac{C_y}{C_x}\right)^2} \; \frac{\left(\mathbf{R}_B\frac{\partial \mathbf{R}^{\mathrm{f}}}{\partial \theta_x}\mathbf{R}^{\mathrm{r}}\mathbf{C}_0\right)_y C_x - C_y\left(\mathbf{R}_B\frac{\partial \mathbf{R}^{\mathrm{f}}}{\partial \theta_x}\mathbf{R}^{\mathrm{r}}\mathbf{C}_0\right)_x}{C_x^2} \tag{B.12}$$

$$\frac{\partial \alpha_i}{\partial \theta_y} = \frac{1}{1+\left(\frac{C_y}{C_x}\right)^2} \; \frac{\left(\mathbf{R}_B\frac{\partial \mathbf{R}^{\mathrm{f}}}{\partial \theta_y}\mathbf{R}^{\mathrm{r}}\mathbf{C}_0\right)_y C_x - C_y\left(\mathbf{R}_B\frac{\partial \mathbf{R}^{\mathrm{f}}}{\partial \theta_y}\mathbf{R}^{\mathrm{r}}\mathbf{C}_0\right)_x}{C_x^2} \tag{B.13}$$

$$\frac{\partial \alpha_i}{\partial \theta_z} = \frac{1}{1+\left(\frac{C_y}{C_x}\right)^2} \; \frac{\left(\mathbf{R}_B\frac{\partial \mathbf{R}^{\mathrm{f}}}{\partial \theta_z}\mathbf{R}^{\mathrm{r}}\mathbf{C}_0\right)_y C_x - C_y\left(\mathbf{R}_B\frac{\partial \mathbf{R}^{\mathrm{f}}}{\partial \theta_z}\mathbf{R}^{\mathrm{r}}\mathbf{C}_0\right)_x}{C_x^2} \tag{B.14}$$

$$\frac{\partial \alpha_i}{\partial \phi} = \frac{1}{1+\left(\frac{C_y}{C_x}\right)^2} \; \frac{\left(\mathbf{R}_B\mathbf{R}^{\mathrm{f}}\frac{\partial \mathbf{R}^{\mathrm{r}}}{\partial \phi}\mathbf{C}_0\right)_y C_x - C_y\left(\mathbf{R}_B\mathbf{R}^{\mathrm{f}}\frac{\partial \mathbf{R}^{\mathrm{r}}}{\partial \phi}\mathbf{C}_0\right)_x}{C_x^2} \tag{B.15}$$

$$\frac{\partial \alpha_i}{\partial \theta} = \frac{1}{1+\left(\frac{C_y}{C_x}\right)^2} \; \frac{\left(\mathbf{R}_B\mathbf{R}^{\mathrm{f}}\frac{\partial \mathbf{R}^{\mathrm{r}}}{\partial \theta}\mathbf{C}_0\right)_y C_x - C_y\left(\mathbf{R}_B\mathbf{R}^{\mathrm{f}}\frac{\partial \mathbf{R}^{\mathrm{r}}}{\partial \theta}\mathbf{C}_0\right)_x}{C_x^2} \tag{B.16}$$

$$\frac{\partial \alpha_i}{\partial \psi} = \frac{1}{1+\left(\frac{C_y}{C_x}\right)^2} \; \frac{\left(\mathbf{R}_B\mathbf{R}^{\mathrm{f}}\frac{\partial \mathbf{R}^{\mathrm{r}}}{\partial \psi}\mathbf{C}_0\right)_y C_x - C_y\left(\mathbf{R}_B\mathbf{R}^{\mathrm{f}}\frac{\partial \mathbf{R}^{\mathrm{r}}}{\partial \psi}\mathbf{C}_0\right)_x}{C_x^2} \tag{B.17}$$

Selection of the combined rotation $\mathbf{T}_q$

With reference to Sec. 5.6., let us recall eq. 6.143 from the mathematical derivation of current formulation,

$$q = \mathbf{t}_2 \mathbf{T}_q \boldsymbol{\chi} \tag{B.18}$$

The equation as such is a linear relationship between the pitch rate q and the DoF of the coupled system, signified by $\boldsymbol{\chi}$. The generalized nonlinear set of equations that defines the aircraft orientation is given,

$$\begin{cases} p = \dot{\phi} - \dot{\psi}\sin\theta \\ q = \dot{\psi}\cos\theta\sin\phi + \dot{\theta}\cos\phi \\ r = \dot{\psi}\cos\theta\cos\phi - \dot{\theta}\sin\phi \end{cases} \tag{B.19}$$

Let $\boldsymbol{\delta}$ be the nonlinear deformed configuration. The set of equation B.19 is now expanded about the deformed configuration,

$$\begin{cases} p = p(\boldsymbol{\delta}) + \left(\dfrac{\partial p}{\partial \phi}\right)_{\boldsymbol{\delta}} \phi + \left(\dfrac{\partial p}{\partial \theta}\right)_{\boldsymbol{\delta}} \theta + \left(\dfrac{\partial p}{\partial \psi}\right)_{\boldsymbol{\delta}} \psi + o(2) \\ q = q(\boldsymbol{\delta}) + \left(\dfrac{\partial q}{\partial \phi}\right)_{\boldsymbol{\delta}} \phi + \left(\dfrac{\partial q}{\partial \theta}\right)_{\boldsymbol{\delta}} \theta + \left(\dfrac{\partial q}{\partial \psi}\right)_{\boldsymbol{\delta}} \psi + o(2) \\ r = r(\boldsymbol{\delta}) + \left(\dfrac{\partial r}{\partial \phi}\right)_{\boldsymbol{\delta}} \phi + \left(\dfrac{\partial r}{\partial \theta}\right)_{\boldsymbol{\delta}} \theta + \left(\dfrac{\partial r}{\partial \psi}\right)_{\boldsymbol{\delta}} \psi + o(2) \end{cases} \tag{B.20}$$

Recalling that $p(\boldsymbol{\delta}) = q(\boldsymbol{\delta}) = r(\boldsymbol{\delta}) = 0$, and neglecting higher order terms in the Taylor expansion, the set of equations becomes,

$$\begin{cases} p \approx \left(\dfrac{\partial p}{\partial \phi}\right)_{\boldsymbol{\delta}} \phi + \left(\dfrac{\partial p}{\partial \theta}\right)_{\boldsymbol{\delta}} \theta + \left(\dfrac{\partial p}{\partial \psi}\right)_{\boldsymbol{\delta}} \psi \\ q \approx \left(\dfrac{\partial q}{\partial \phi}\right)_{\boldsymbol{\delta}} \phi + \left(\dfrac{\partial q}{\partial \theta}\right)_{\boldsymbol{\delta}} \theta + \left(\dfrac{\partial q}{\partial \psi}\right)_{\boldsymbol{\delta}} \psi \\ r \approx \left(\dfrac{\partial r}{\partial \phi}\right)_{\boldsymbol{\delta}} \phi + \left(\dfrac{\partial r}{\partial \theta}\right)_{\boldsymbol{\delta}} \theta + \left(\dfrac{\partial r}{\partial \psi}\right)_{\boldsymbol{\delta}} \psi \end{cases} \tag{B.21}$$

or equivalently, in matrix format,

$$\begin{bmatrix} p \\ q \\ r \end{bmatrix} = \begin{bmatrix} \dfrac{\partial p}{\partial \phi} & \dfrac{\partial p}{\partial \phi} & \dfrac{\partial p}{\partial \phi} \\ \dfrac{\partial q}{\partial \phi} & \dfrac{\partial q}{\partial \phi} & \dfrac{\partial q}{\partial \phi} \\ \dfrac{\partial r}{\partial \phi} & \dfrac{\partial r}{\partial \phi} & \dfrac{\partial r}{\partial \phi} \end{bmatrix}_{\boldsymbol{\delta}} \begin{bmatrix} \phi \\ \theta \\ \psi \end{bmatrix} \tag{B.22}$$

recognizing that the matrix is nothing other than the Jacobian of the angular velocity $\boldsymbol{\omega}$ with respect to the Euler angles,

$$\boldsymbol{\omega} = \mathbf{J}_{\boldsymbol{\delta}} \begin{bmatrix} \phi \\ \theta \\ \psi \end{bmatrix} \tag{B.23}$$

and finally, the system can be written solely as a function of the state $\boldsymbol{\chi}$ as follows,

$$\boldsymbol{\omega} = \begin{bmatrix} \mathbf{0} & \mathbf{0} \\ \mathbf{0} & \mathbf{J}_{\boldsymbol{\delta}} \end{bmatrix} \chi \tag{B.24}$$

The term $\mathbf{T}_q$ is derived from the Jacobian where the partial derivatives in p and r are set to zero,

$$\mathbf{T}_q^0 = \begin{bmatrix} 0 & 0 & 0 \\ \dfrac{\partial q}{\partial \phi} & \dfrac{\partial q}{\partial \phi} & \dfrac{\partial q}{\partial \phi} \\ 0 & 0 & 0 \end{bmatrix}_{\boldsymbol{\delta}} \tag{B.25}$$

and thus,

$$\mathbf{T}_q = \begin{bmatrix} \mathbf{0} & \mathbf{0} \\ \mathbf{0} & \mathbf{T}_q^0 \end{bmatrix} \tag{B.26}$$

The matrix thus built is indeed linear about the nonlinear configuration $\boldsymbol{\delta}$ and is adopted in the derivation of the coupled system in the present formulation.

C
Coupling Terms in the Wake Equation

Hereby the column-wise terms of the matrix Ξ_1 are given.

$$\mathbf{B}_\alpha \mathbf{T}_\alpha^1 \mathbf{H}_{\mathrm{SA}} \tag{C.1}$$

$$\mathbf{B}_\alpha \mathbf{T}_\alpha^2 \mathbf{H}_{\mathrm{SA}} \tag{C.2}$$

$$\mathbf{B}_\alpha \mathbf{T}_\alpha^3 \mathbf{H}_{\mathrm{SA}} \tag{C.3}$$

$$\mathbf{B}_\alpha \mathbf{T}_\alpha^4 \tag{C.4}$$

$$\mathbf{B}_{\mathrm{pitch}} \mathbf{T}_1 \mathbf{H}_{\mathrm{SA}} \tag{C.5}$$

$$\mathbf{B}_{\mathrm{pitch}} \mathbf{T}_2 \mathbf{H}_{\mathrm{SA}} \tag{C.6}$$

$$\mathbf{B}_{\mathrm{pitch}} \mathbf{T}_3 \mathbf{H}_{\mathrm{SA}} \tag{C.7}$$

$$\mathbf{B}_{\mathrm{pitch}} \mathbf{t}_2 \tag{C.8}$$

$$-\frac{1}{V_\infty} \mathbf{B}_\alpha \mathbf{N}_1 \mathbf{H}_{\mathrm{SA}} \tag{C.9}$$

$$-\frac{1}{V_\infty} \mathbf{B}_\alpha \mathbf{N}_2 \mathbf{H}_{\mathrm{SA}} \tag{C.10}$$

$$-\frac{1}{V_\infty} \mathbf{B}_\alpha \mathbf{N}_3 \mathbf{H}_{\mathrm{SA}} \tag{C.11}$$

$$-\frac{1}{V_\infty} \mathbf{B}_\alpha \mathbf{n}_1 \tag{C.12}$$

$$-\frac{1}{V_\infty} \mathbf{B}_\alpha \mathbf{n}_2 \tag{C.13}$$

$$-\frac{1}{V_\infty} \mathbf{B}_\alpha \mathbf{n}_3 \tag{C.14}$$

D

Coupling Terms in the Aerodynamic Force Equation

Hereby the column-wise terms of the matrix Ξ_2 are given.

$$\mathbf{L}_9 \mathbf{B}_\alpha \mathbf{T}_\alpha^1 \mathbf{H}_{\text{SA}} \tag{D.1}$$

$$\mathbf{L}_9 \mathbf{B}_\alpha \mathbf{T}_\alpha^2 \mathbf{H}_{\text{SA}} \tag{D.2}$$

$$\mathbf{L}_9 \mathbf{B}_\alpha \mathbf{T}_\alpha^3 \mathbf{H}_{\text{SA}} \tag{D.3}$$

$$\mathbf{L}_9 \mathbf{B}_\alpha \mathbf{T}_\alpha^4 \tag{D.4}$$

$$\left(\mathbf{L}_9 \mathbf{B}_{\text{pitch}} + \mathbf{L}_7 \mathbf{B}_\alpha\right) \mathbf{T}_1 \mathbf{H}_{\text{SA}} \tag{D.5}$$

$$\left(\mathbf{L}_9 \mathbf{B}_{\text{pitch}} + \mathbf{L}_7 \mathbf{B}_\alpha\right) \mathbf{T}_2 \mathbf{H}_{\text{SA}} \tag{D.6}$$

$$\left(\mathbf{L}_9 \mathbf{B}_{\text{pitch}} + \mathbf{L}_7 \mathbf{B}_\alpha\right) \mathbf{T}_3 \mathbf{H}_{\text{SA}} \tag{D.7}$$

$$\left(\mathbf{L}_9 \mathbf{B}_{\text{pitch}} + \mathbf{L}_7 \mathbf{B}_\alpha\right) \mathbf{t}_2 \tag{D.8}$$

$$-\frac{1}{V_\infty} \mathbf{L}_9 \mathbf{B}_\alpha \mathbf{N}_1 \mathbf{H}_{\text{SA}} \tag{D.9}$$

$$-\frac{1}{V_\infty} \mathbf{L}_9 \mathbf{B}_\alpha \mathbf{N}_2 \mathbf{H}_{\text{SA}} \tag{D.10}$$

$$-\frac{1}{V_\infty} \mathbf{L}_9 \mathbf{B}_\alpha \mathbf{N}_3 \mathbf{H}_{\text{SA}} \tag{D.11}$$

$$-\frac{1}{V_\infty} \mathbf{L}_9 \mathbf{B}_\alpha \mathbf{n}_1 \tag{D.12}$$

$$-\frac{1}{V_\infty} \mathbf{L}_9 \mathbf{B}_\alpha \mathbf{n}_2 \tag{D.13}$$

$$-\frac{1}{V_\infty} \mathbf{L}_9 \mathbf{B}_\alpha \mathbf{n}_3 \tag{D.14}$$

The column-wise terms of the matrix $\mathbf{H}_3$ are given.

$$\mathbf{L}_7\mathbf{B}_{\text{pitch}}\mathbf{T}_1\mathbf{H}_{\text{SA}} \tag{D.15}$$

$$\mathbf{L}_7\mathbf{B}_{\text{pitch}}\mathbf{T}_2\mathbf{H}_{\text{SA}} \tag{D.16}$$

$$\mathbf{L}_7\mathbf{B}_{\text{pitch}}\mathbf{T}_3\mathbf{H}_{\text{SA}} \tag{D.17}$$

$$\mathbf{L}_7\mathbf{B}_{\text{pitch}}\mathbf{t}_2\mathbf{H}_{\text{SA}} \tag{D.18}$$

$$-\frac{1}{V_\infty}\mathbf{L}_7\mathbf{B}_\alpha\mathbf{N}_1\mathbf{H}_{\text{SA}} \tag{D.19}$$

$$-\frac{1}{V_\infty}\mathbf{L}_7\mathbf{B}_\alpha\mathbf{N}_2\mathbf{H}_{\text{SA}} \tag{D.20}$$

$$-\frac{1}{V_\infty}\mathbf{L}_7\mathbf{B}_\alpha\mathbf{N}_3\mathbf{H}_{\text{SA}} \tag{D.21}$$

$$-\frac{1}{V_\infty}\mathbf{L}_7\mathbf{B}_\alpha\mathbf{n}_1 \tag{D.22}$$

$$-\frac{1}{V_\infty}\mathbf{L}_7\mathbf{B}_\alpha\mathbf{n}_2 \tag{D.23}$$

$$-\frac{1}{V_\infty}\mathbf{L}_7\mathbf{B}_\alpha\mathbf{n}_3 \tag{D.24}$$

E

Blended-Wing-Body Aircraft

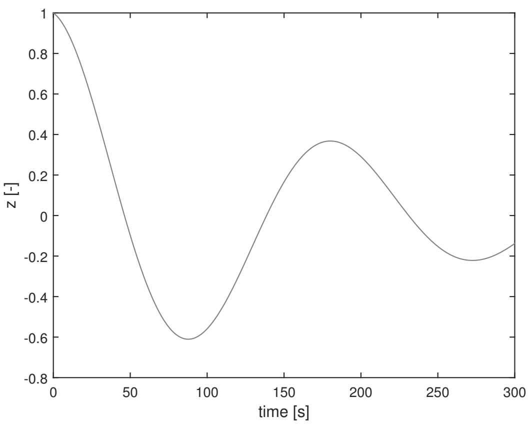

(a) $M = 0.2$ at sea level.

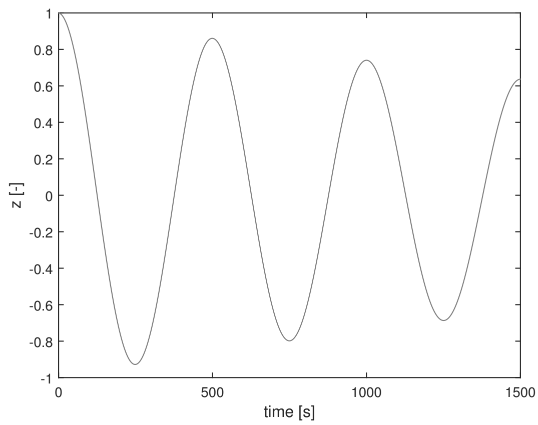

(b) $M = 0.7$ at sea level.

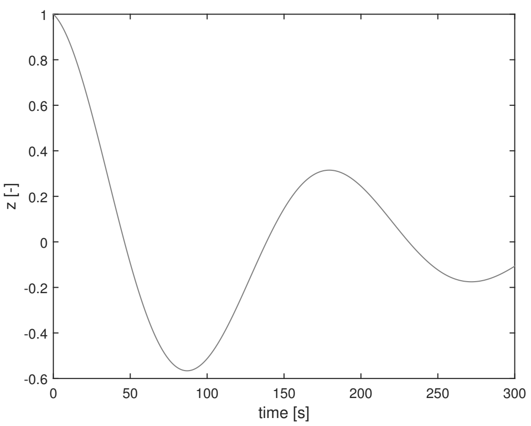

(c) $M = 0.2$ at $H = 15000\,\mathrm{m}$.

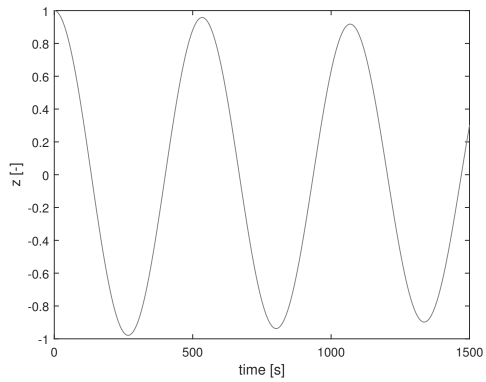

(d) $M = 0.7$ at $H = 15000\,\mathrm{m}$.

Figure E.1: Phugoid modes.

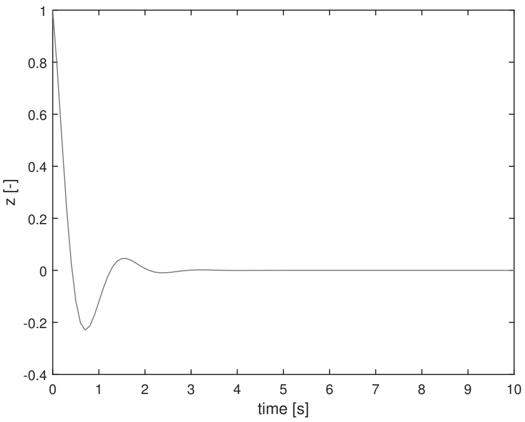

(a) $M = 0.2$ at sea level.

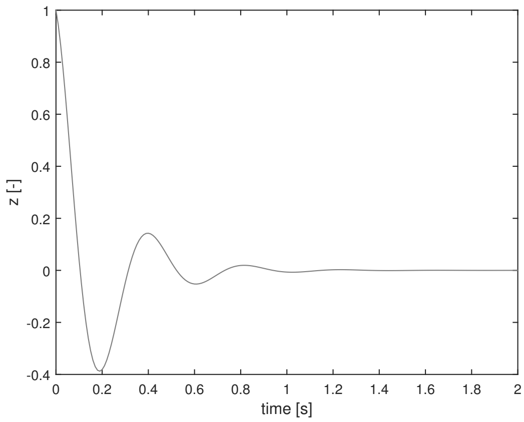

(b) $M = 0.7$ at sea level.

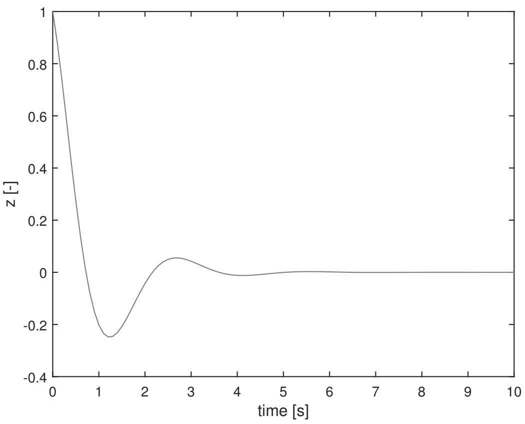

(c) $M = 0.2$ at $H = 15000\,\mathrm{m}$.

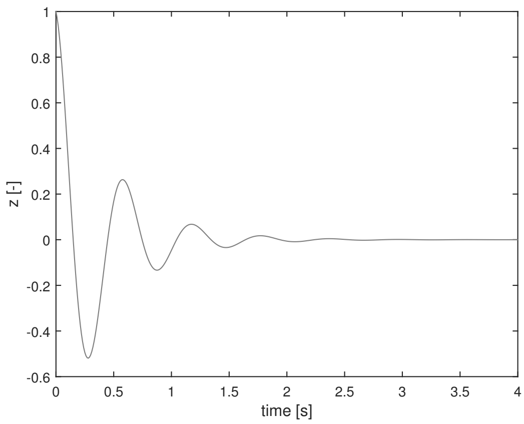

(d) $M = 0.7$ at $H = 15000\,\mathrm{m}$.

Figure E.2: Short-period modes.

F

Flying-wing Configuration

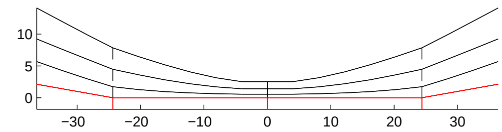

(a) Vertical displacement at 0, $T/8$, $3T/8$, $T/4$.

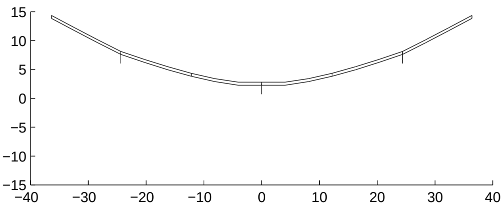

(b) Maximum vertical elevation during the short-period oscillation at $T/4$.

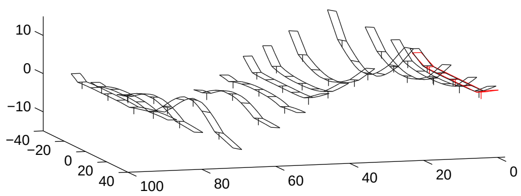

(c) 3D view.

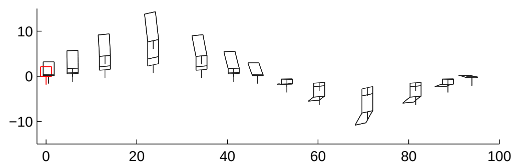

(d) Lateral view.

Figure F.1: Short-period oscillation. In red the initial undeformed configuration.

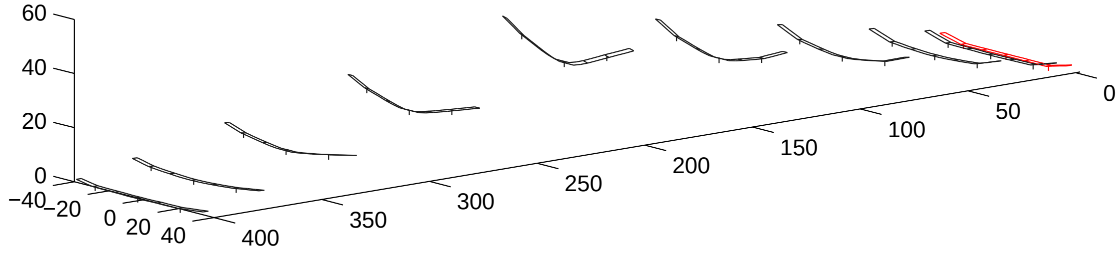

(a) 3D view. Frames are captured every ($\Delta t = 10$ s).

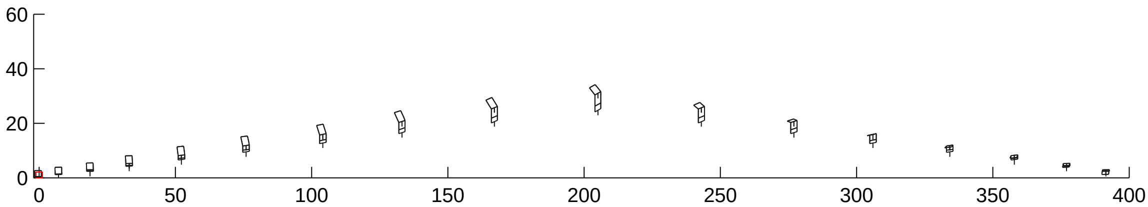

(b) Lateral view ($\Delta t = 5$ s).

Figure F.2: Phugoid oscillation. In red the initial undeformed configuration.

Bibliography

Battini, J. M. and Pacoste, C. (2002). Co-rotational beam elements with warping effects in instability problems. *Computational Methods in Applied Mechanical Engineering, 191 (2002), 1755-1789.*

Birkoff, G. and MacLane, S. (1996). A survey of modern algebra. *Wellesley, MA.*

Brown, L. (2003). Integrated strain actuation in aircraft with highly flexible composite wings. *Ph.D. Dissertation, Massachusetts Institute of Technology, Cambridge, MA, Feb. 2003.*

Cesnik, C. and Brown, L. (2002). Modeling of high aspect ratio active flexible wings for roll control. *43rd AIAA/ASME/ASCE/AHS/ASC Structures, Structural Dynamics, and Materials Conference, Denver, CO, Apr. 22-25, 2002.*

Cesnik, C., Patil, M., and Hodges, D. (1996). Aeroelastic analysis of composite wings. *Proceedings of the 37th Structures, Structural Dynamics, and Material Conference, Salt Lake City, UT, April 18-19, 1996, pp. 1113-1123.*

Cesnik, C., Patil, M., and Hodges, D. (2000). Nonlinear aeroelastic analysis of complete aircraft in subsonic flow. *Journal of Aircraft, Vol.37, 2000, No. 5, pp. 753-760.*

Cesnik, C., Patil, M., and Hodges, D. (2001). Nonlinear aeroelasticity and flight dynamics of high-altitude long endurance aircraft. *Journal of Aircraft, Vol.38, 2001, No. 1, pp. 88-94.*

Cesnik, C. and Shearer, M. (2005). Nonlinear flight dynamics of very flexible aircraft. *AIAA Atmospheric Flight Mechanics Conference and Exhibit, Aug. 15-18, 2005, San Francisco, CA.*

Cesnik, C. and Su, W. (2005a). Nonlinear aeroelastic modeling and analysis of fully flexible aircraft. *AIAA-2005-1945, 46th AIAA/ASME/ASCE/AHS/ASC Structures, Structural Dynamics, and Materials Conference, Austin, TX, Apr. 18-21, 2005.*

Cesnik, C. and Su, W. (2005b). Nonlinear aeroelastic modeling and analysis of fully flexible aircraft. *46^{th} AIAA/ASME/ASCE/AHS/ASC Structures, Structural Dynamics, and Material Conference, AIAA 2005-2169, Austin, TX, USA, April 2005.*

Cesnik, C. and Su, W. (2009). Nonlinear aeroelasticity of a very flexible blended-wing-body aircraft. *50^{th} AIAA/ASME/ASCE/AHS/ASC Structures, Structural Dynamics, and Material Conference, AIAA 2009-2402, Palm Springs, CA, USA, May 2009.*

Cesnik, C. and Su, W. (2011). Dynamic response og highly flexible flying wings. *AIAA Journal, 49(2): 324-339, Feb. 2011. doi: 10.2514/1.J050496.*

Chang, C., Hodges, D., and Patil, M. (2008). Flight dynamics of highly flexible aircraft. *Journal of Aircraft, Vol.45, 2008, No. 2, pp. 538-545.*

Chen, L. W. and Chern, H. K. (1993). The vibrations of pre-twisted rotating beams of general orthotropy. *Journal of Sound and Vibration, 167(3): 529-539.*

Crisfield, M. and Jelenic, G. (1999). Geometrically exact 3d beam theory: implementation of a strin-invariant finite element for statics and dynamics. *Comput. Methods Appl. Mech. Engrg. 171, 141-171.*

D. A. Peters, M. A. H. and Torrero, A. (2006). State-space airloads theory for flexible airfoils. *Annual Forum of the American Helicopter Society, Phoenix, AZ, USA, 2006.*

Dowell, E., Edwards, J., and Strganac, T. (2003). Nonlinear aeroelasticity. *44th AIAA/ASME/ASCE/AHS Structures, Structural Dynamics and Materials Conference, Norfolk, VA, Apr. 7-10, 2003.*

Drela, M. (1999). Integrated simulation model for preliminary aerodynamic, structural, and control-law design of aircraft. *Proceedings of the 40th Structures, Structural Dynamics, and materials Conference, Saint Louis, MO, April 12-15, 1999, pp. 1644-1656.*

Drela, M. (2012). Aswing 5.81 technical description, 2008. *http://web.mit.edu/drela/Public/web/aswing/, Last revision in 2012.*

Goland, M. (1945). The flutter of a uniform cantilever beam. *Journal of Aircraft Mechanics, Vol. 12, No. 4, December 1945, pp. A197 - A208.*

Gurdal, Z., Haftka, R., and Hajela, P. (1999). Design and optimization of laminated composite materials. *John Wiley and Sons, Inc.*

Hammer, V., Bendsoe, M., and Pedersem, P. (1998). Parametrization in laminate design for optimal compliance. *International Journal of Solids and Structures, 34(4): 415-434.*

Livne, E. and Weishaar, T. (2003). Aeroelasticity of nonconventional airplane configurations - past and future. *Journal of Aircraft, Vol.40, 2003, No. 6, pp. 1047-1065.*

Lockyer, A., Drake, A., Bartley-Cho, J., Vartio, E., Solomon, D., and Shimko, T. (2005). High lift over drag active (hilda) wing. *Northrop Grumman Corp., Rept. AFRL-VA-WP.TR 2005-3066.*

Meirovitch, L. and Tuzcu, I. (2007). The lure of the mean axes. *Journal of Applied Mechanics, 74: 497-504, May 2007. doi: 10.1115/1.2338060.*

Milne, R. D. (1962). Dynamics of the deformable aeroplane, parts i and ii. *Aeronautical Research Council Reports and Memoranda, No. 3345, 1962.*

Murua, J. (2012). Flexible aircraft dynamics with a geometrically-nonlinear description of the unsteady aerodynamics. *Ph.D. Dissertation, Imperial College, London, United Kingdom, May 2012.*

Newman, B. and Schmidt, D. (1991). Numerical and literal aeroelastic-vehicle-model reduction for feedback control synthesis. *Journal of Guidance, Control and Dynamics, Vol. 14, No. 5, Sep.-Oct. 1991, pp. 943-953.*

Nguyen, N., Trinh, K., Nguyen, D., and Tuzcu, I. (2012). Nonlinear aeroelasticity of a flexible wing structure coupled with aircraft flight dynamics. *53rd AIAA Structures, Structural Dynamics and Materials Conference, Apr. 23-26, 2012, Honolulu, Hawaii.*

Nguyen, N. and Tuzcu, I. (2012). Flight dynamics of flexible aircraft with aeroelastic and inertia forces interaction. *53rd AIAA Structures, Structural Dynamics and Materials Conference, Apr. 23-26, 2012, Honolulu, Hawaii.*

Palacios, R. and Cesnik, C. (2005). Static nonlinear aeroelasticity of flexible slender wings in compressible flow. *AIAA-2005-1945, 46th AIAA/ASME/ASCE/AHS/ASC Structures, Structural Dynamics, and Materials Conference, Austin, TX, Apr. 18-21, 2005.*

Patil, M. (1997). Aeroelastic tailoring of composite box beams. *Proceedings of the 35th Aerospace Sciences Meeting and Exhibit, Reno, NV, Jan. 1997.*

Patil, M. (1999). Nonlinear aeroelastic analysis, flight dynamics, and control of a complete aircraft. *PhD Thesis, Georgia Institute of Technology, May, 1999, Atlanta, GA.*

Patil, M. J. and Hodges, D. H. (2005). Flight dynamics of highly flexible flying wings. *International Forum on Aeroelasticity and Structural Dynamics, Munich, Germany, Jun. 28 - Jul. 1, 2005.*

Pendaries, C. (1999). From the hale gnopter to the ornithopter - or how to take advantage of aircraft flexibility. *Proceedings of the 21st Congress of the International Council of the Aeronautical Sciences, Melbourne, Australia, Sept. 13-18, 1998, A98-31715.*

Sabuncu, M. and Evran, K. (2006). Dynamic stability of a rotating pre-twisted asymmetric corss-section timoshenko beam subject to an axial periodic force. *International Journal of Mechanical Sciences, 48: 579-590.*

Shabana, A. A. (1997). Flexible multibody dynamics: Review of past and recent developments. *Multibody System Dynamics, 1(2): 189-222, June 1997, doi: 10.1023/A:1009773505418.*

Shearer, C. (2006). Flight dynamics, aeroelasticity and control of very flexible aircraft. *Ph.D. Dissertation, The University of Michigan, Ann Arbor, MI, Aug. 2006.*

Shirk, M., Hertz, T., and Weisshaar, T. (1986). Aeroelastic tailoring - theory, practice, promise. *Journal of Aircraft, Vol. 23, 1986, No. 1, pp. 6-18.*

Su, W. (2008). Coupld nonlinear aeroelasticity and flight dynamics of fully flexible aircraft. *PhD Thesis, The University of Michigan, 2008, Ann Arbor, MI.*

Svanberg, K. (2002). A class of globally convergent optimization methods based on conservative convex separable approximations. *SIAM Journal on Optimization, Vol. 12, No. 2, 2002, pp. 555-573.*

VanSchoor, M. and VonFlotow, A. (1990). Aeroelastic characteristics of a highly flexible aircraft. *Journal of Aircraft, Vol. 27, No. 10, October 1990, pp. 901-908.*

Waszak, M. and Schmidt, D. (1990). Flight dynamics of aeroelastic vehicles. *Journal of Aircraft, Vol.27, No.10, October 1990, pp. 901-908.*

Weishaar, T. (1987). Aeroelastic tailoring - creative uses of unusual materials. *AIAA/ASME/ASCE/AHS 28th Structures, Structural Dynamics and Materials Conference, 1987.*

Werter, N. P. M. and Breuker, R. D. (2015). Aeroelastic tailoring and structural optimisation using an advanced dynamic aeroelasic framework. *International Forum on Aeroelasticity and Structural Dynamics, June 2015, Saint Petersburg, Russia.*

Werter, N. P. M., Breuker, R. D., and Abdalla, M. (2015). Continuus-time state-space unsteady aerodynamic modelling for efficient aeroelastic load analysis. *International Forum on Aeroelasticity and Structural Dynamics, June 2015, Saint Petersburg, Russia.*

Willaert, M., Abdalla, M., and Gurdal, Z. (2010). A simple finite element cross-sectional modeling of thin-walled beams. *Proceedings f the 2nd Aircraft Structural Design Conference.*